From IEEE Trans. Antennas and Propagation, 1974, pp. 266-274

Interaction Notes

Note 119

September 1972

Natural-Mode Representation of Transient Scattering From Rotationally Symmetric, Perfectly Conducting Bodies and Numerical Results for a Prolate Spheroid

Lennart Marin*
Northrop Corporate Laboratories
Pasadena, California

Abstract

A procedure for calculating the natural frequencies and the current distribution of the natural modes of a perfectly conducting body of revolution is presented. The analysis is based on the magnetic-field integral equation simplified to account for rotational symmetry. A computer code is developed for the numerical evaluation of the natural frequencies and modes of a perfectly conducting, rotationally symmetric body. The code is used in a numerical sample calculation of the natural frequency, the current distribution and the charge density of some of the natural modes of a prolate spheroid.

The general method of treating transient electromagnetic interaction problems developed in a previous note is specialized to perfectly conducting bodies of revolution. In particular, interaction of a step-function plane wave with a prolate spheroid is treated numerically in great detail. The time response of the current and the induced charge on the scattering body is constructed from the natural modes much in the same way as in network theory. The convergence of the solution, as the number of modes is increased, is also considered.

---

* Now with the Dikewood Corporation, Westwood Research Branch, California.

Interaction Notes

Note 119

September 1972

Natural-Mode Representation of Transient Scattering From Rotationally Symmetric, Perfectly Conducting Bodies and Numerical Results for a Prolate Spheroid

Lennart Marin*
Northrop Corporate Laboratories
Pasadena, California

Abstract

A procedure for calculating the natural frequencies and the current distribution of the natural modes of a perfectly conducting body of revolution is presented. The analysis is based on the magnetic-field integral equation simplified to account for rotational symmetry. A computer code is developed for the numerical evaluation of the natural frequencies and modes of a perfectly conducting, rotationally symmetric body. The code is used in a numerical sample calculation of the natural frequency, the current distribution and the charge density of some of the natural modes of a prolate spheroid.

The general method of treating transient electromagnetic interaction problems developed in a previous note is specialized to perfectly conducting bodies of revolution. In particular, interaction of a step-function plane wave with a prolate spheroid is treated numerically in great detail. The time response of the current and the induced charge on the scattering body is constructed from the natural modes much in the same way as in network theory. The convergence of the solution, as the number of modes is increased, is also considered.

*Now with the Dikewood Corporation, Westwood Research Branch, California.

I. Introduction

In two previous notes[1,11] it has been shown that the temporal behavior of the scattered field due to an incident delta-function plane wave can be described by damped sinusoidal oscillations alone. This fact enables one to get a series representation of the operator inverse to the integral operator describing the electromagnetic scattering problem. In the case of slender structures, where resonance phenomena are especially pronounced, only a few terms in this series representation suffices to describe the scattered field. This makes the singularity expansion method especially useful when solving transient scattering problems involving slender structures. Missiles and aircraft in free space or above a ground plane and subject to a nuclear EMP are examples of such problems.

The natural frequencies of a thin wire have been calculated by many investigators[2-9]. Some have studied a thin cylinder together with the so-called thin-wire approximation of the electric field integral equation[6-9], while others have considered a thin prolate spheroid as the scattering object[2-5]. Recently in a note in this series, transient scattering from thin wires has been investigated using the singularity expansion method[9]. In that note some of the natural frequencies and modes of a thin wire have been calculated.

Based on the theory developed in reference [11] we will, in this note, consider electromagnetic scattering from rotationally symmetric bodies. In particular, we will calculate some of the natural frequencies and modes of a prolate spheroid. One reason for investigating a spheroid is to gain some insight into the behavior of the natural modes for structures not necessarily thin. By varying only one parameter, namely the eccentricity, the shape of a spheroid can be changed from a thin wire to a sphere. Thus, the results obtained in references [9] and [10] combined with the results obtained in this note will serve as a guideline for the behavior of the natural modes for many differently shaped bodies. Although the calculations performed in this note are limited to a prolate spheroid, the method used in determining the natural frequency, current distribution and coupling vector of each natural mode is general and can be used in determining, for example, the same quantities for a missile and an aircraft in free space or above the ground.

We want to point out that scattering from a prolate spheroid can also be treated by using the method of separation of variables. Some calculations of the fundamental natural modes using this method have been reported in the literature[3]. These results and the results for a sphere[10] provide useful checks on our numerical calculations.

The analysis in this note is based on the theory developed in a previous note[11]. In the case of a rotationally symmetric body we simplify, in section II, the surface integral equation to a set of one dimensional integral equations. Based on the integral equations for fields independent of the azimuthal angle we deduce, in section III, approximations necessary for the numerical calculations of the natural modes. The results of these numerical calculations are presented in section IV in graphical form for the location of the natural frequencies in the complex frequency plane. We also graph the current distributions of some of the natural modes. In order to get some idea of the number of natural modes needed to accurately describe an actual scattering situation we calculate the time response of the induced current on a prolate spheroid due to a step-function incident plane wave as a function of the number of natural modes used in the series expansion of the inverse operator.

Although the sphere has been the subject of many investigations we determine, in Appendix A, the eigenvalues and eigenfunctions of the integral operator derived from the magnetic-field formulation. In one example we can demonstrate the connections between the singularity expansion method[1,11] (natural modes) and the theory of characteristic modes[13-16]. We want to point out that the singularity expansion method is based on the properties in the complex frequency plane of the operator inverse to the integral operator of the electromagnetic scattering problem, whereas the theory of characteristic modes gives the properties of the same operator only for real frequencies.

A description of the method used in determining the natural frequencies and modes from an integral equation is given in Appendix D. The method we use is general and can be used in any formulation of the electromagnetic scattering problem and is not limited to any particular shape of the scattering body.

A knowledge of the order of each pole is necessary when solving transient electromagnetic scattering problems by using the singularity expansion method.

For a perfectly conducting, arbitrarily shaped, finite body there seems to exist, as of now, no general analytical method that enables one to determine the order of each pole. In Appendix E we discuss a general numerical method to determine the order of each pole.

II. The Magnetic Field Integral Equation for a Rotationally Symmetric Body

In this section we will consider electromagnetic scattering from a perfectly conducting, rotationally symmetric body. In this case, the surface integral equation for the induced surface current density on the scattering body can be reduced to a set of one dimensional integral equations.

Based on the magnetic field formulation we have the following integral equation for the surface current density, $\underline{j}$, on the body

$$(\tfrac{1}{2}\,\underline{\underline{I}} - \underline{\underline{L}})\cdot\underline{j} = \underline{j}^{inc} \tag{2.1}$$

where $\underline{\underline{I}}$ is the identity operator, $\underline{\underline{L}}$ an integral operator defined by

$$\underline{\underline{L}}\cdot\underline{j} = \int_S \underline{n}\times(\nabla G\times\underline{j})\,dS, \tag{2.2}$$

$\underline{j}^{inc} = \underline{n}\times\underline{H}^{inc}$, $\underline{H}^{inc}$ is the magnetic field of the incident wave, $\underline{n}$ the outward unit normal to S (the surface of the perfectly conducting scattering body) G is the free space Green's function,

$$G(\underline{r},\underline{r}';\gamma) = (4\pi|\underline{r} - \underline{r}'|)^{-1}\, e^{-\gamma|\underline{r}-\underline{r}'|}, \tag{2.3}$$

$\gamma(= -ik)$ is the propagation constant of the incident wave, and ∇ operates on the first argument of $G(\underline{r},\underline{r}';\gamma)$.

Let the axis of the rotationally symmetric body coincide with the z-axis in a Cartesian coordinate system (x,y,z). A point on the surface of the scattering body can be represented by two orthogonal coordinates (ξ,ϕ) so that for points on S we have

$$\begin{aligned} x &= \rho(\xi)\cos\phi \\ y &= \rho(\xi)\sin\phi \\ z &= z(\xi) \end{aligned} \tag{2.4}$$

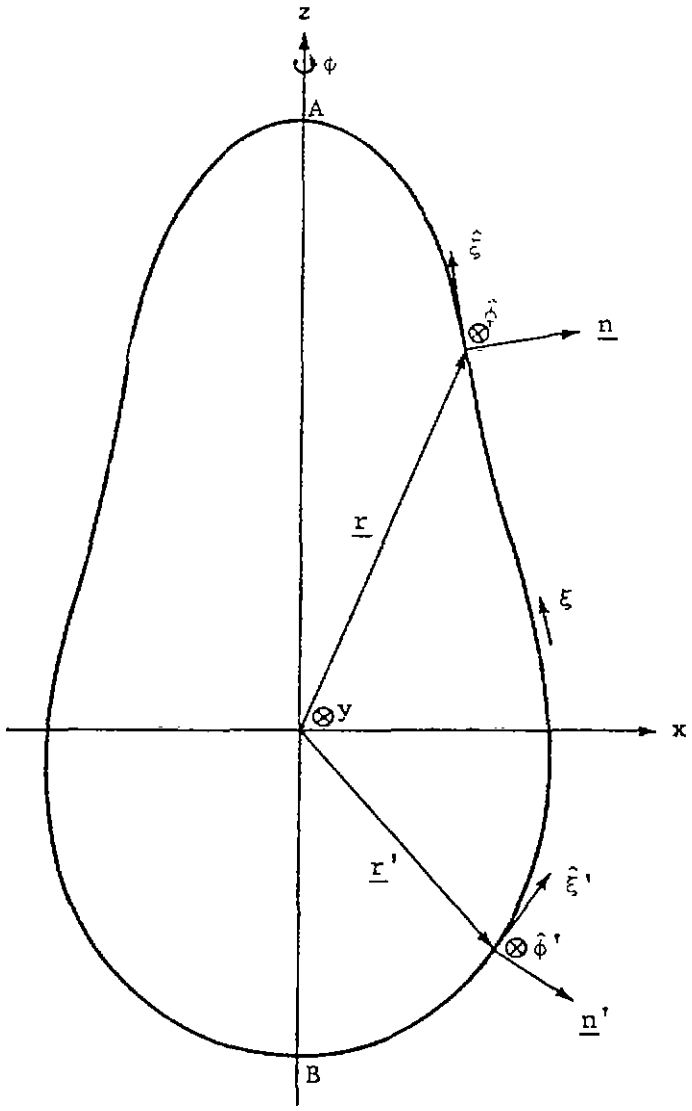

Figure 1. A rotationally symmetric body with a local orthogonal curvlinear coordinate system. The coordinate ξ is used to represent the arclength measured from the bottom point B. At the top point A, ξ takes the value ξ_o.

where $0 \le \xi \le \xi_o$ and $0 \le \phi \le 2\pi$ (see figure 1).

Expanding $\underline{j}$ and $\underline{j}^{inc}$ in a Fourier series in ϕ,

$$\underline{j} = j_\xi \hat{\xi} + j_\phi \hat{\phi}, \tag{2.5}$$

$$\underline{j}^{inc} = j_\xi^{inc} \hat{\xi} + j_\phi^{inc} \hat{\phi} \tag{2.6}$$

where

$$j_\xi(\xi,\phi) = \sum_{m=0}^{\infty} j'_{\xi m}(\xi)\cos m\phi + \sum_{m=1}^{\infty} j''_{\xi m}(\xi)\sin m\phi, \tag{2.7}$$

$$j_\phi(\xi,\phi) = \sum_{m=1}^{\infty} j'_{\phi m}(\xi)\sin m\phi - \sum_{m=0}^{\infty} j''_{\phi m}(\xi)\cos m\phi, \tag{2.8}$$

$$j_\xi^{inc}(\xi,\phi) = \sum_{m=0}^{\infty} j'^{inc}_{\xi m}(\xi)\cos m\phi + \sum_{m=1}^{\infty} j''^{inc}_{\xi m}(\xi)\sin m\phi, \tag{2.9}$$

$$j_\phi^{inc}(\xi,\phi) = \sum_{m=1}^{\infty} j'^{inc}_{\phi m}(\xi)\sin m\phi - \sum_{m=0}^{\infty} j''^{inc}_{\phi m}(\xi)\cos m\phi \tag{2.10}$$

we get, after some tedious calculations, the following two sets of coupled one dimensional integral equations, $m = 0,1,2,\ldots,$

$$\frac{1}{2} j'_{\xi m}(\xi) - \int_0^{\xi_o} A_m(\xi,\xi')\rho(\xi')j'_{\xi m}(\xi')d\xi' - \int_0^{\xi_o} B_m(\xi,\xi')\rho(\xi')j'_{\phi m}(\xi')d\xi' = j'^{inc}_{\xi m}(\xi),$$

$$\frac{1}{2} j'_{\phi m}(\xi) - \int_0^{\xi_o} C_m(\xi,\xi')\rho(\xi')j'_{\xi m}(\xi')d\xi' - \int_0^{\xi_o} D_m(\xi,\xi')\rho(\xi')j'_{\phi m}(\xi')d\xi' = j'^{inc}_{\phi m}(\xi), \tag{2.11}$$

$$\frac{1}{2} j''_{\xi m}(\xi) - \int_0^{\xi_o} A_m(\xi,\xi')\rho(\xi')j''_{\xi m}(\xi')d\xi' - \int_0^{\xi_o} B_m(\xi,\xi')\rho(\xi')j''_{\phi m}(\xi')d\xi' = j''^{inc}_{\xi m}(\xi),$$

$$\frac{1}{2} j''_{\phi m}(\xi) - \int_0^{\xi_o} C_m(\xi,\xi')\rho(\xi')j''_{\xi m}(\xi')d\xi' - \int_0^{\xi_o} D_m(\xi,\xi')\rho(\xi')j''_{\phi m}(\xi')d\xi' = j''^{inc}_{\phi m}(\xi) \tag{2.12}$$

where

$$A_m(\xi,\xi') = a(\xi,\xi')\alpha_m(\xi,\xi') + a'(\xi,\xi')\beta_m(\xi,\xi'),$$

$$B_m(\xi,\xi') = b(\xi,\xi')\sigma_m(\xi,\xi'),$$

$$C_m(\xi,\xi') = c(\xi,\xi')\sigma_m(\xi,\xi'),$$

$$D_m(\xi,\xi') = d(\xi,\xi')\alpha_m(\xi,\xi') + d'(\xi,\xi')\beta_m(\xi,\xi'),$$

$$a(\xi,\xi') = (z' - z)\sin\theta' - \rho'\cos\theta',$$

$$a'(\xi,\xi') = \rho\cos\theta',$$

$$b(\xi,\xi') = z - z',$$

$$c(\xi,\xi') = \rho'\sin\theta\cos\theta' - \rho\cos\theta\sin\theta' + (z - z')\sin\theta\sin\theta',$$

$$d(\xi,\xi') = (z' - z)\sin\theta + \rho\cos\theta,$$

$$d'(\xi,\xi') = -\rho'\cos\theta,$$

$$\alpha_m(\xi,\xi') = \int_0^{2\pi} f(R)\cos\psi\cos m\psi d\psi,$$

$$\beta_m(\xi,\xi') = \int_0^{2\pi} f(R)\cos m\psi,$$

$$\sigma_m(\xi,\xi') = \int_0^{2\pi} f(R)\sin\psi\sin m\psi d\psi,$$

$$f(R) = \mathscr{P}(1 + \gamma R)(4\pi R^3)^{-1}\exp(-\gamma R),$$

$$R = \left[\rho^2 + \rho'^2 - 2\rho\rho'\cos\psi + (z - z')^2\right]^{\frac{1}{2}},$$

$$\rho = \rho(\xi), \qquad \rho' = \rho(\xi'),$$

$$z = z(\xi), \qquad z' = z(\xi'),$$

$$\theta = \theta(\xi), \qquad \theta' = \theta(\xi'),$$

and

$$\theta(\xi) = -\arcsin[\underline{n}(\xi)\cdot\hat{z}].$$

The advantages of transforming a surface integral equation into a set of one-dimensional integral equations are obvious in numerical computations and have been discussed in the literature[12]. Notice that for $m \neq 0$ the only difference between the set of integral equations (2.11) and the set (2.12) is the right-hand side. Since the natural frequencies and natural modes are determined by the kernel of the integral equation it follows that the natural modes can be determined from the set of equations (2.11). The only difference between the solution of equations (2.11) and (2.12) is in the coupling coefficients given by

$$\langle \underline{j}_n^{inc}, \underline{h}_n \rangle$$

(c.f. section VI of [11]).

Next, let us consider the case $m = 0$. In this case the set of coupled integral equations decouple and we have the two integral equations

$$\frac{1}{2} j'(\xi) - \int_0^{\xi_o} A(\xi,\xi')\rho(\xi')j'(\xi')d\xi' = j'^{inc}(\xi), \tag{2.13}$$

$$\frac{1}{2} j''(\xi) - \int_0^{\xi_o} D(\xi,\xi')\rho(\xi')j''(\xi')d\xi' = j''^{inc}(\xi) \tag{2.14}$$

where

$$A(\xi,\xi') = A_o(\xi,\xi'),$$

$$D(\xi,\xi') = D_o(\xi,\xi'),$$

$$j'(\xi) = j'_{\xi_o}(\xi),$$

$$j'^{inc}(\xi) = j'^{inc}_{\xi o}(\xi),$$

$$j''(\xi) = j''_{\phi o}(\xi),$$

and

$$j''^{inc}(\xi) = j''^{inc}_{\phi o}(\xi).$$

When the scattering body is a sphere the integral equation (2.13) gives the surface current density of transverse magnetic fields (no radial component of the magnetic field) and the integral equation (2.14) gives the surface current density of transverse electric fields (no radial component of the electric field). An investigation of the integral equations (2.13) and (2.14) when the scattering body is a sphere is given in Appendix A.

Let the z - x plane be the plane spanned by the unit-vector in the z-direction and the unit vector in the direction of propagation of the incident wave. If the incident magnetic field is perpendicular to this plane we have $j'^{inc} = 0$, and if the incident electric field is perpendicular to this plane we have $j''^{inc} = 0$.

We now go on to consider the integral equation

$$(\tfrac{1}{2}\,\underline{\underline{I}} - \underline{\underline{L}}^T)\cdot\underline{h}^* = \underline{h}^{inc} \tag{2.15}$$

when the scattering body is a rotationally symmetric body. Here $\underline{\underline{L}}^T = \underline{\underline{L}}^{\dagger *}$ where the asterisk denotes complex conjugation and $\underline{\underline{L}}^\dagger$ is the adjoint-operator of $\underline{\underline{L}}$ (c.f. Appendix C of [11]). Expanding $\underline{h}^*$ and $\underline{h}^{inc}$ in the Fourier series (2.5) through (2.10) the surface integral equation (2.15) can be transformed into the following set of one dimensional integral equations

$$\begin{aligned}
&\tfrac{1}{2}\,h'^*_{\xi m}(\xi) - \int_0^{\xi_o} A_m(\xi',\xi)\rho(\xi')h'^*_{\xi m}(\xi')d\xi' - \int_0^{\xi_o} B_m(\xi',\xi)\rho(\xi')h'^*_{\phi m}(\xi')d\xi' = h'^{inc}_{\xi m}(\xi), \\
&\tfrac{1}{2}\,h'^*_{\phi m}(\xi) - \int_0^{\xi_o} C_m(\xi',\xi)\rho(\xi')h'^*_{\xi m}(\xi')d\xi' - \int_0^{\xi_o} D_m(\xi',\xi)\rho(\xi')h'^*_{\phi m}(\xi')d\xi' = h'^{inc}_{\phi m}(\xi),
\end{aligned} \tag{2.16}$$

$$\frac{1}{2} h''^{*}_{\xi m}(\xi) - \int_0^{\xi_o} A_m(\xi',\xi)\rho(\xi')h''^{*}_{\xi m}(\xi')d\xi' - \int_0^{\xi_o} B_m(\xi',\xi)\rho(\xi')h''^{*}_{\phi m}(\xi')d\xi' = h''^{inc}_{\xi m}(\xi),$$

$$\frac{1}{2} h''^{*}_{\phi m}(\xi) - \int_0^{\xi_o} C_m(\xi',\xi)\rho(\xi')h''^{*}_{\xi m}(\xi')d\xi' - \int_0^{\xi_o} D_m(\xi',\xi)\rho(\xi')h''^{*}_{\phi m}(\xi')d\xi' = h''^{inc}_{\phi m}(\xi) \tag{2.17}$$

and especially for m = 0 we have

$$\frac{1}{2} h'^{*}(\xi) - \int_0^{\xi_o} A(\xi',\xi)\rho(\xi')h'^{*}(\xi')d\xi' = h'^{inc}(\xi), \tag{2.18}$$

$$\frac{1}{2} h''^{*}(\xi) - \int_0^{\xi_o} D(\xi',\xi)\rho(\xi')h''^{*}(\xi')d\xi' = h''^{inc}(\xi) \tag{2.19}$$

where

$$h'^{*}(\xi) = h'^{*}_{\xi o}(\xi),$$

$$h''^{*}(\xi) = h''^{*}_{\phi o}(\xi),$$

$$h'^{inc}(\xi) = h'^{inc}_{\xi o}(\xi),$$

$$h''^{inc}(\xi) = h''^{inc}_{\phi o}(\xi).$$

In the next section we will discuss the numerical solution of the integral equations (2.13) and (2.14) with the aid of equations (2.18) and (2.19).

III. Numerical Calculation of the Natural Modes

In this section we will give a numerical method for computing the natural modes of a rotationally symmetric body. In reference [11] we have shown that the natural frequency and the current distribution of a natural mode can be determined from the eigenvalue problem

$$\underline{\underline{A}}(\gamma_n)\cdot\underline{j}_n = 0 \tag{3.1}$$

where $\underline{\underline{A}}(\gamma) = \frac{1}{2}\underline{\underline{I}} - \underline{\underline{L}}(\gamma)$ and $\underline{j}_n \neq 0$. We have also shown in reference [11] that there exists $\underline{h}_n \neq 0$ such that

$$\underline{\underline{A}}^T(\gamma_n)\cdot\underline{h}_n^* = 0. \tag{3.2}$$

From the preceeding section [c.f. equations (2.13), (2.14), (2.18) and (2.19)] it follows that in the case of a rotationally symmetric body we can, for the ϕ-independent modes, reduce equations (3.1) and (3.2) to

$$\frac{1}{2}\, j_n'(\xi) - \int_0^{\xi_o} A(\xi,\xi';\gamma_n')\rho(\xi')j_n'(\xi')d\xi' = 0, \tag{3.3}$$

$$\frac{1}{2}\, j_n''(\xi) - \int_0^{\xi_o} D(\xi,\xi';\gamma_n'')\rho(\xi')j_n''(\xi')d\xi' = 0, \tag{3.4}$$

$$\frac{1}{2}\, h_n'^*(\xi) - \int_0^{\xi_o} A(\xi',\xi;\gamma_n')\rho(\xi')h_n'^*(\xi')d\xi' = 0, \tag{3.5}$$

$$\frac{1}{2}\, h_n''^*(\xi) - \int_0^{\xi_o} D(\xi',\xi;\gamma_n'')\rho(\xi')h_n''^*(\xi')d\xi' = 0. \tag{3.6}$$

In the following we will analyze in detail the numerical solution of equations (3.3) and (3.5). The numerical solution of equations (3.4) and (3.6) can, of course, be obtained in a similar way. The numerical method we will use is based on a zoning technique. Divide the surface of the scattering body into N segments, and approximate each segment of the surface by a frustum of a cone.

Moreover, on each frustum we assume that the current density is constant. The left hand side of equation (3.3) can then be approximated by the sum

$$\frac{1}{2} j'(\xi) - \int_0^{\xi_o} A(\xi,\xi',\gamma)\rho(\xi')j'(\xi')d\xi' \approx \frac{1}{2} j'(\xi) - \sum_{\ell=1}^{N} K(\xi,\xi_\ell;\gamma)w_\ell j'(\xi_\ell) \qquad (3.7)$$

where

$$K(\xi,\xi_\ell;\gamma)\bar{w}_\ell = \int_{-\delta_\ell}^{\delta_\ell} A(\xi,\xi_\ell + \xi';\gamma)\rho(\xi_\ell + \xi')d\xi' \approx \sum_{k_\ell} A(\xi,\xi_{k_\ell};\gamma)w_{k_\ell},$$

and ξ_ℓ is the midpoint of the ℓ^{th} interval, which consists of all ξ such that $\xi_\ell - \delta_\ell \le \xi \le \xi_\ell + \delta_\ell$. Furthermore,

$$w_{\ell_k} = \rho(\xi_{\ell_k})r_{\ell_k} \quad \text{and} \quad w_\ell = \sum_{k_\ell} w_{k_\ell}$$

where r_{k_ℓ} are the weight factors and ξ_{k_ℓ} are the abscissas used in the Gaussian quadrature formula on the interval $(\xi_\ell - \delta_\ell, \xi_\ell + \delta_\ell)$. In order to form a set of algebraic equations we proceed as follows: multiply equation (3.7) by $\rho(\xi)$ and integrate the expression thus formed over the interval $(\xi_\ell - \delta_\ell, \xi_\ell + \delta_\ell)$. Setting each resulting expression equal to zero we can form the following system of algebraic equations from the integral equation (3.3),

$$\frac{1}{2} w_i j_i - \sum_{\ell=1}^{N} w_i P_{i\ell}(\gamma) w_\ell j_\ell = 0, \qquad 1 \le i \le N \qquad (3.8)$$

or

$$\sum_{\ell=1}^{N} \left[\frac{1}{2}\delta_{i\ell} - P_{i\ell}(\gamma)w_\ell\right] j_\ell = 0, \qquad 1 \le i \le N \qquad (3.9)$$

since $w_i \neq 0$. Here

$$j_\ell = j'(\xi_\ell),$$

and

$$w_i w_\ell P_{i\ell}(\gamma) = \sum_{k_i,k_\ell} w_{k_i} w_{k_\ell} A(\xi_{k_i},\xi_{k_\ell};\gamma).$$

The set of equations (3.9) can be written in the matrix form

$$M(\gamma)\cdot\bar{j} = 0 \tag{3.10}$$

where $\bar{j}$ is a column vector with elements j_i and $M(\gamma)$ is a $N \times N$ matrix with elements $m_{i\ell}(\gamma)$, defined by

$$m_{i\ell}(\gamma) = \frac{1}{2}\,\delta_{i\ell} - P_{i\ell}(\gamma)w_\ell .$$

Similarly, it can be shown that the integral equation (3.4) can be approximated by the following set of algebraic equations

$$\frac{1}{2}\,h_i^* - \sum_{\ell=1}^{N} P_{\ell i}(\gamma)w_\ell h_\ell^* = 0, \tag{3.11}$$

where

$$h_\ell^* = h'^*(\xi_\ell).$$

Multiplying equation (3.11) by w_i and introducing

$$q_\ell = w_\ell h_\ell^* \tag{3.12}$$

we get the following matrix equation

$$M^T(\gamma)\cdot\bar{q} = 0 \tag{3.13}$$

where $M^T(\gamma)$ is the transposed matrix of $M(\gamma)$ and $\bar{q}$ is a column vector with elements q_i.

Thus, by finding those γ_n for which

$$\det\{M(\gamma_n)\} = 0 \tag{3.14}$$

and the corresponding nontrivial solutions, $\bar{j}_n$ and $\bar{q}_n$, of the equations

$$M(\gamma_n)\cdot\bar{j}_n = 0, \tag{3.15}$$

and

$$M^T(\gamma_n)\cdot\bar{q}_n = 0 \tag{3.16}$$

we can determine j_n' and $h_n'^*$ numerically. A detailed analysis of how to determine γ_n, $\bar{j}_n$ and $\bar{q}_n$ from equations (2.13) and (2.18) is given in Appendix D.

We now go on to consider the construction of the solution of the non-homogeneous integral equation

$$\underline{\underline{A}}(\gamma)\cdot\underline{j} = \underline{j}^{inc}, \qquad \gamma \neq \gamma_n. \tag{3.17}$$

Let us consider the special case where the inverse operator $\underline{\underline{A}}^{-1}(\gamma)$ has only simple poles. Furthermore, we assume that for each pole there is only one linear independent nontrivial solution $\underline{j}_n$ of the equation

$$\underline{\underline{A}}(\gamma_n)\cdot\underline{j}_n = 0, \tag{3.18}$$

and thus only one linear independent nontrivial solution $\underline{h}_n^*$ of the equation

$$\underline{\underline{A}}^T(\gamma_n)\cdot\underline{h}_n^* = 0. \tag{3.19}$$

We also assume that $\underline{j}^{inc}$ is an analytic function in the entire γ-plane. The solution of the integral equation (3.17) then takes the following form

$$\underline{j}(\underline{r},\gamma) = \sum_{ext} (\gamma - \gamma_n)^{-1} \left[\langle \underline{\underline{B}}_n\cdot\underline{j}_n, \underline{h}_n\rangle\right]^{-1} \langle \underline{j}_n^{inc}, \underline{h}_n\rangle \underline{j}_n \tag{3.20}$$

(c.f. equation (6.29) in [11]). When the incident wave is a step-function in time we have the following time response for the induced current density $\underline{J}(\underline{r},t)$,

$$\underline{J}(\underline{r},t) = U(ct - \eta_o) \sum_{ext} \gamma_n^{-1} \langle \underline{n}\times\underline{H}_o \exp[\gamma_n(\eta' - \eta_o)], \underline{h}_n\rangle$$
$$\left[\langle \underline{\underline{B}}_n\cdot\underline{j}_n, \underline{h}_n\rangle\right]^{-1} \underline{j}_n \exp[\gamma_n(\eta_o - ct)]. \tag{3.21}$$

Here $\eta_o = \hat{e}\cdot\underline{r}_o$ where $\hat{e}$ is the direction of propagation of the incident wave, $\underline{r}_o$ is the point on S first hit by the incident wave, $\underline{\underline{B}}_n$ is an integral operator defined by

$$(\underline{\underline{B}}_n\cdot\underline{f})(\underline{r}) = -(4\pi)^{-1}\int_S \underline{n}(\underline{r})\times[\nabla \exp(-\gamma_n|\underline{r}-\underline{r}'|)]\times\underline{f}(\underline{r}')dS',$$

and

$$\langle\underline{f},\underline{g}\rangle = \int_S \underline{f}(\underline{r})\cdot\underline{g}^*(\underline{r})dS.$$

For the ϕ-independent modes we get the following approximative expressions

$$(\underline{\underline{B}}_n\cdot\underline{j}_n)(\xi_i) \approx \sum_\ell b_{i\ell}(\gamma_n)w_\ell j_\ell^{(n)}, \tag{3.22}$$

and

$$\langle\underline{\underline{B}}_n\cdot\underline{j}_n,\underline{h}_n\rangle \approx \sum_{i,\ell} b_{i\ell}(\gamma_n)w_i h_i^{*(n)}\, w_\ell j_\ell^{(n)} = \sum_{i,\ell} b_{i\ell}(\gamma_n)q_i^{(n)}\, w_\ell j_\ell^{(n)} \tag{3.23}$$

where

$$w_i w_\ell b_{i\ell}(\gamma_n) = \sum_{k_i,k_\ell} B(\xi_{k_i},\xi_{k_\ell};\gamma)w_{k_i}w_{k_\ell},$$

$$B(\xi,\xi';\gamma) = a(\xi,\xi')\lambda_1(\xi,\xi') + a'(\xi,\xi')\lambda_o(\xi,\xi'),$$

$$\lambda_m(\xi,\xi') = \int_0^{2\pi} g(R)\cos m\psi,$$

and

$$g(R) = \frac{1}{2}\exp(-\gamma R).$$

Furthermore, the coupling coefficient for the ϕ-independent modes takes the form

$$\langle\underline{j}_n^{inc},\underline{h}_n\rangle \approx 2\pi\sum_i j_n^{inc}(\xi_i)q_i^{(n)}. \tag{3.24}$$

In the next section we will present the results of the numerical calculations obtained by using the method outlined in this section. Some alternative numerical methods are presented in Appendix C, and certain properties of the convergence of the numerical solution is given in Appendix B.

IV. Numerical Results

In this section we will discuss the results of the numerical calculations that have been performed on the basis of the theory outlined in sections II and III. First, we will present the calculations of the natural frequency the current distribution, and the charge density of some of the natural modes. Then, we will continue with the construction of the time history of the current and charge induced on a prolate spheroid by a step function incident plane wave.

For practical purposes we are mainly interested in electromagnetic interaction of a plane wave and relatively slender structures (aircraft and missiles are examples of such structures). For slender structures the most important current density is independent of the azimuthal angle ϕ and satisfies the integral equation (2.13). Therefore, the numerical calculations will be limited to the solution of the integral equations (2.13) and (2.18).

A. Numerical Determination of the Natural Modes

The prolate spheroid used as a scattering object together with a coordinate system is depicted in figure 2. The semiminor axis is denoted by a and the semimajor axis by b.

In order to determine the natural frequency, current distribution and coupling vector of each natural mode it is necessary to find the nontrivial solutions of equations (3.10) and (3.13). Throughout all the numerical calculations the prolate spheroid was divided into 32 segments (see figure 2). However, since the current distribution and coupling vector of each mode is either an even or an odd function with respect to the x-y-plane all matrices involved consist of 16 rows and 16 columns.

The location of a natural frequency is determined from the equation

$$\det\{M(\gamma)\} = 0 \tag{4.1}$$

(c.f. equation (3.10)). In Appendix D we have shown that equation (4.1) is satisfied for those values of γ that satisfy the equation

$$t_{NN}(\gamma) = 0. \tag{4.2}$$

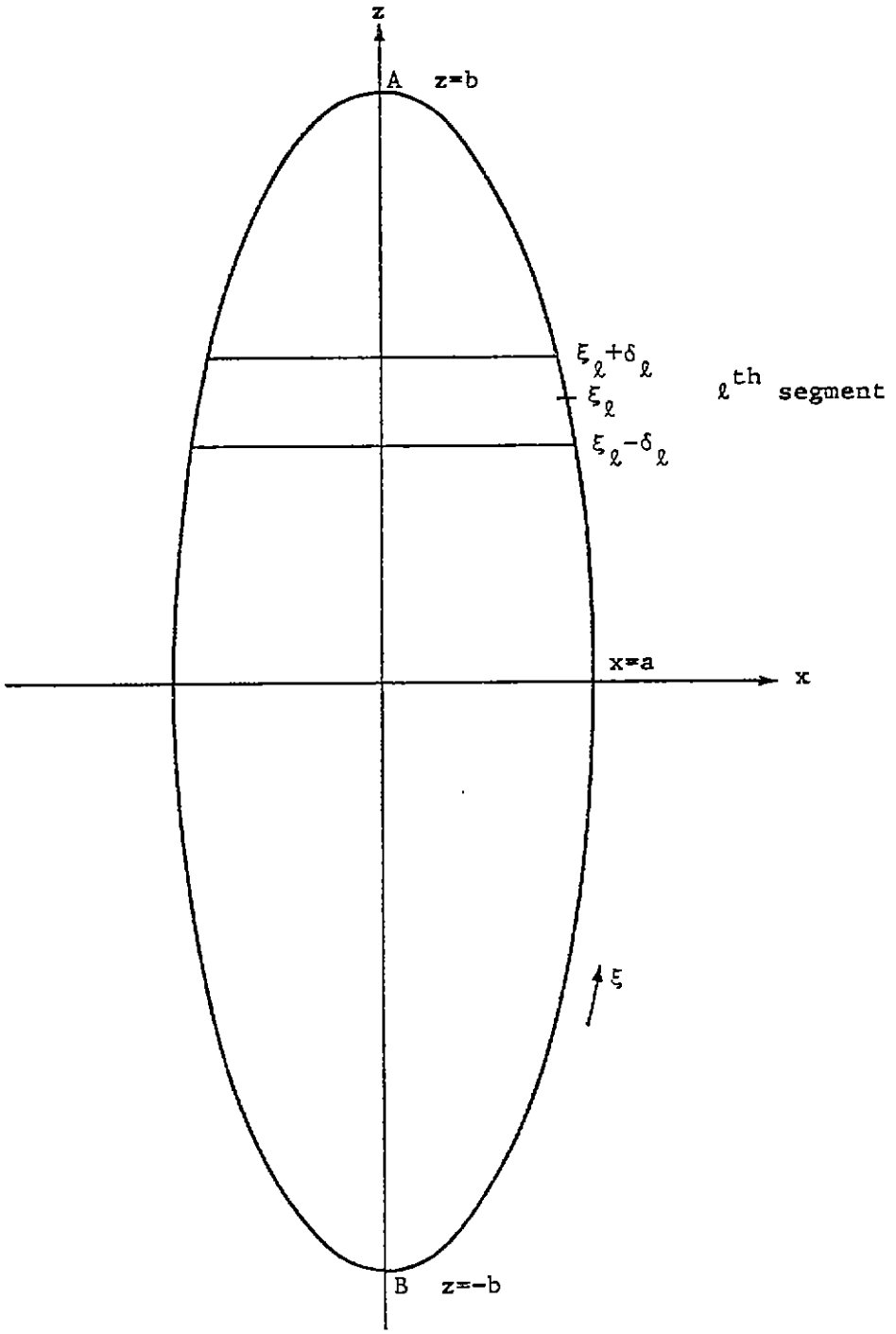

Figure 2. A prolate spheroid with the segments and sample points used in the numerical calculations.

Here, $t_{NN}(\gamma)$ is the last diagonal element in the triangular matrix obtained by applying the Householder triangularization method to the matrix $M(\gamma)$. An iterative method was used to find the solutions of equation (4.2). Each iteration was started by an initial guess of the natural frequency. A method similar to the Newton-Raphson method of finding zeros of a real function was then used to find the natural frequency. Each iteration was stopped when the absolute value of the difference of γb between two consecutive iterations was less than .001. The value of $|t_{NN}(\gamma)|$ was then found to be less than .0001, whereas $|t_{ii}(\gamma)|$, $1 \leq i \leq N - 1$, varied between .1 and 1. It was also found numerically that all zeros of $\det\{M(\gamma)\}$ are simple zeros. Note that each zero of $\det\{M(\gamma)\}$ is a pole of $M^{-1}(\gamma)$, the inverse of $M(\gamma)$.

The result of the numerical search in the complex γ-plane for the poles of $M^{-1}(\gamma)$ is shown in figure 3. In calculating the results presented in figure 3a the ratio of the minor axis to the major axis of the spheroid was chosen to be .1. Since all poles of $M^{-1}(\gamma)$ have negative real part and since all poles except those on the negative real axis occur in complex conjugate pairs we only present the second quadrant of the complex γ-plane in figure 3a. In figure 3a we observe that the poles of $M^{-1}(\gamma)$ occur in layers. This fact has also been observed in previous studies of the natural frequencies of a thin wire and a sphere[9,10]. Following the notation introduced previously[9], we use the index ℓ to describe each layer of poles and the index n to describe a pole within each layer. Here ℓ is a positive integer and n is a nonnegative integer. Poles on the negative real axis have index $n = 0$. Poles in the third quadrant can then be characterized by a negative value of n. We have also listed some natural frequencies in table I.

In figures 3b and 3c we have graphed the locus of some of the natural frequencies as the length of the minor axis (2a) varies, but the length of the major axis (2b) is fixed. In figure 3b we have graphed the normalized quantity γb and in figure 3c we have graphed γd. Here, 4d is the circumference of an ellipse with minor axis 2a and major axis 2b, i.e.,

$$d = b \int_0^{\pi/2} [1 - (1 - a^2/b^2)\sin^2\phi]^{\frac{1}{2}} \, d\phi. \tag{4.3}$$

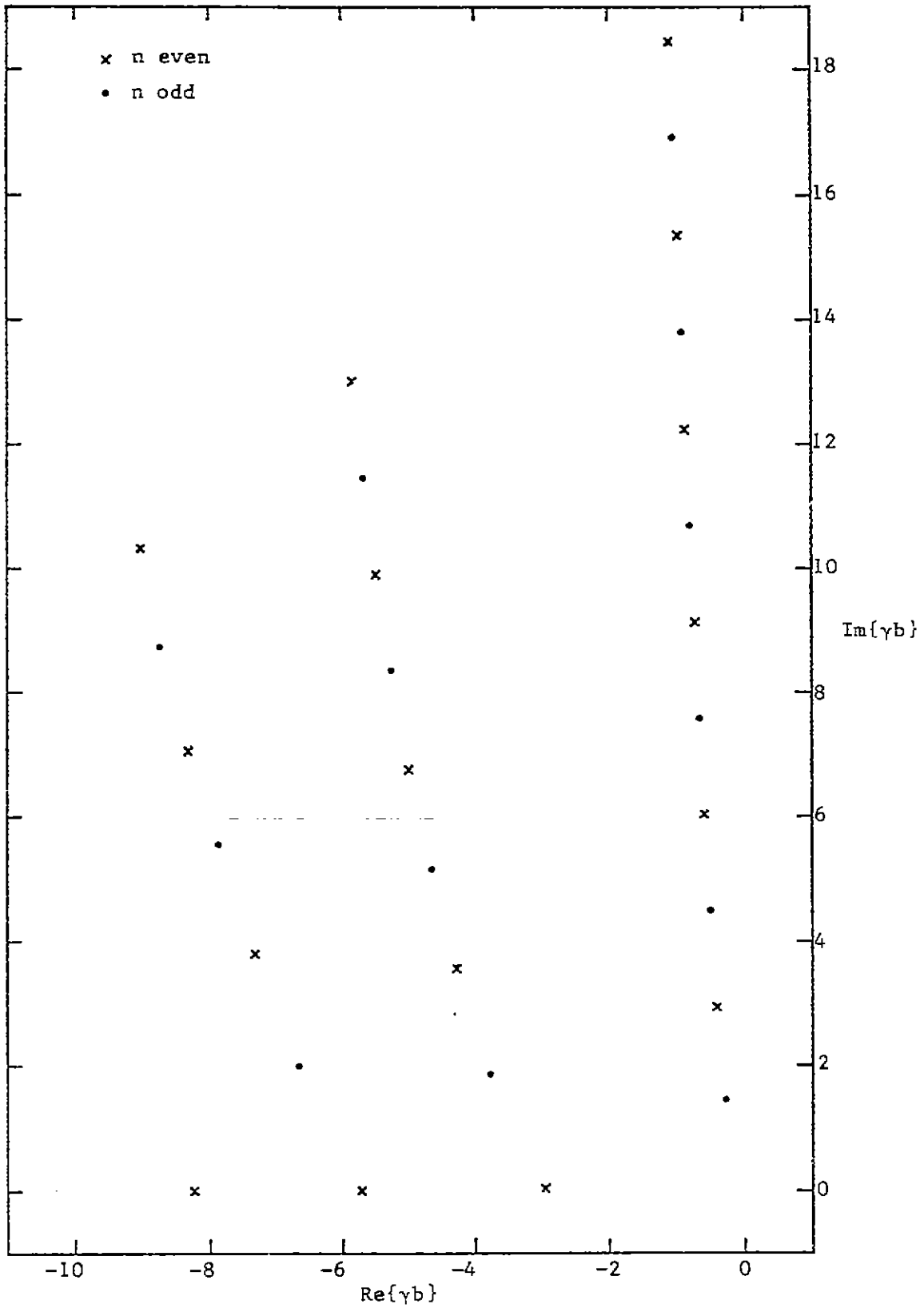

Figure 3a. Natural frequencies of a prolate spheroid where a/b=.1.

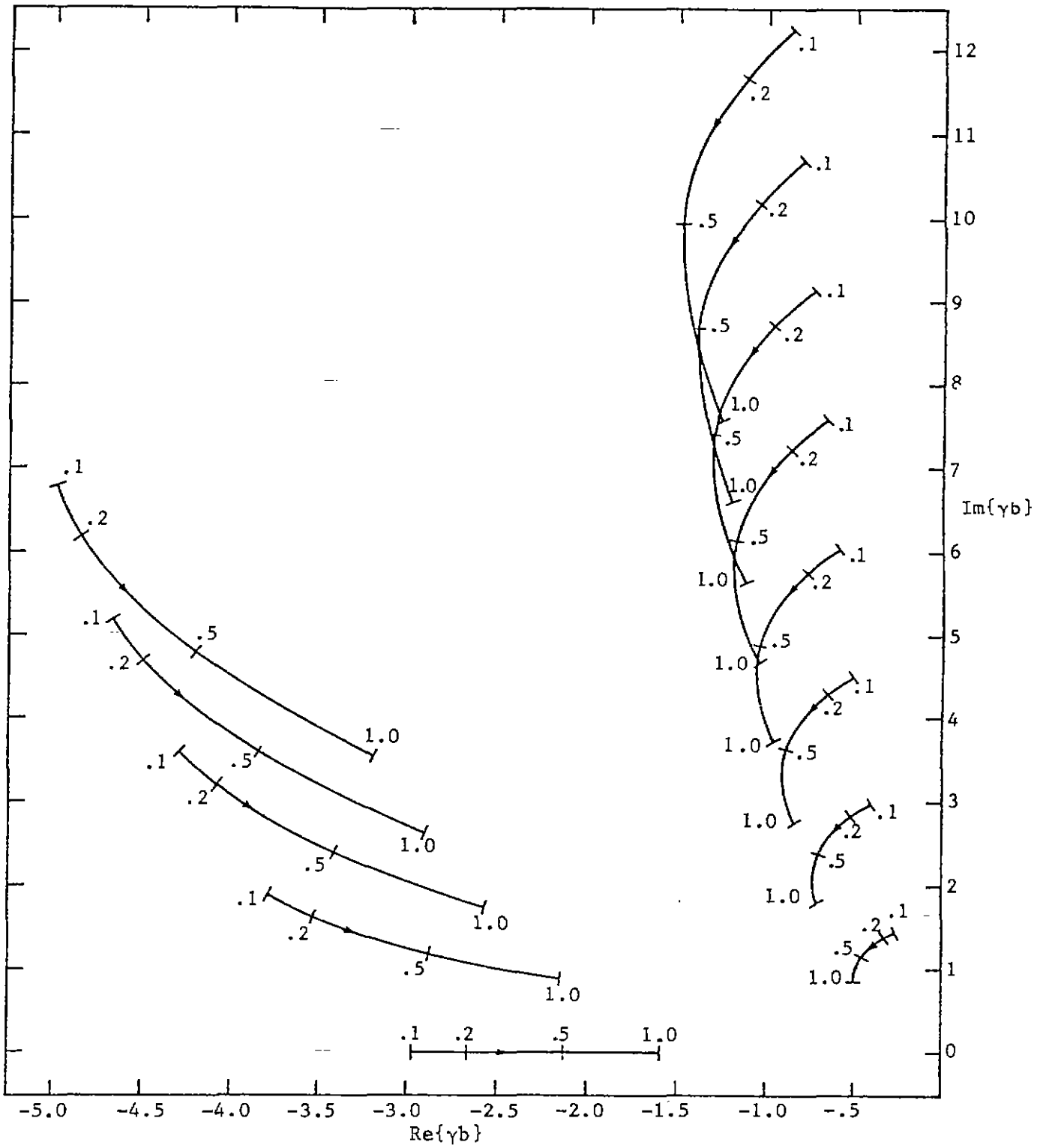

Figure 3b. The locus of natural frequencies when .1≤a/b≤1. The location of the natural frequencies for a/b=.1, .2, .5, 1 is indicated on the curves. The arrow indicates the direction in which the natural frequencies move for increasing values of a/b.

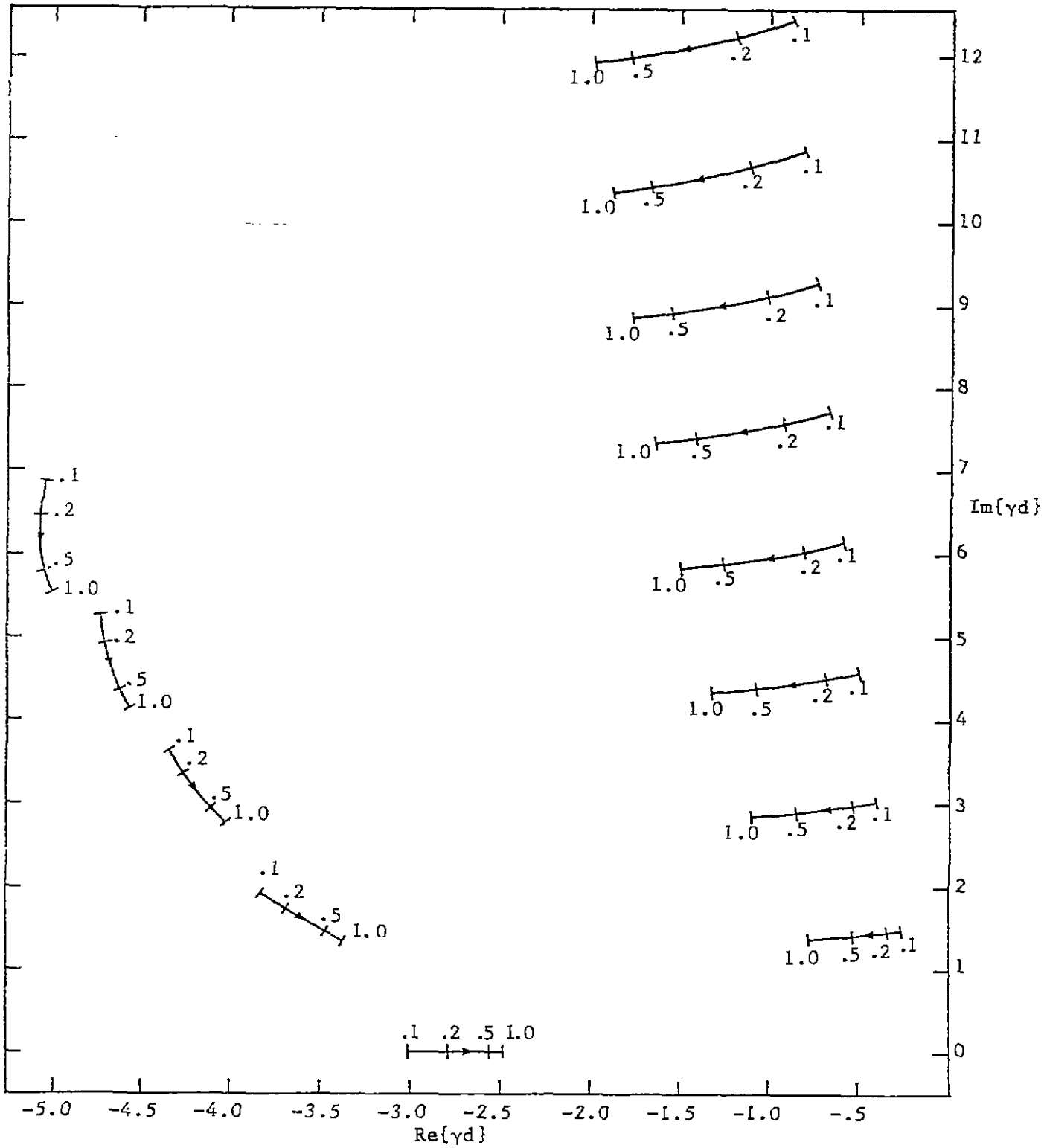

Figure 3c. The locus of natural frequencies when .1≤a/b≤1. The location of the natural frequencies for a/b=.1, .2, .5, 1 is indicated on the curves. The arrow indicates the direction in which the natural frequencies move for increasing values of a/b.

Table 1. Natural frequencies of a prolate spheroid where a/b = .1

ℓ	n	Re{γb}	Im{γb}
1	1	-.265	1.458
	2	-.400	2.977
	3	-.497	4.510
	4	-.582	6.051
	5	-.658	7.598
	6	-.727	9.149
	7	-.793	10.703
	8	-.855	12.260
	9	-.915	13.818
	10	-.973	15.377
	11	-1.030	16.937
	12	-1.086	18.450
	13	-1.141	20.006
2	0	-2.969	0
	1	-3.776	1.888
	2	-4.278	3.575
	3	-4.670	5.194
	4	-4.975	6.782
	5	-5.248	8.352
	6	-5.493	9.911
3	0	-5.697	0
	1	-6.658	2.012
	2	-7.311	3.812
	3	-7.834	5.509
	4	-8.290	7.146
	5	-8.717	8.727
	6	-9.003	10.306

Table 2. Natural frequencies of prolate spheroids where a/b = .1, .2, .5, 1

ℓ	n	a/b = .1		a/b = .2		a/b = .5		a/b = 1	
		Re{γb}	Im{γb}	Re{γb}	Im{γb}	Ke{γb}	Im{γb}	Re{γb}	Im{γb}
1	1	-.265	1.458	-.336	1.374	-.453	1.152	-.500	.866
	2	-.400	2.977	-.516	2.817	-.703	2.380	-.702	1.807
	3	-.497	4.510	-.655	4.277	-.890	3.623	-.843	2.758
	4	-.582	6.051	-.773	5.745	-1.042	4.876	-.954	3.715
	5	-.658	7.598	-.876	7.220	-1.171	6.136	-1.048	4.676
	6	-.727	9.149	-.970	8.698	-1.286	7.401	-1.129	5.642
	7	-.793	10.703	-1.057	10.180	-1.388	8.669	-1.201	6.610
	8	-.855	12.260	-1.138	11.666	-1.480	9.938	-1.267	7.580
2	0	-2.969	0	-2.672	0	-2.130	0	-1.596	0
	1	-3.776	1.888	-3.522	1.652	-2.879	1.210	-2.157	.871
	2	-4.278	3.575	-4.070	3.195	-3.408	2.410	-2.571	1.752
	3	-4.660	5.194	-4.491	4.694	-3.830	3.609	-2.908	2.644
	4	-4.975	6.782	-4.839	6.174	-4.187	4.810	-3.195	3.545

For poles in the $\ell = 1$ layer we note that the absolute value of the real part of γd is a monotonically increasing function of a, whereas the imaginary part of γd stays almost constant. Making a comparison with circuit theory this means that the Q-value of each mode is a decreasing function of a when b is fixed. Another way of expressing the same fact is to say that thin spheroids are more resonant as compared to thick spheroids. For poles in the $\ell = 2$ layer we note that the absolute value of the real part of γd is a decreasing function of a. In table 2 we have tabulated some of the natural frequencies of a prolate spheroid for different values of a/b.

Comparison with previous calculations[3] of the location of the first pole in the first layer was made and good agreement was found in those cases where a comparison could be made. Unfortunately, for $.3 < a/b < .02$ it is hard to make accurate comparisons with the results presented in [3] since the series expressions used there converge very slowly for $.3 < a/b < .02$.

The current distribution of some of the natural modes is depicted in figure 4. In figure 4 we have chosen to normalize the current density, $j_{\ell n}$, so that its absolute value is less than or equal to one. To get some idea of the total current associated with each mode we have also graphed the current distribution multiplied by ρ/a. Here, $\rho = \rho(z)$ is the "local radius" of the spheroid. The current distribution is an odd (even) function with respect to the x-y-plane for modes where the index n is an even (odd) integer. Moreover, the current distribution is a real function for modes whose natural frequency is on the negative real axis in the complex s-plane. In the case of a sphere we note that (1) the current distribution can be represented by real functions (spherical harmonics) and (2) that the current distribution of modes with indices $\ell = 1$, $n = 2$ and $\ell = 2$, $n = 0$ are identical. For spheroids with an arbitrary eccentricity it can be observed from figure 4 that the current distribution is almost real. This fact has also been observed in the case of a thin cylinder[9]. Estimates of the accuracy of the numerical calculations indicate that the complex values obtained are not due to numerical errors. This means that the current distribution indeed is a complex function.

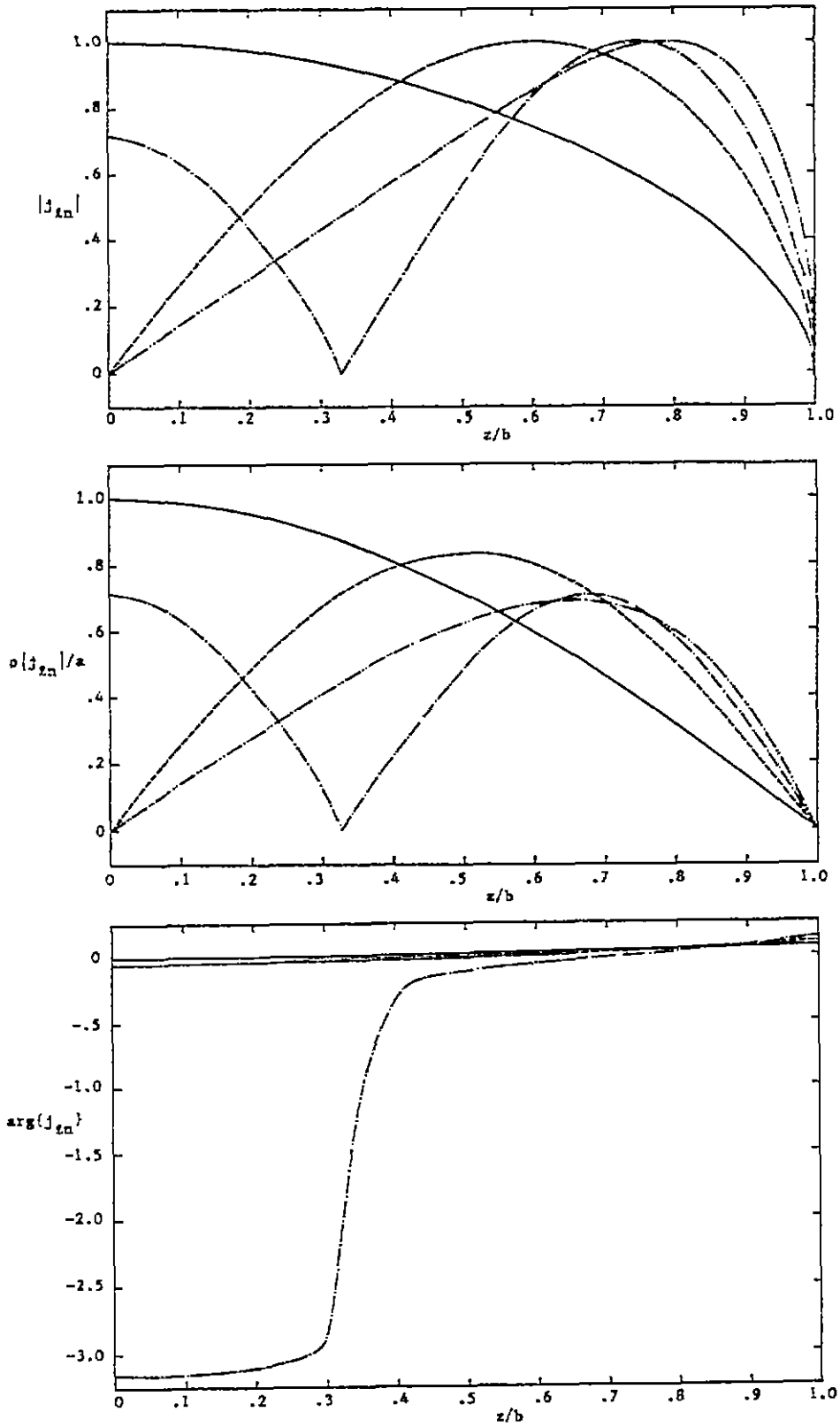

Figure 4a. The current distribution of natural modes of a prolate spheroid where a/b=.1.

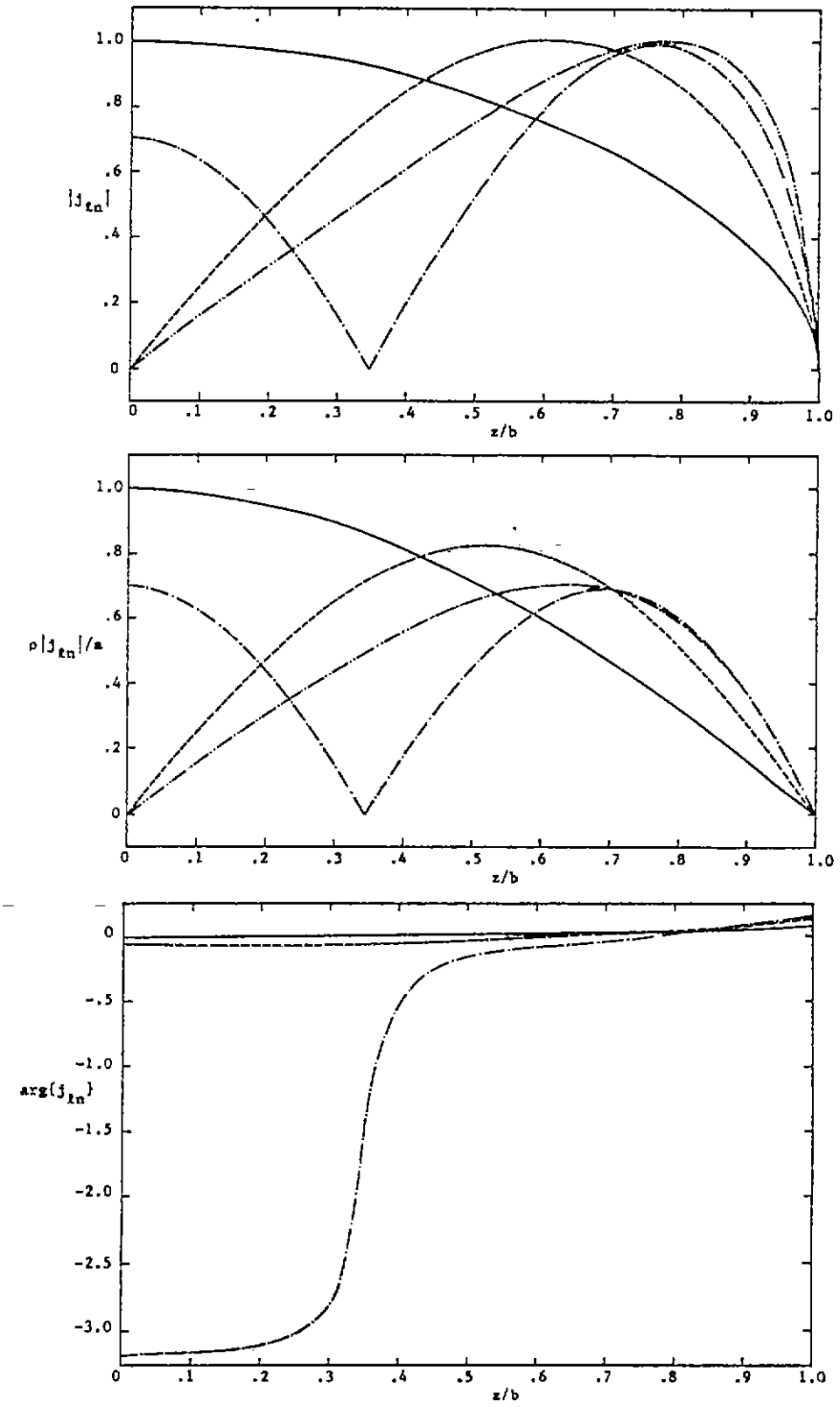

Figure 4b. The current distribution of natural modes of a prolate spheroid where a/b=.2.

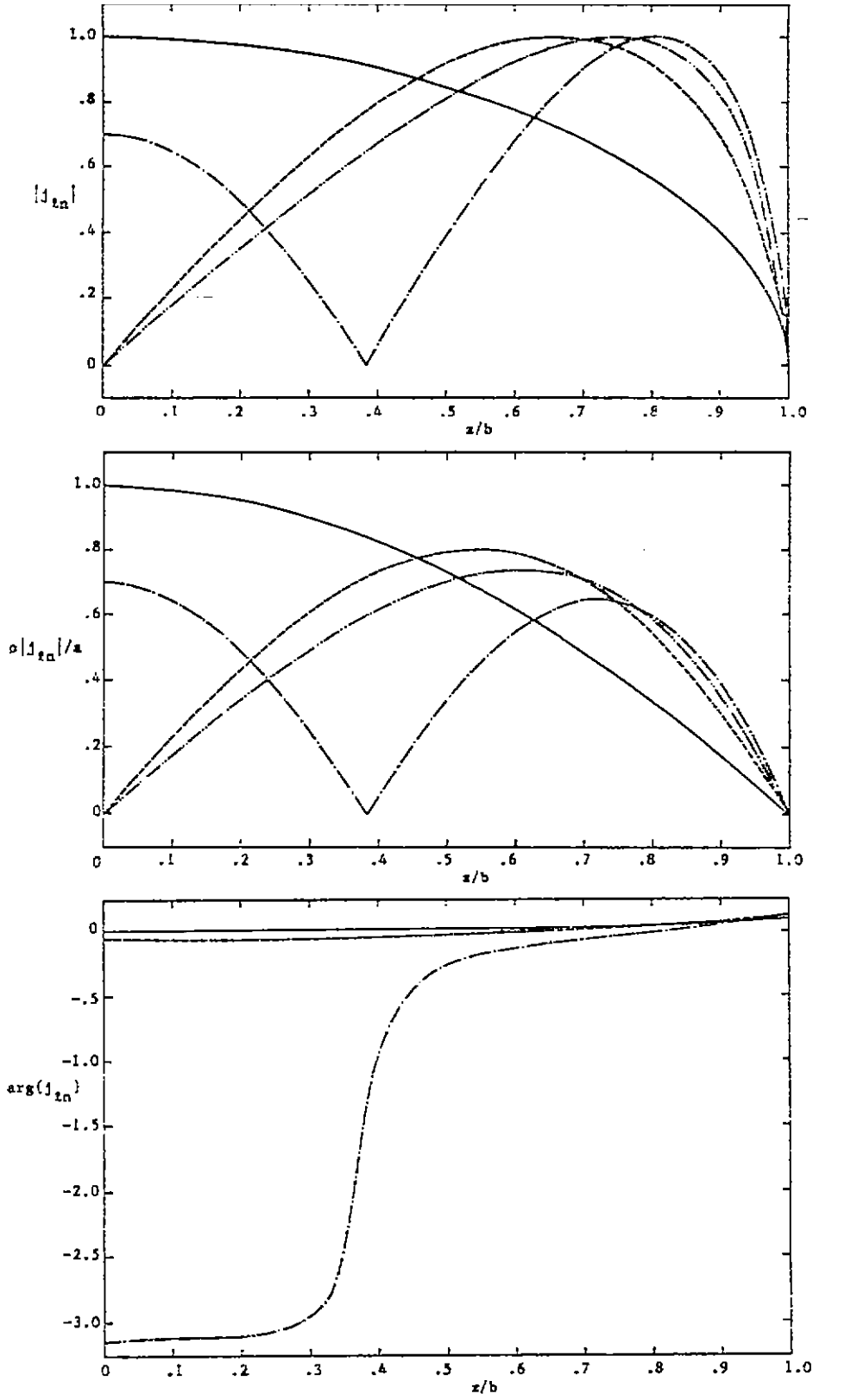

Figure 4c. The current distribution of natural modes of a prolate spheroid where a/b=.5.

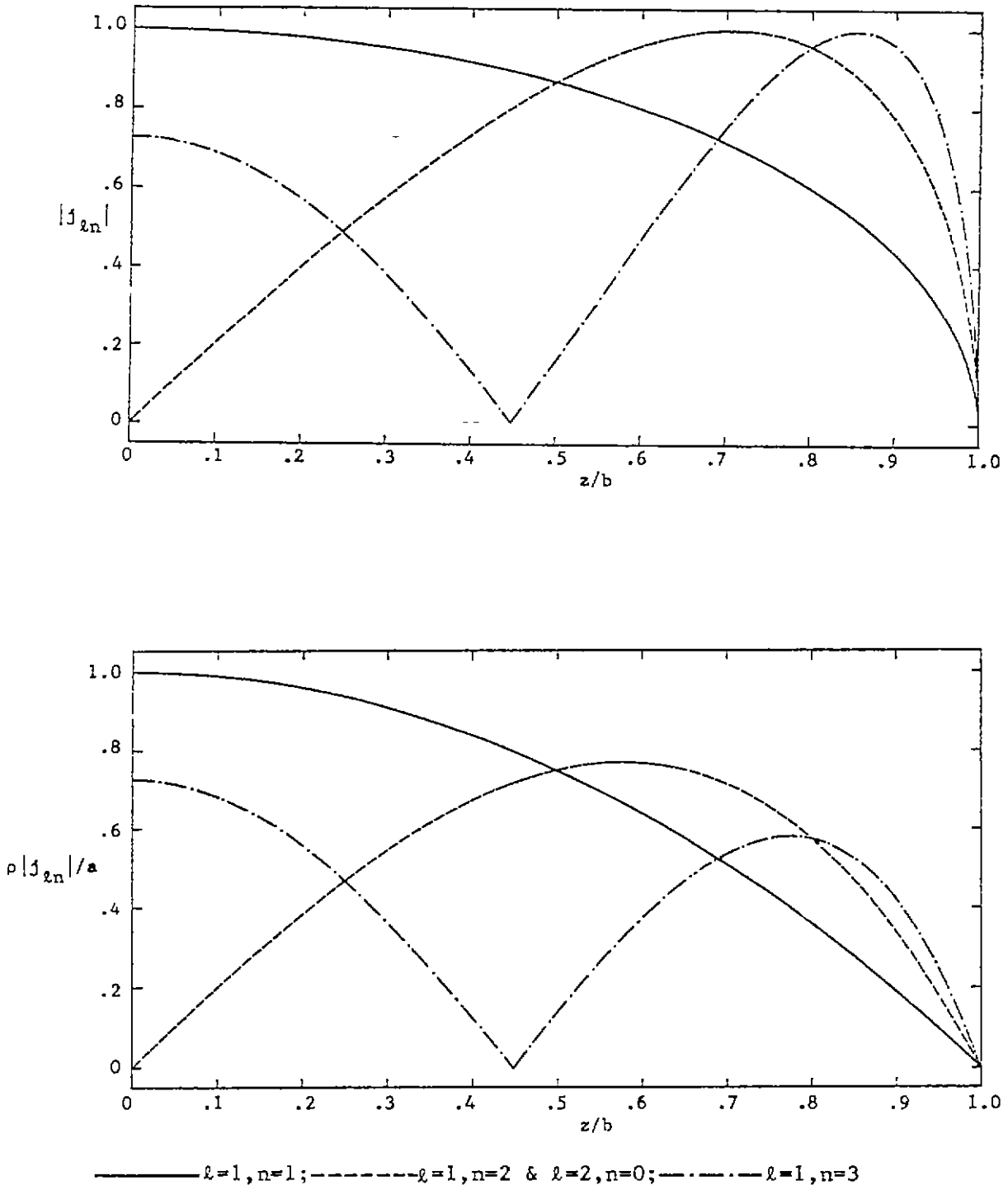

Figure 4d. The current distribution of natural modes of a prolate spheroid where a/b=1 (a sphere).

The continuity equation enables us to calculate the charge density, $q_{\ell n}$, of each mode from the current density, $j_{\ell n}$,

$$q_{\ell n} = (\rho j_{\ell n})' / (c\rho\gamma_{\ell n}). \tag{4.4}$$

Here the prime denotes differentiation with respect to ξ. The charge density of some of the natural modes is depicted in figure 5. In figure 5 we have chosen the same normalization as in figure 4, i.e., so that

$$\max_z \{|j_{\ell n}(z)|\} = 1.$$

In order to get some idea about the total charge associated with each mode we have also graphed the charge density multiplied by ρ/a. Note that the charge density is an even (odd) function with respect to the x-y-plane for modes where the index n is an even (odd) integer.

The results presented in figure 5 were obtained from the current density, $j_{\ell n}$, by performing a numerical differentiation of $\rho j_{\ell n}$ (c.f. (4.4)). Therefore, we expect the results for the charge density to be less accurate than the current density (especially close to the poles of the ellipsoid).

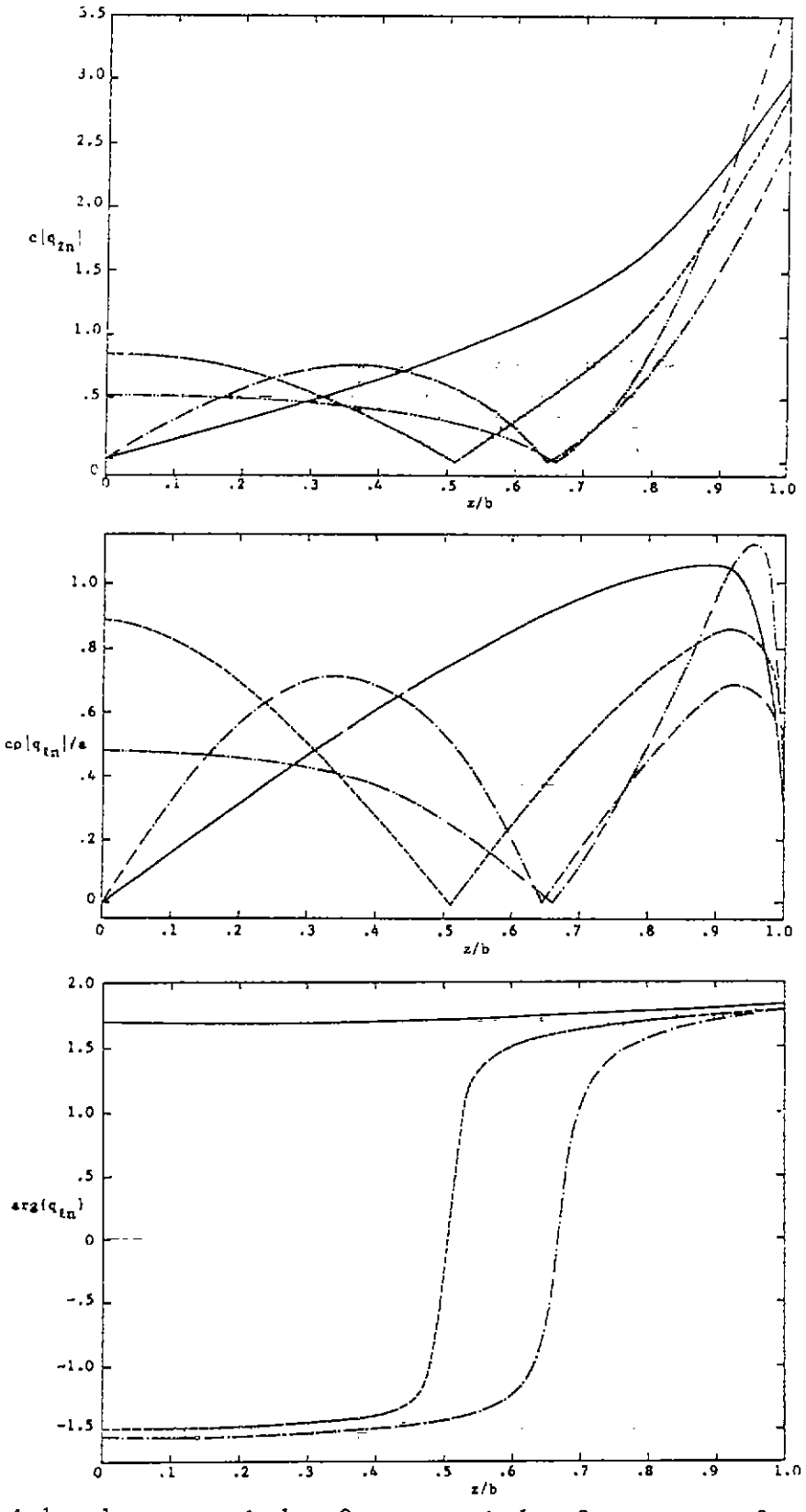

————ℓ=1, n=1; – – – – – ℓ=1, n=2; — · — · — ℓ=1, n=3; — · · — · · — ℓ=2, n=0

Figure 5a. [illegible] charge density of natural modes of a prolate spheroid [illegible]ere a/b=.1.

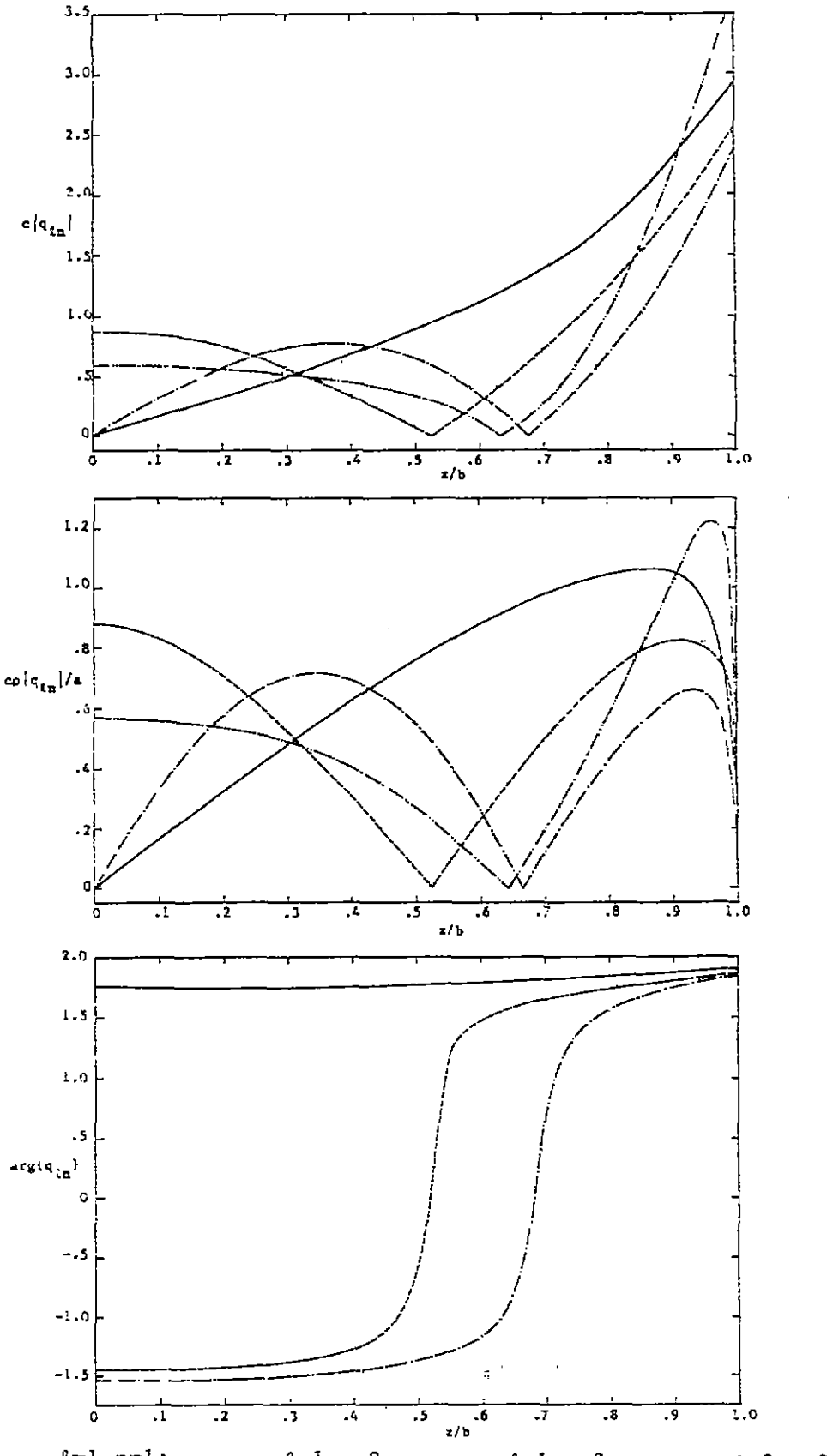

Figure 5b. The charge density of natural modes of a prolate spheroid where a/b=.2.

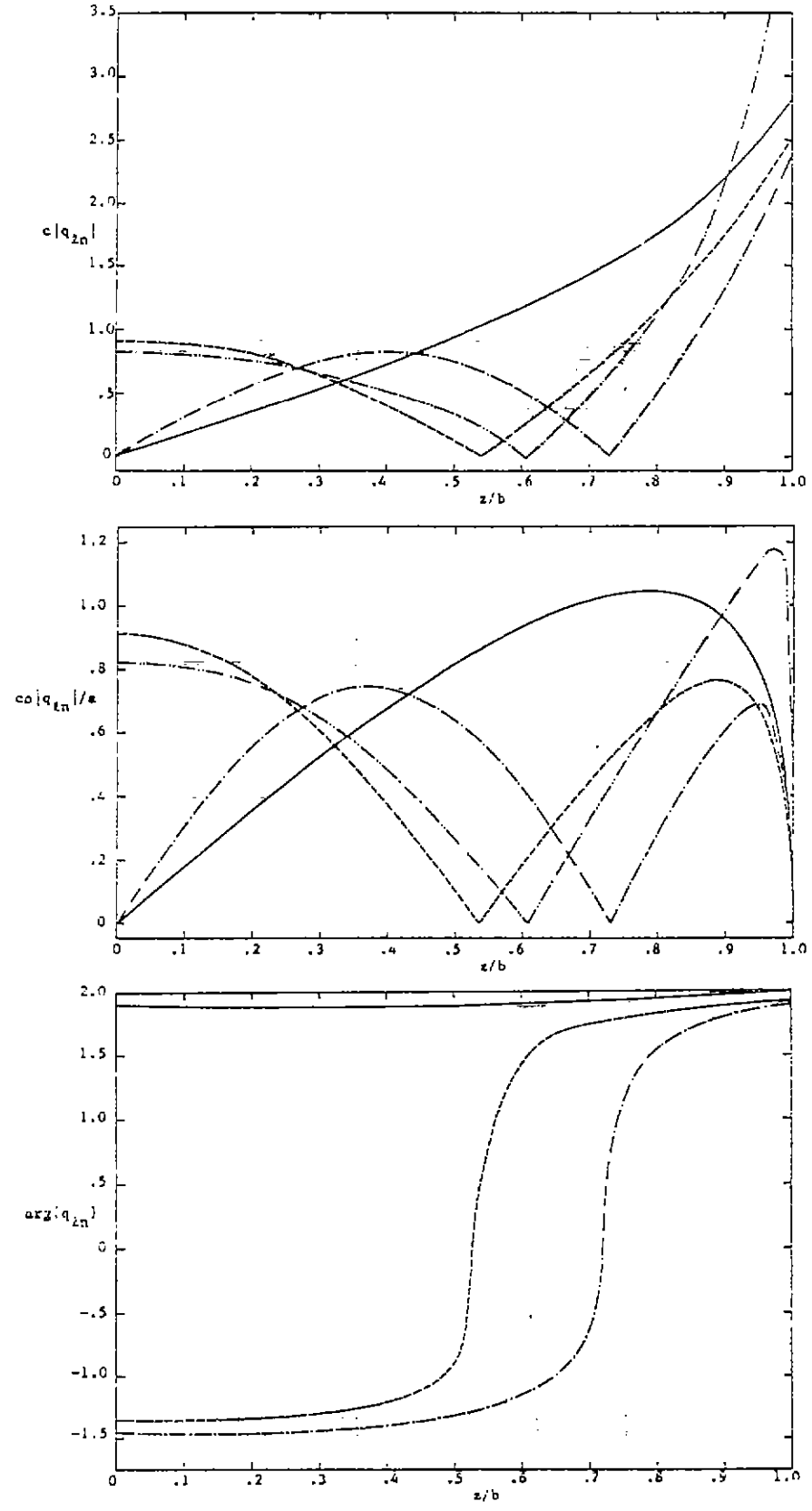

Figure 5c. The charge density of natural modes of a prolate spheroid where a/b=.5.

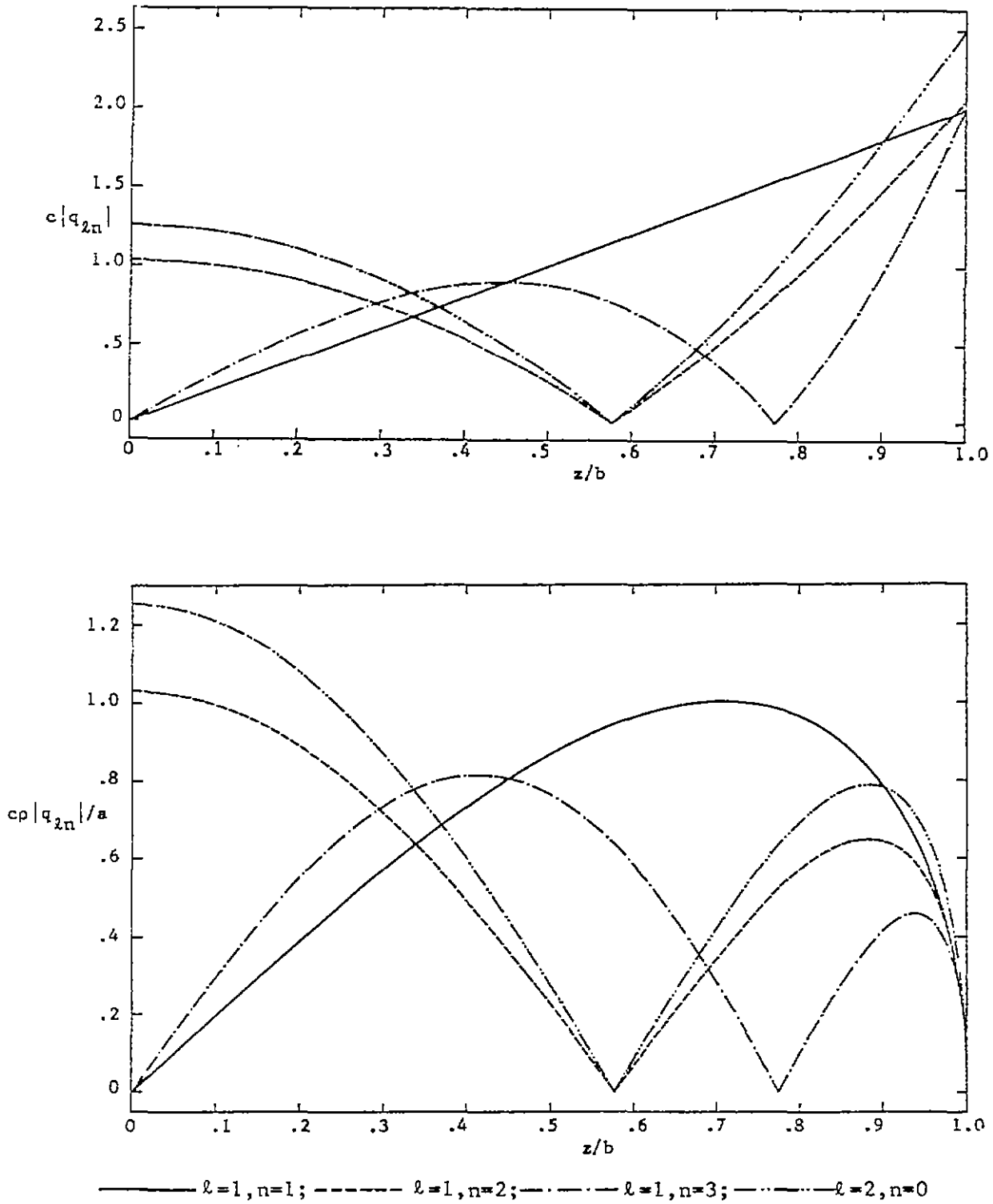

Figure 5d. The charge density of natural modes of a prolate spheroid where a/b=1 (a sphere).

B. The Coupling Coefficient

Assume that the perfectly conducting prolate spheroid is struck by an incident step-function plane wave. The angle of incidence and the polarization of the incident wave is shown in figure 6. It is desired to obtain the total induced axial current on the scatterer as a function of time and space.

The current density can be calculated from equation (3.21). Let us introduce a normalized coupling coefficient $C_{\ell n}$, defined by the expression

$$C_{\ell n} = (\underline{j}_{\ell n}^{inc}, \underline{h}_{\ell n})[(\underline{E}_{\ell n} \cdot \underline{j}_{\ell n}, \underline{h}_{\ell n})]^{-1} \tag{4.5}$$

where

$$\underline{j}_{\ell n}^{inc} = \underline{n} \times \hat{y} \exp[\gamma_{\ell n}(x \sin \theta + z \cos \theta)].$$

Here the incident wave is a step-function plane wave passing through the origin of the coordinate system at $t = 0$. The coupling coefficient as defined by equation (4.3) is independent of the normalization of the coupling vector $\underline{h}_{\ell n}^{*}$, whereas it depends on the normalization of $\underline{j}_{\ell n}$. As mentioned previously we have normalized $\underline{j}_{\ell n}$ so that

$$\max_{z}\{|\underline{j}_{\ell n}(z)|\} = 1.$$

The variation of $C_{\ell n}$ with the angle of incidence for four different modes is depicted in figure 7. We note that

(1) all coupling coefficients investigated are zero for $\theta = 0^{o}$, which means that no modes are excited where the current distribution is independent of the azimuthal angle ϕ;

(2) for $\theta = 90^{o}$ (broad side incidence) no modes are excited where the current distribution is an odd function with respect to the x-y-plane.

The only quantity that varies with the incident field is $(\underline{j}_{\ell n}^{inc}, \underline{h}_{\ell n})$. Thus, varying the angle of incidence or the shape of the incident waveform requires very little extra calculation time once the natural modes of a given structure have been determined.

Due to the normalization chosen when calculating $q_{\ell n}$, we have, of course, the same coupling coefficient, $C_{\ell n}$, for the charge density as for the current density.

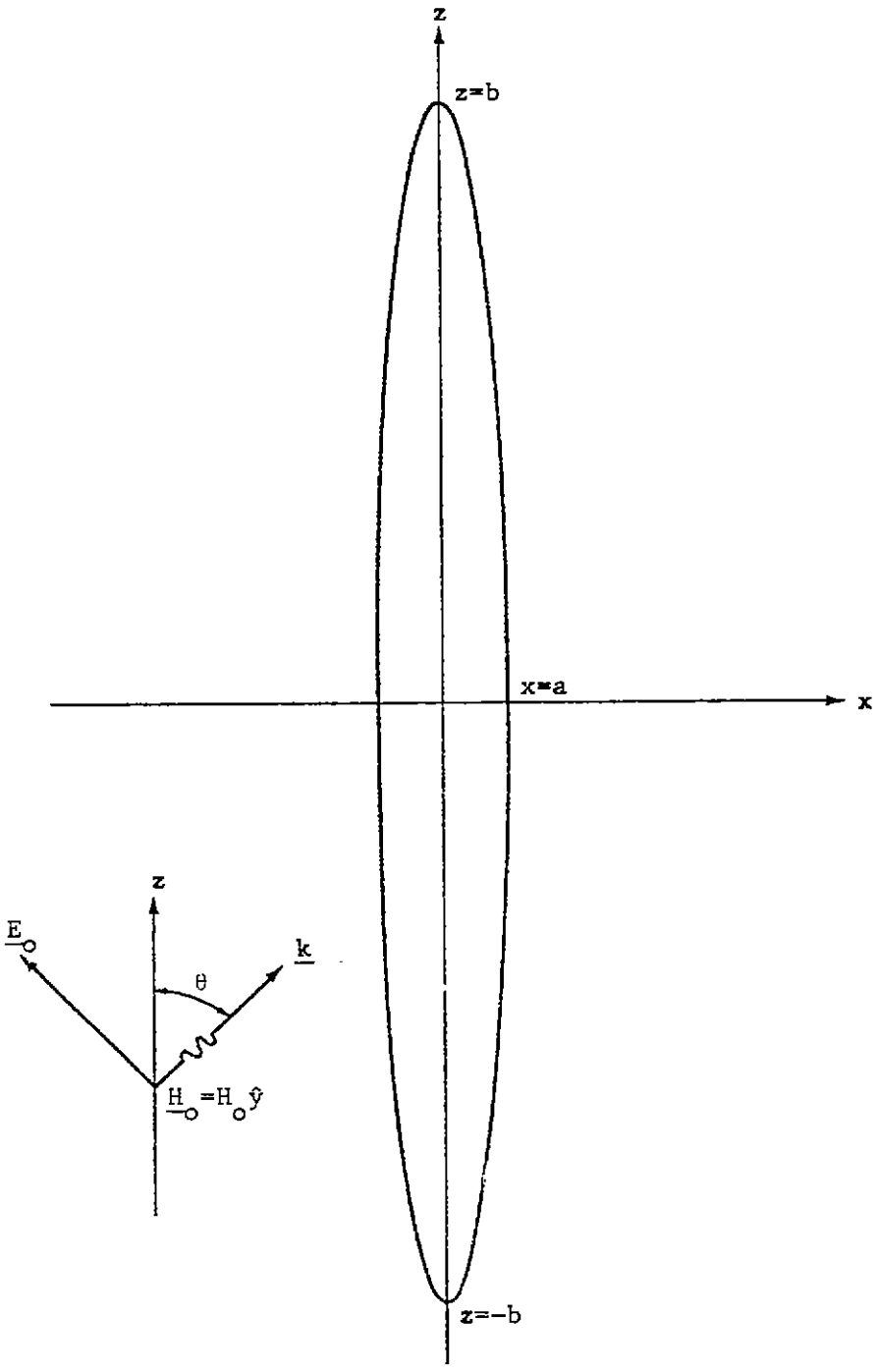

Figure 6. A plane wave impinging on a perfectly conducting, prolate spheroid.

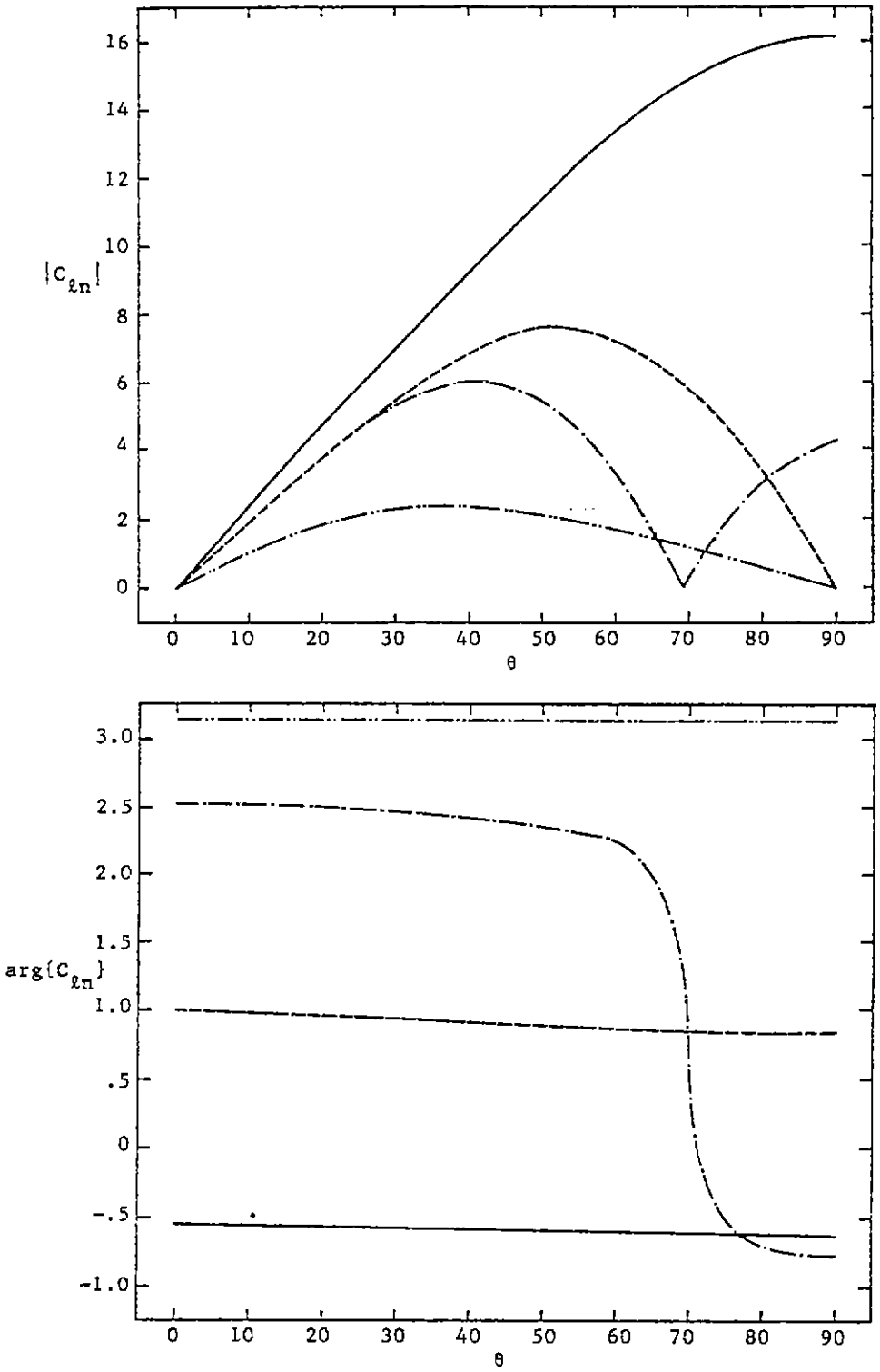

Figure 7. Variation with the angle of incidence θ of the coupling coefficient of the first three poles in the ℓ=1 layer and the first pole in the ℓ=2 layer, where a/b=.1.

C. The Time Domain Response

One representation of the current density induced by a step-function plane wave is given by equation (3.21),

$$\underline{J}(\underline{r},t) = U(ct - \eta_o) \sum_{ext} \Big[\gamma_{\ell n}^{-1} \langle \underline{n}\times\underline{H}_o \exp[\gamma_{\ell n}(\eta' - \eta_o)], \underline{h}_{\ell n} \rangle$$

$$[\langle \underline{\underline{B}}_{\ell n} \cdot \underline{j}_{\ell n}, \underline{h}_{\ell n} \rangle]^{-1} \underline{j}_{\ell n} \exp[\gamma_{\ell n}(\eta_o - ct)] \Big] \qquad (4.6)$$

Another representation of $\underline{J}(\underline{r},t)$ is given by[9,11]

$$\underline{J}(\underline{r},t) = U(ct - \eta) \sum_{ext} \Big[\gamma_{\ell n}^{-1} \langle \underline{n}\times\underline{H}_o \exp(\gamma_{\ell n}\eta') U(ct - \eta'), \underline{h}_{\ell n} \rangle$$

$$[\langle \underline{\underline{B}}_{\ell n} \cdot \underline{j}_{\ell n}, \underline{h}_{\ell n} \rangle]^{-1} \underline{j}_{\ell n} \exp(-\gamma_{\ell n} ct) \Big] \qquad (4.7)$$

For $t < t_o$ both (4.6) and (4.7) give $\underline{J}(\underline{r},t) \equiv 0$. Here t_o is the time when the wavefront first hits the scattering body,

$$t_o = c^{-1} \min_{\underline{r}\in S} \{\hat{e}\cdot\underline{r}\}.$$

The representations (4.6) and (4.7) are both sums of damped sinusoidal oscillations for $t > t_1$. Here t_1 is the time when the wavefront just passes the scattering body,

$$t_1 = c^{-1} \max_{\underline{r}\in S} \{\hat{e}\cdot\underline{r}\}.$$

For intermediate times, $t_o < t < t_1$, (4.6) consists of a sum of damped sinusoidal oscillations whereas (4.7) does not. The representation (4.6) is numerically unstable for $t_o < t < t_1$ whereas (4.7) converges for all times.

From the numerical point of view it is important to know how to truncate the sum (4.7) and still maintain a given accuracy. Therefore, we have numerically studied the convergence of the sum (4.7) as the number of poles is increased. The results of this study are presented in figures 8 through 13 in form of graphs of the time history of the induced total current on the spheroid at z/b = -.5, 0, .5

with the number of poles and the angle of incidence as parameters. In figures 8 through 13 we have introduced a normalized axial current, $I = I(z,t)$, defined by

$$I(z,t) = 2\pi\rho J(z,t)/(bH_o).$$

Throughout this time-domain study the shape of the spheroid remained fixed with $a/b = .1$. The time scale is chosen so that $t = 0$ when the wavefront first hits the scattering body.

The time domain current response as shown in figures 8 through 13 has been obtained by combining the contributions from poles in the second quadrant with the contributions from their complex conjugate poles, i.e., poles in the third quadrant. The accumulated contribution from the first nine poles in the $\ell = 1$ layer is considered together with a solution, labeled "all poles", which consists of 13 poles from the $\ell = 1$ layer, 7 poles from the $\ell = 2$ layer and 7 poles from the $\ell = 3$ layer. A comparison with the conventional method of first solving the integral equation along the ik axis and then performing a numerical inverse Fourier transform was also made. Excellent agreement was found and the curves labeled "all poles" also refer to the results obtained by this conventional method.

From these curves we can make the following observations:

(1) There is no contribution to $I(0,t)$ from modes where the index n is an even integer. This follows from the fact that the current distribution is an odd function with respect to the x-y-plane for modes where n is an even integer.

(2) For $t > 12b/c$ only the $\ell = 1$, $n = \pm 1$ poles are needed to accurately describe the induced current.

(3) For $t > 5b/c$ only the first five poles in the $\ell = 1$ layer are needed to accurately describe the induced current.

(4) Poles in the $\ell \geq 2$ layer only contribute appreciably for $t < b/c$.

(5) The effect of the causality is clearly indicated.

(6) The relative importance of the higher order modes as compared to the fundamental mode is a decreasing function of θ. This effect can also be seen in the graph of the coupling coefficients (figure 7).

The ϕ-independent part of the charge density, $\sigma(\xi,t)$, at an arbitrary point on the scattering body can be calculated from the ϕ-independent part of the

induced current density, $\underline{J}(\xi,t)$, by using the continuity equation,

$$\sigma(\xi,t) = -\int_0^t \nabla\cdot\underline{J}(\xi,t')dt'. \tag{4.8}$$

At the "north pole" and the "south pole" of the prolate spheroid (the points A and B in figure 2) equation (4.7) can be integrated to

$$\begin{aligned}\sigma(\xi_o,t) &= -\lim_{\xi\to\xi_o}\left[\int_0^t 2\pi\rho J_\xi(\xi,t')dt'/[S(\xi_o) - S(\xi)]\right]\\ \sigma(0,t) &= \lim_{\xi\to 0}\left[\int_0^t 2\pi\rho J_\xi(\xi,t')dt'/S(\xi)\right]\end{aligned} \tag{4.9}$$

where

$$S(\xi) = \int_0^\xi 2\pi\rho(\xi')d\xi'.$$

When calculating the quantities $\sigma(\xi_o,t)$ and $\sigma(0,t)$ we used the representation (4.7) for $J_\xi(\xi,t)$. A numerical integration, based on the trapezoid formula, was used for $0 < t < t_1$ whereas for $t > t_1$ the sum (4.7) was integrated analytically termwise and summed numerically.

In figure 14 we have graphed the time history of the induced charge density at $z/b = \pm 1$ for $\theta = 30^\circ$, 60°, 90°. The normalized quantity $q = q(z,t)$ used in figure 14 is defined by

$$q(z,t) = \sigma(\xi,t)/(\epsilon_o E_o)$$

where E_o is the strength of the incident electric field. The convergence of the charge density as the number of poles is increased is studied in figure 15. It can be observed that the convergence of the charge density as a function of the number of poles is somewhat faster than the current density.

The following table summarizes the different combinations of parameters for which numerical data are presented in figures 8 through 15.

Figure	Quantity	θ	Time interval	Number of poles
8	current	30°	$0 \leq ct/b \leq 12$	1, 2, 3, 4, 5, all
9	current	30°	$0 \leq ct/b \leq 5$	5, 6, 7, 8, 9, all
10	current	60°	$0 \leq ct/b \leq 12$	1, 2, 3, 4, 5, all
11	current	60°	$0 \leq ct/b \leq 5$	5, 6, 7, 8, 9, all
12	current	90°	$0 \leq ct/b \leq 12$	1, 2, 3, 4, 5, all
13	current	90°	$0 \leq ct/b \leq 5$	5, 6, 7, 8, 9, all
14	charge	30°, 60°, 90°	$0 \leq ct/b \leq 12$	all
15	charge	60°	$0 \leq ct/b \leq 12$	1, 2, 3, 4, 5, all

Note that

(1) the incident field is a step-function plane wave;

(2) the minor-axis-to-major-axis ratio of the prolate spheroid is .1;

(3) $t = 0$ when the wavefront first hits the scattering body;

(4) all data in figures 8 through 13 refer to the total induced current at $z/b = -.5, 0, .5$;

(5) all data in figures, 14 and 15 refer to the induced charge density at $z/b = \pm 1$.

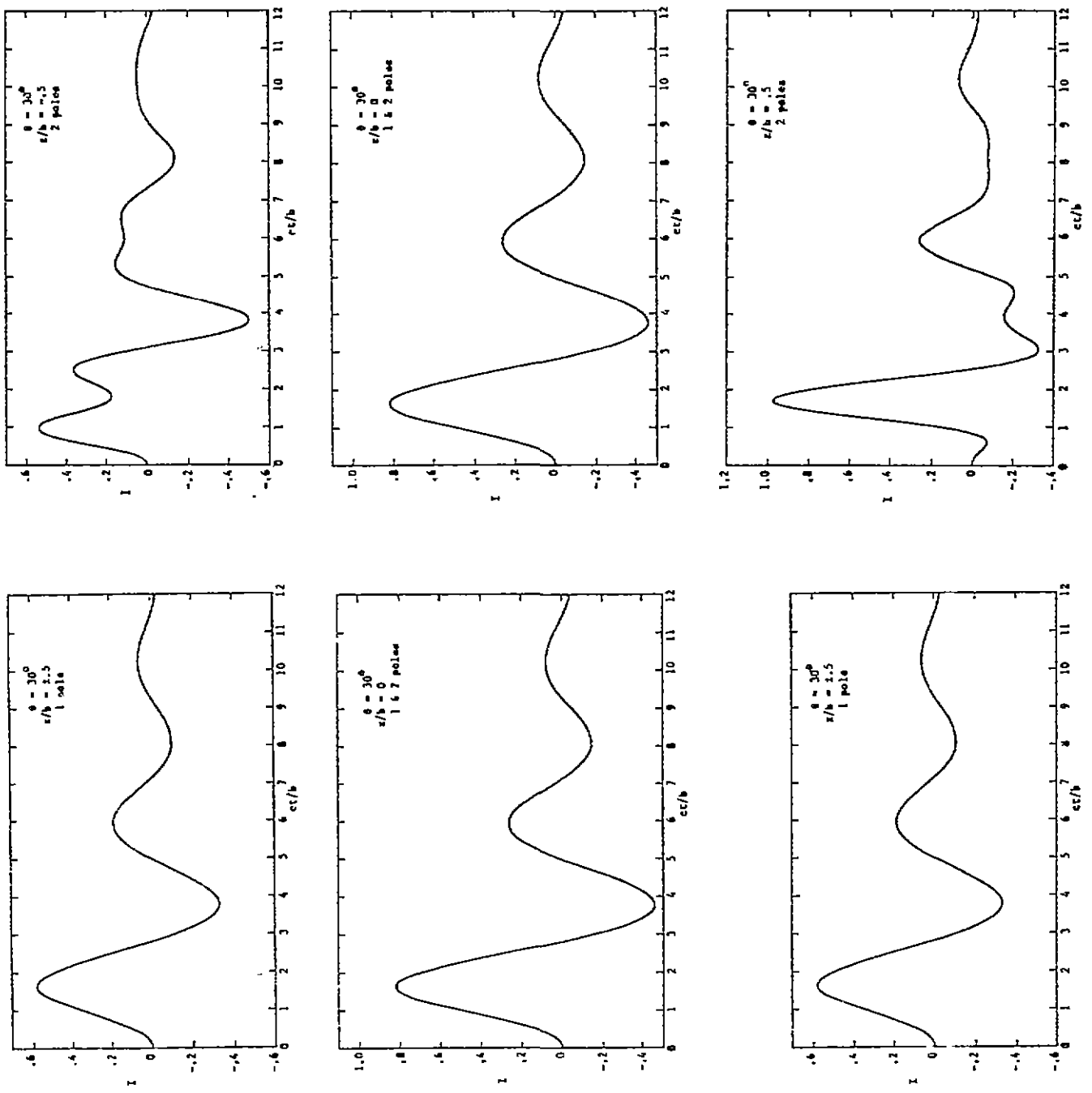

Figure 8a. The time response of the current at three points on a prolate spheroid as a function of the number of poles when the angle of incidence $\theta=30^{o}$.

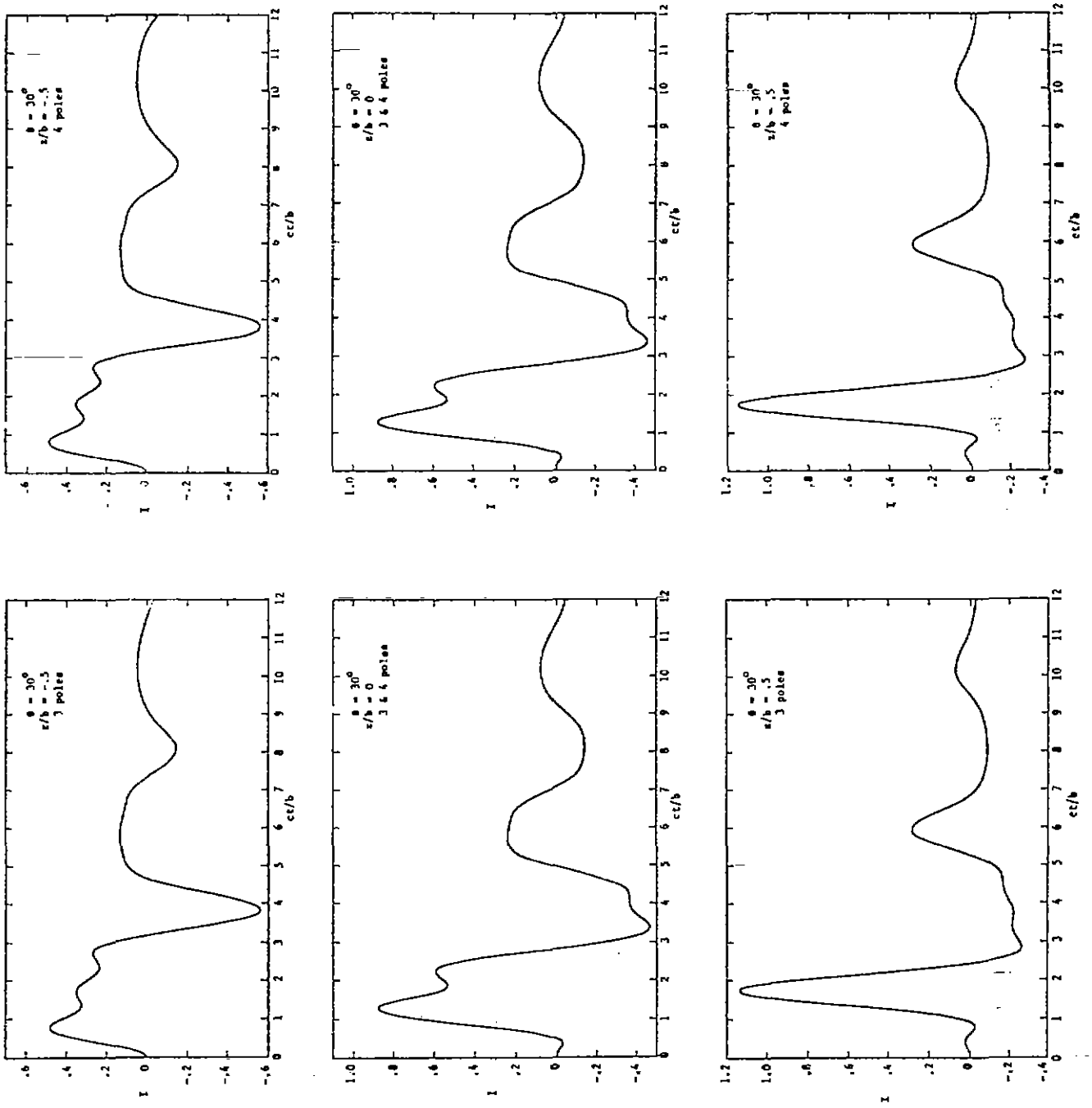

Figure 8b. The time response of the current at three points on a prolate spheroid as a function of the number of poles when the angle of incidence $\theta=30^{\circ}$.

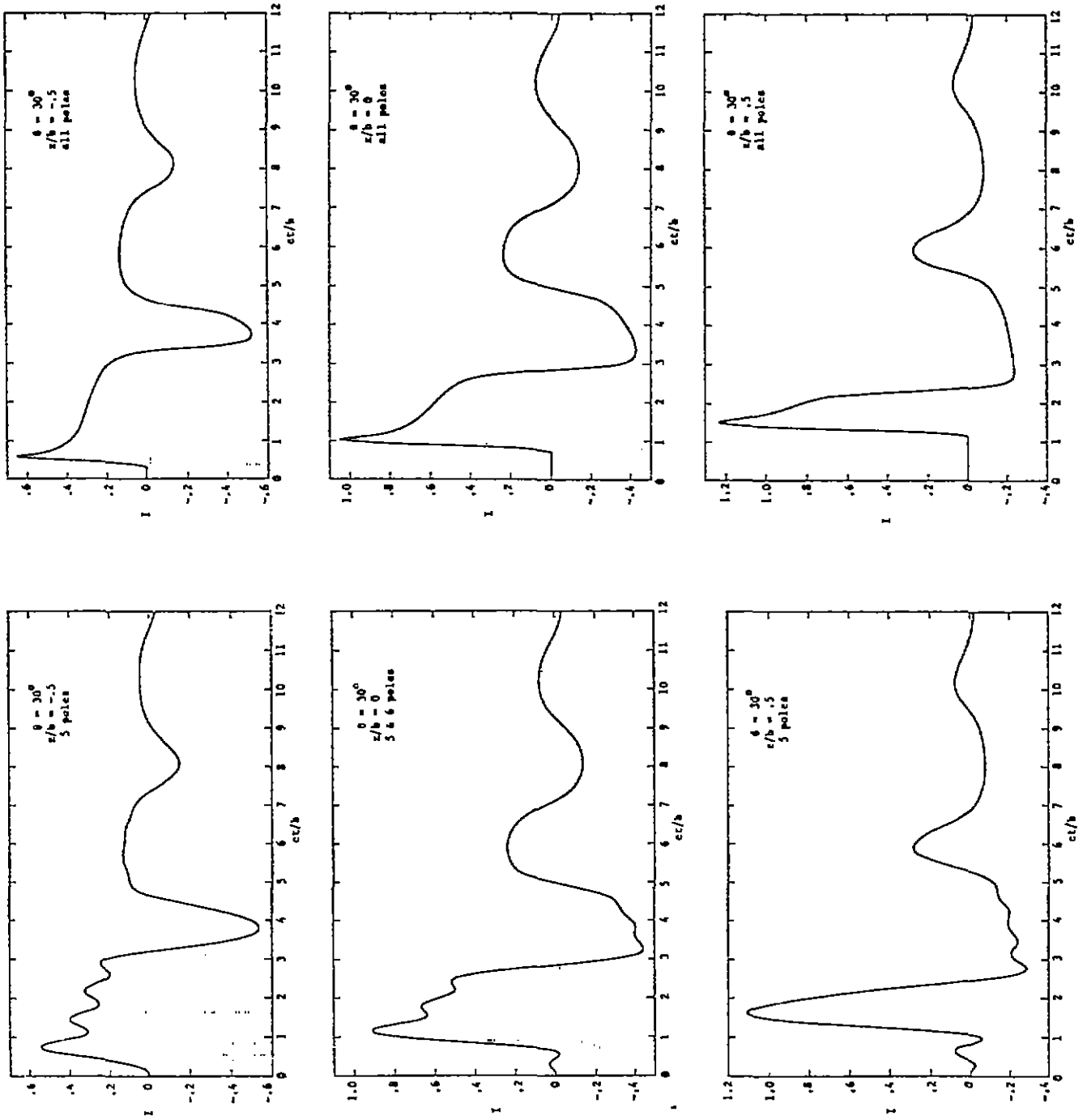

Figure 8c. The time response of the current at three points on a prolate spheroid as a function of the number of poles when the angle of incidence θ=30°.

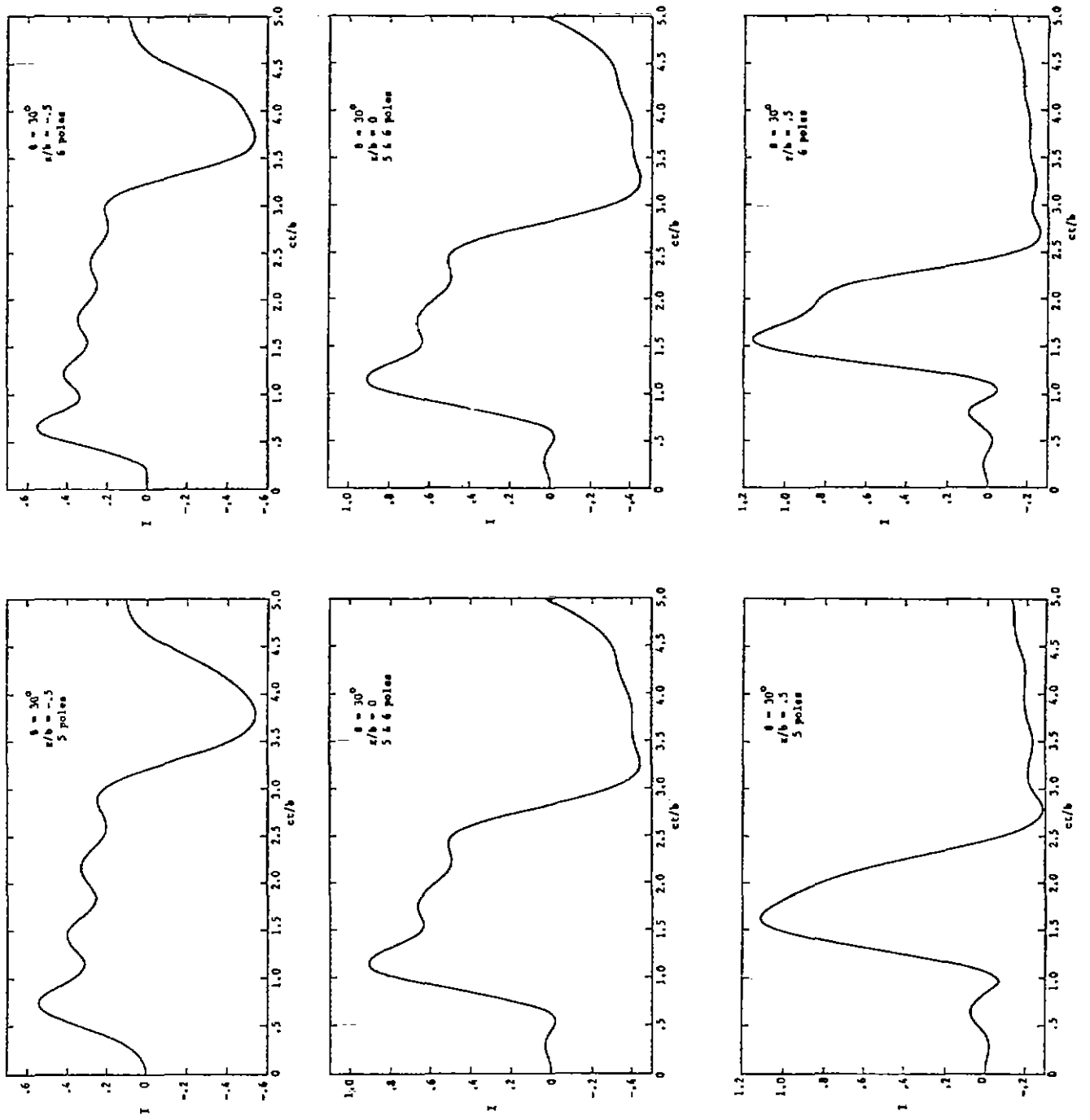

Figure 9a. The time response of the current at three points on a prolate spheroid as a function of the number of poles when the angle of incidence $\theta=30^{\circ}$.

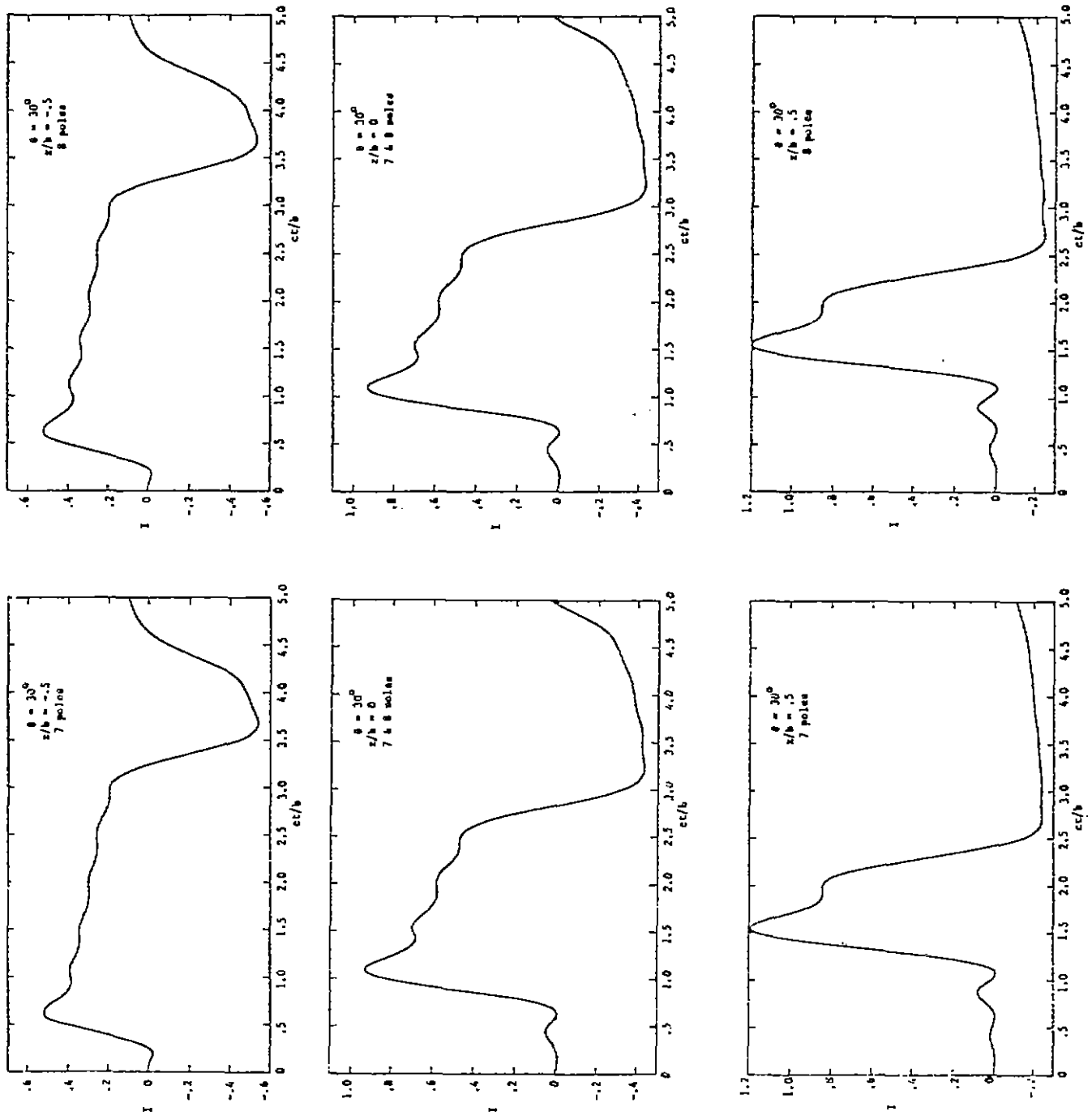

Figure 9b. The time response of the current at three points on a prolate spheroid as a function of the number of poles when the angle of incidence $\theta=30^{\circ}$.

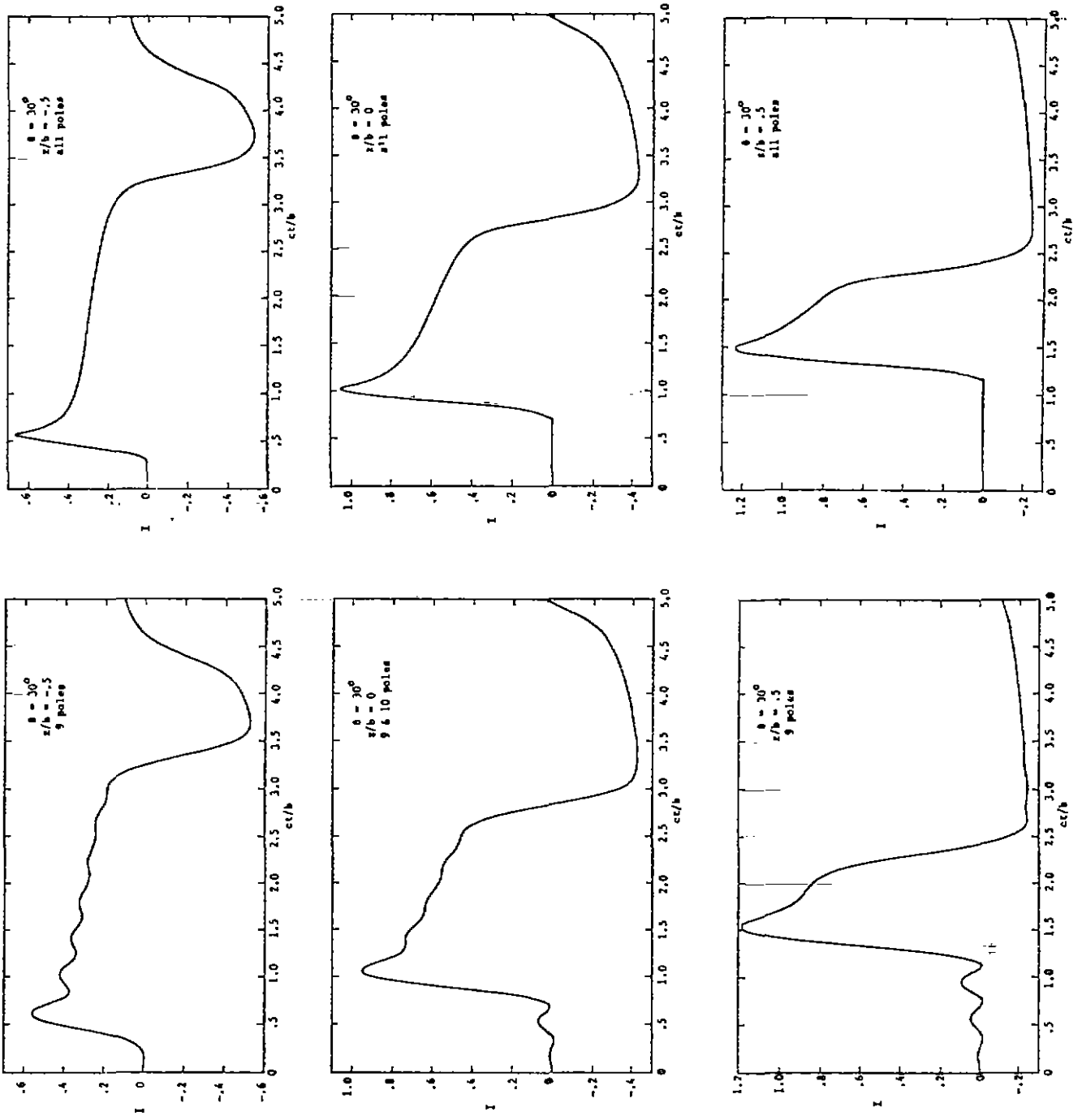

Figure 9c. The time response of the current at three points on a prolate spheroid as a function of the number of poles when the angle of incidence $\theta=30^{\circ}$.

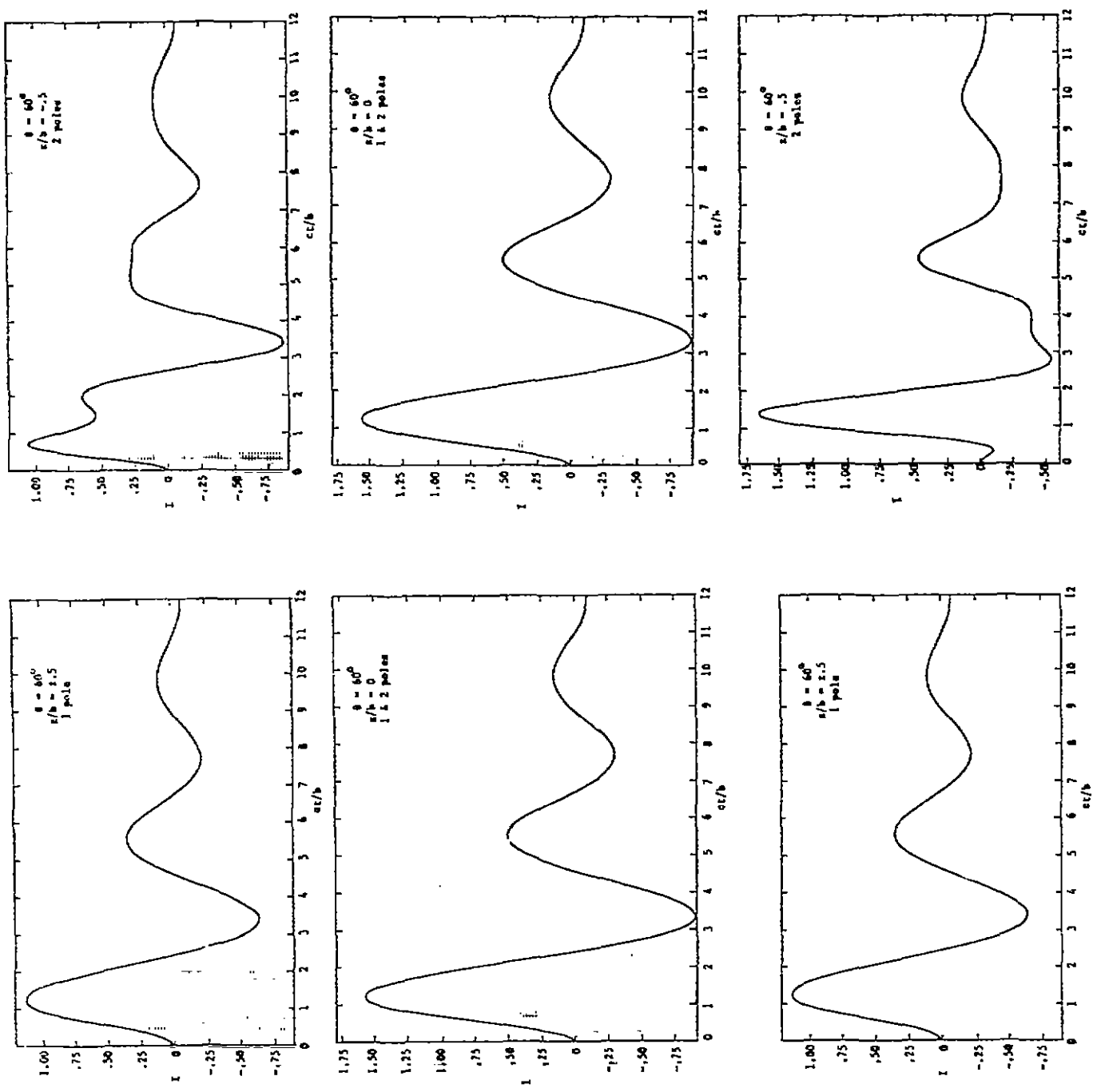

Figure 10a. The time response of the current at three points on a prolate spheroid as a function of the number of poles when the angle of incidence $\theta=60^{\circ}$.

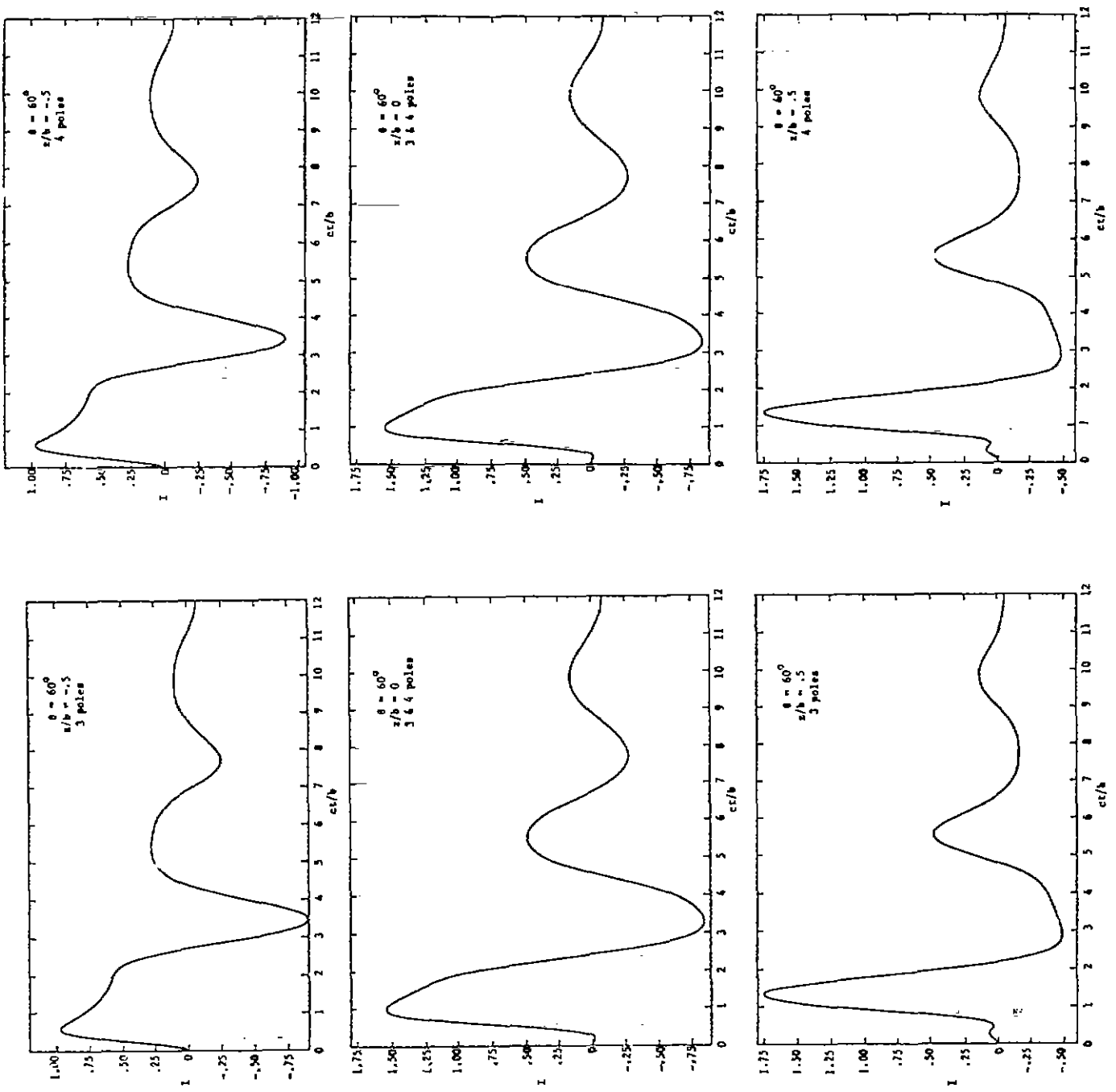

Figure 10b. The time response of the current at three points on a prolate spheroid as a function of the number of poles when the angle of incidence $\theta=60^{\circ}$.

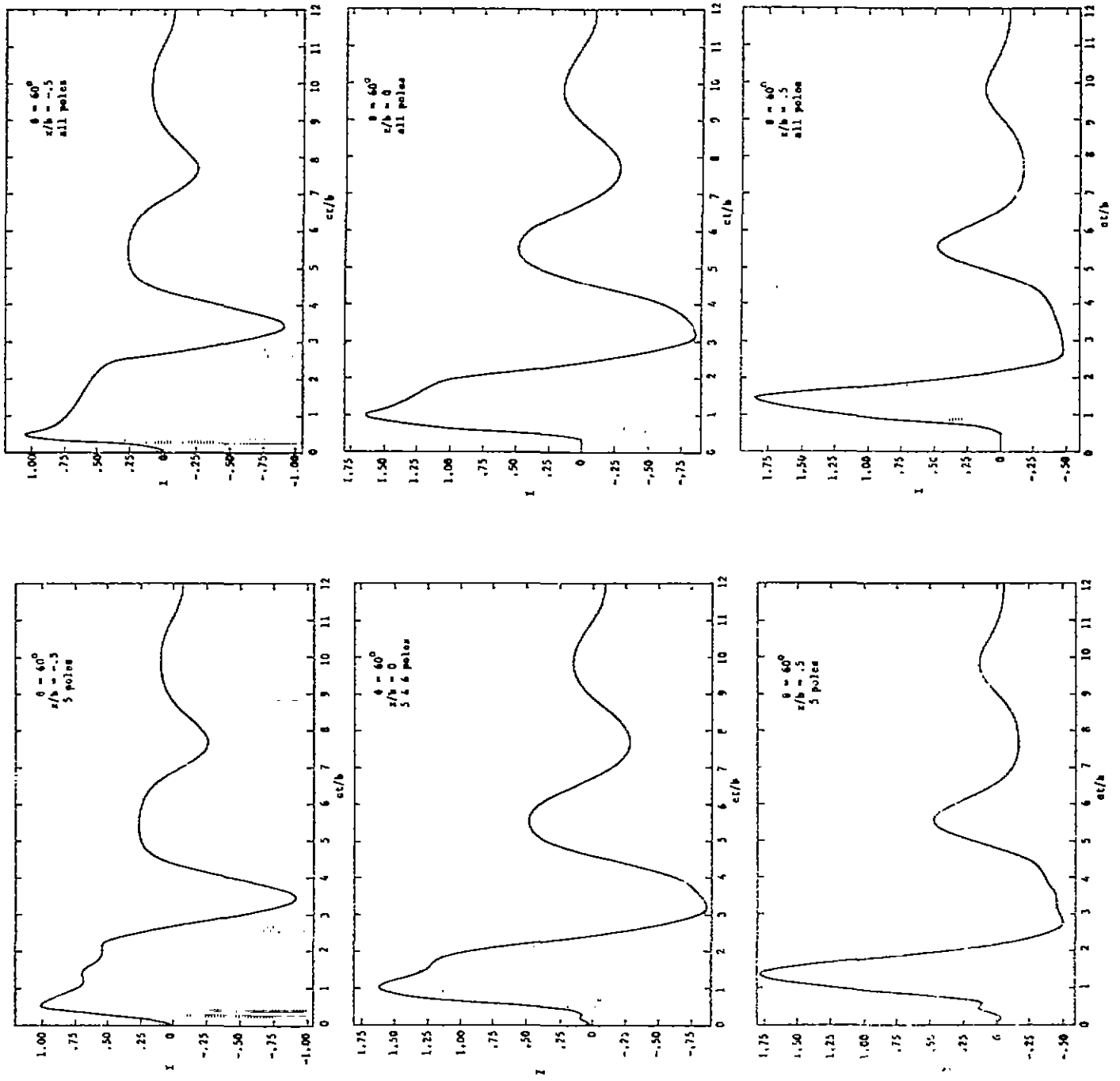

Figure10c. The time response of the current at three points on a prolate spheroid as a function of the number of poles when the angle of incidence $\theta=60^{\circ}$.

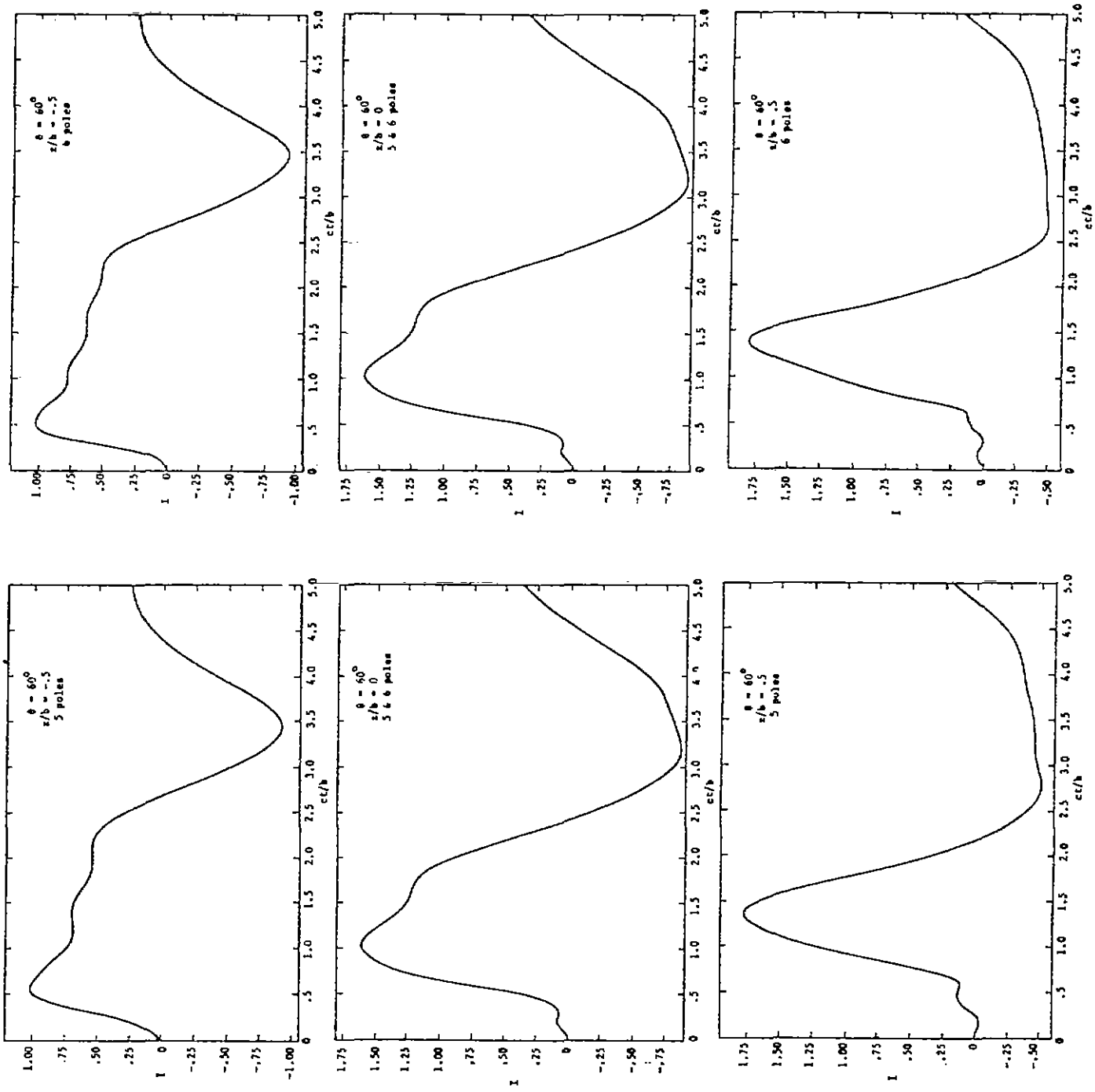

Figure 11a. The time response of the current at three points on a prolate spheroid as a function of the number of poles when the angle of incidence $\theta=60^{\circ}$.

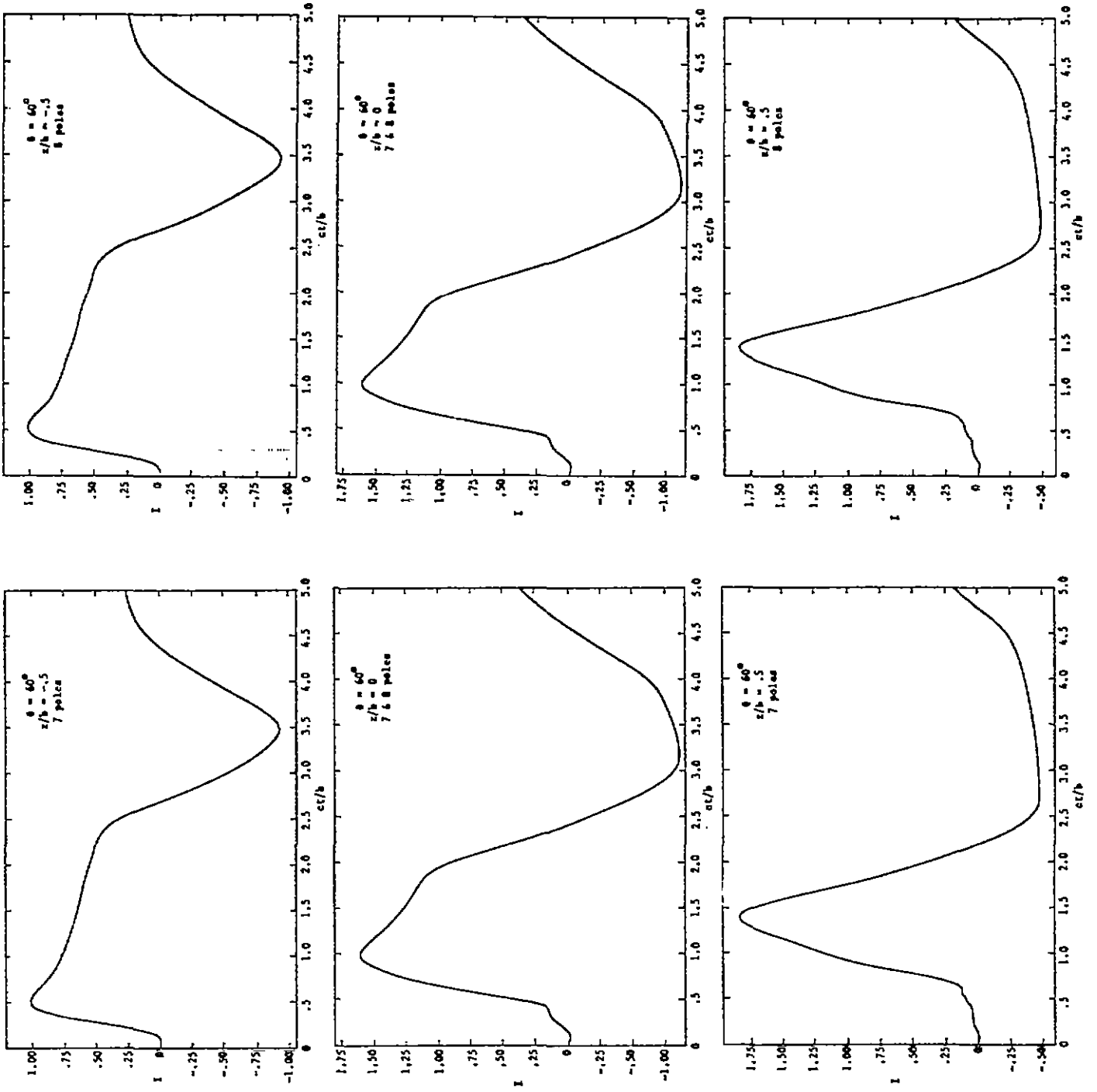

Figure 11b. The time response of the current at three points on a prolate spheroid as a function of the number of poles when the angle of incidence $\theta=60^{o}$.

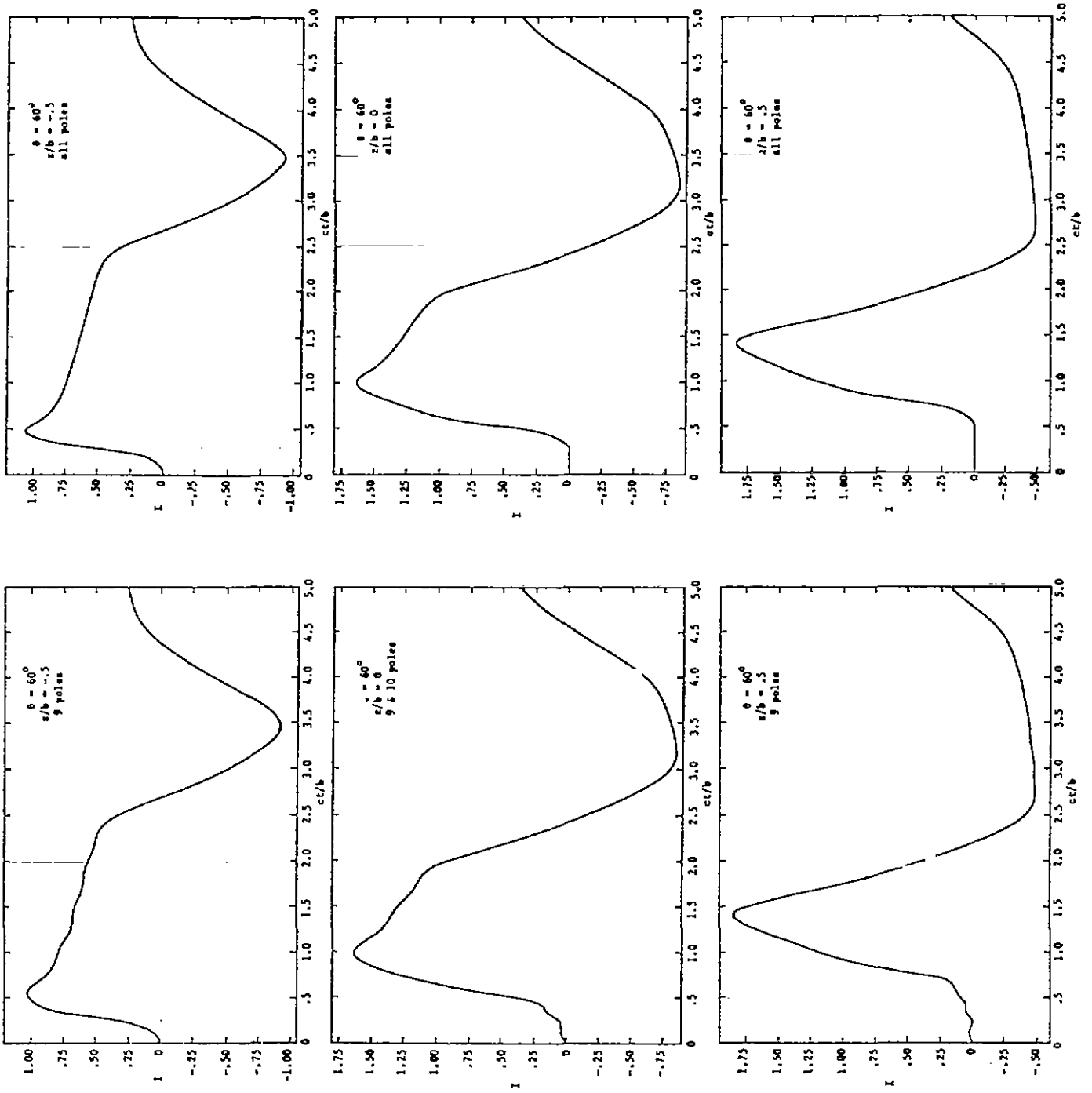

Figure 11c. The time response of the current at three points on a prolate spheroid as a function of the number of poles when the angle of incidence $\theta=60^{\circ}$.

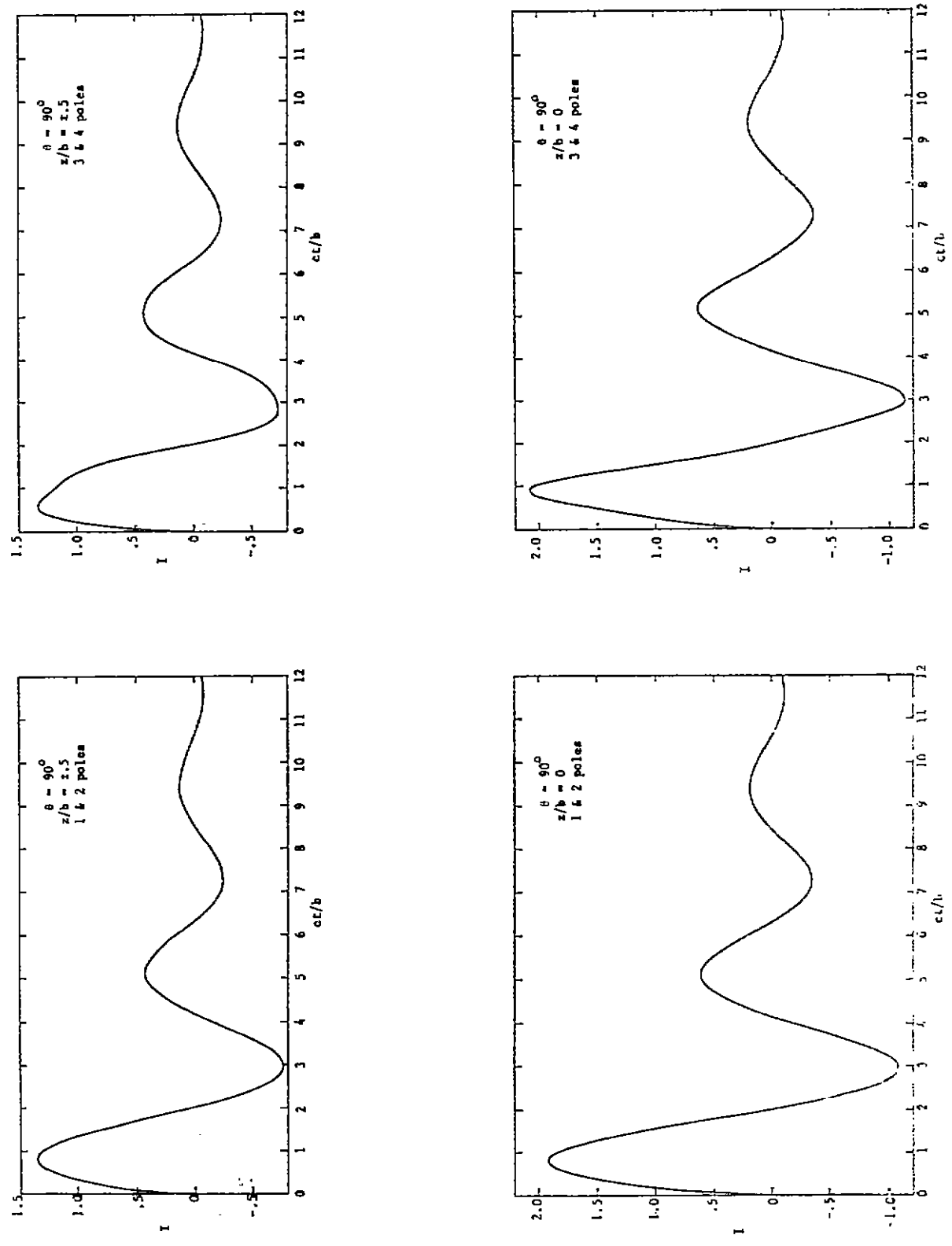

Figure 12a. The time response of the current at three points on a prolate spheroid as a function of the number of poles when the angle of incidence θ=90°.

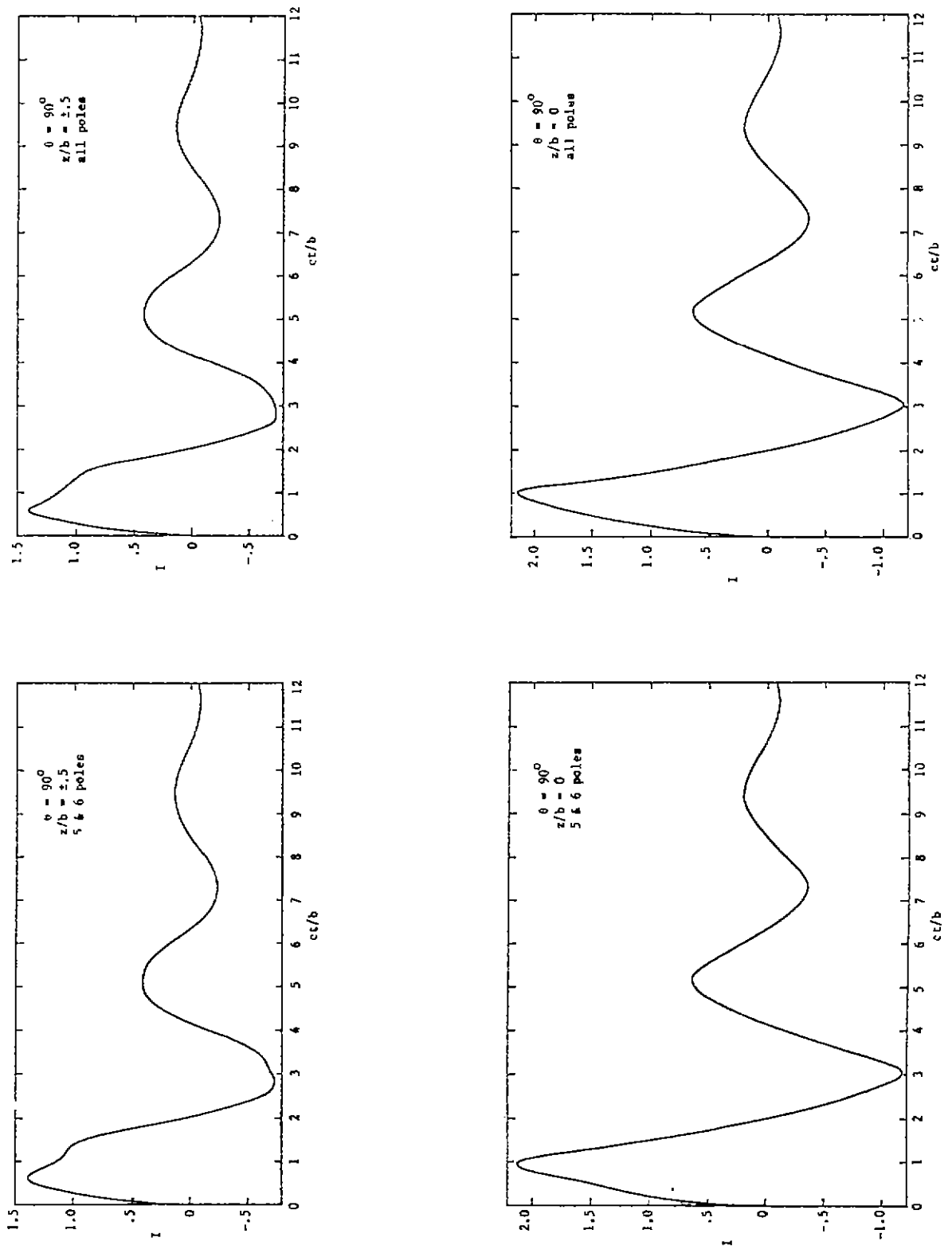

Figure 12b. The time response of the current at three points on a prolate spheroid as a function of the number of poles when the angle of incidence $\theta=90^{o}$.

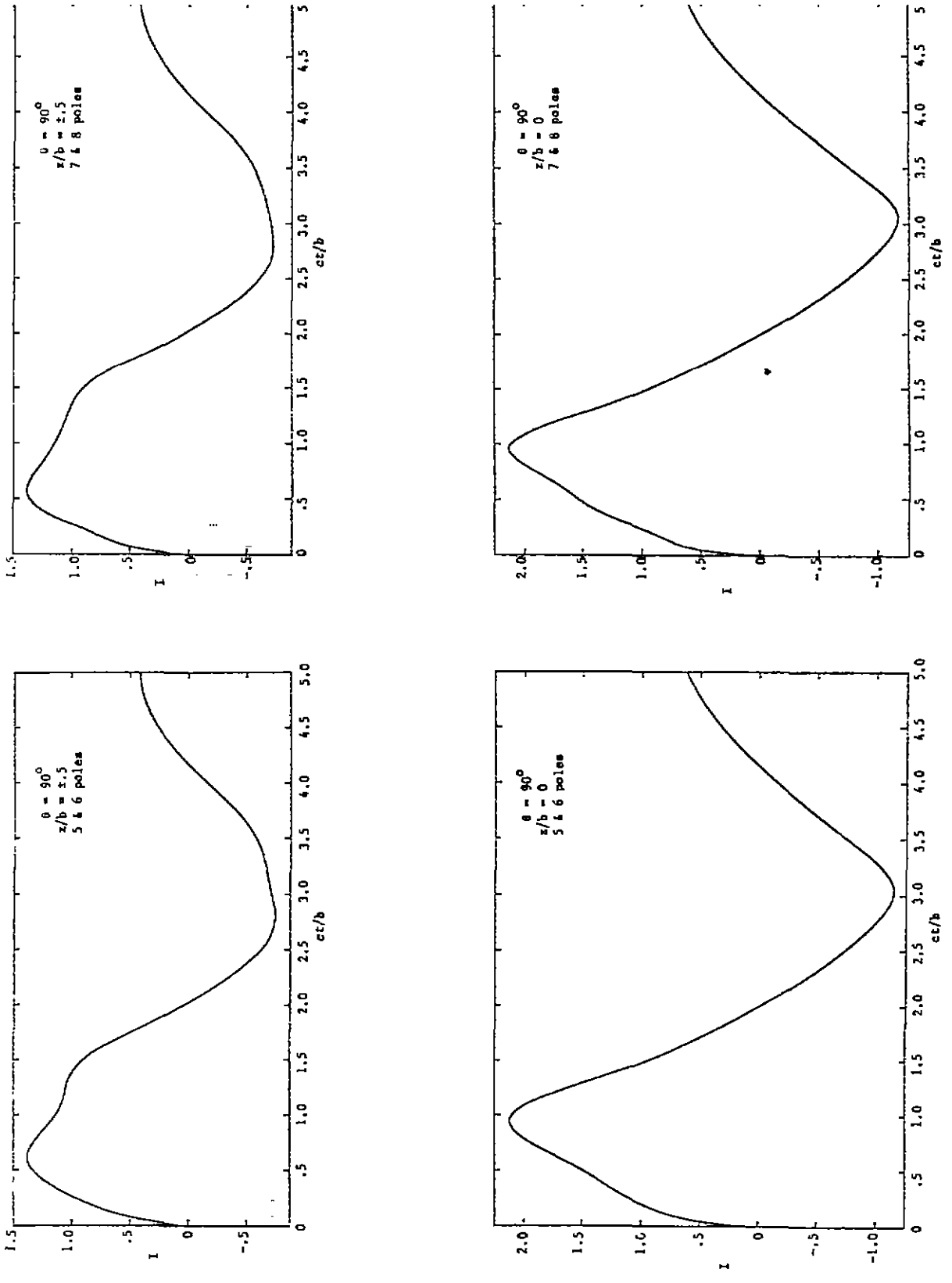

Figure 13a. The time response of the current at three points on a prolate spheroid as a function of the number of poles when the angle of incidence $\theta=90^{\circ}$.

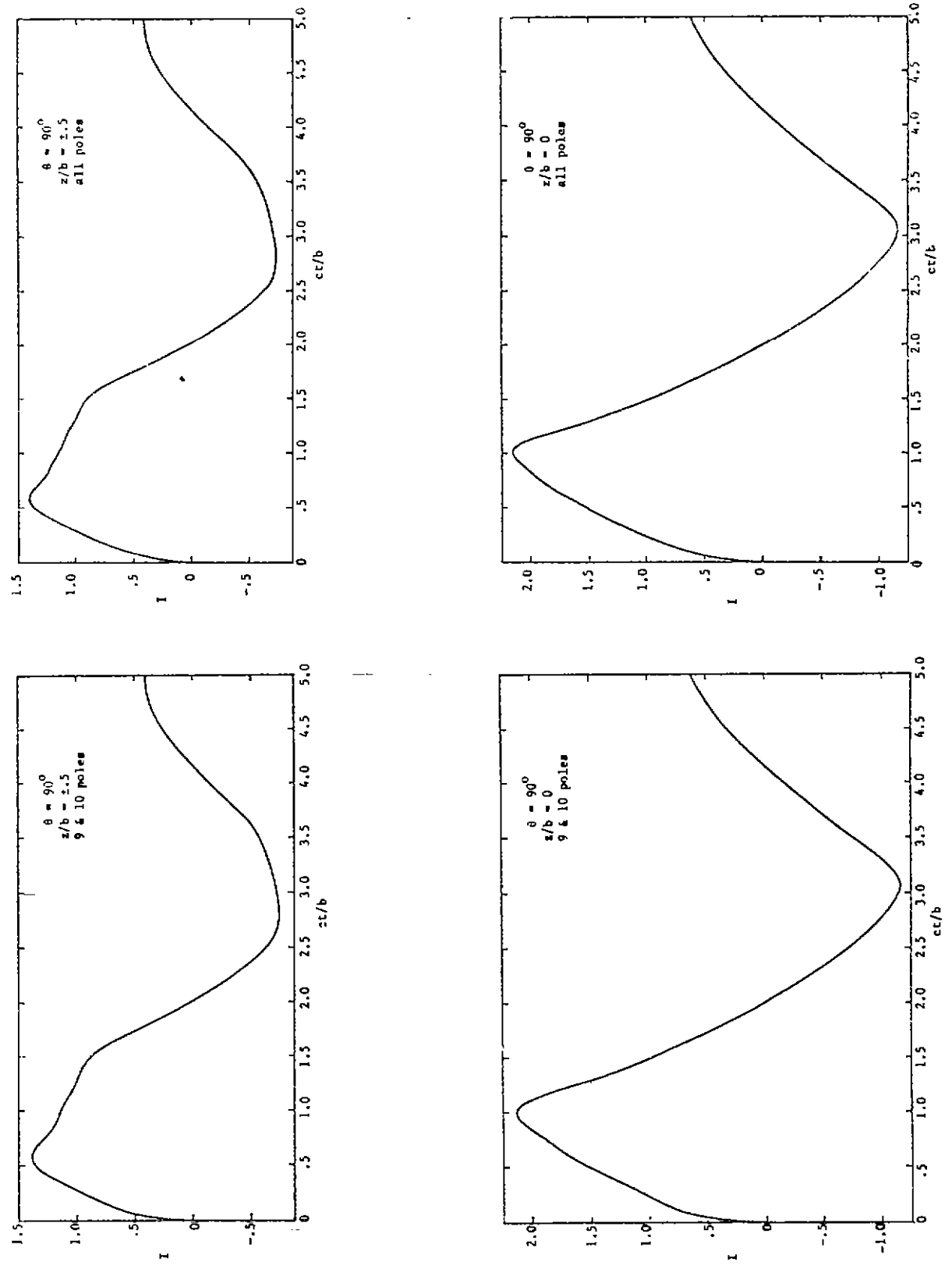

Figure 13b. The time response of the current at three points on a prolate spheroid as a function of the number of poles when the angle of incidence $\theta=90^{\circ}$.

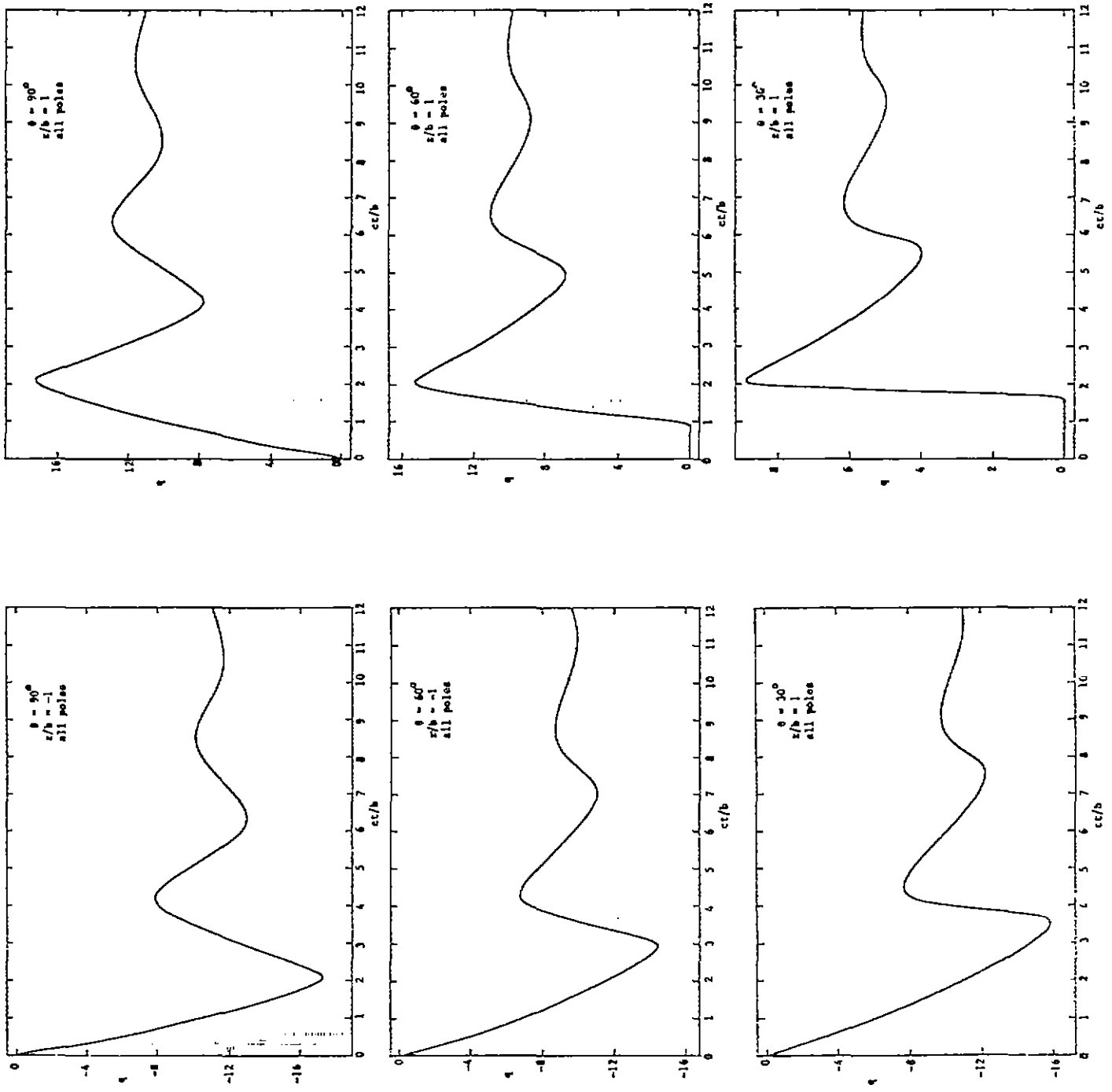

Figure 14. The time response of the charge density at two points on a prolate spheroid when the angle of incidence $\theta = 30^{\circ}, 60^{\circ}, 90^{\circ}$.

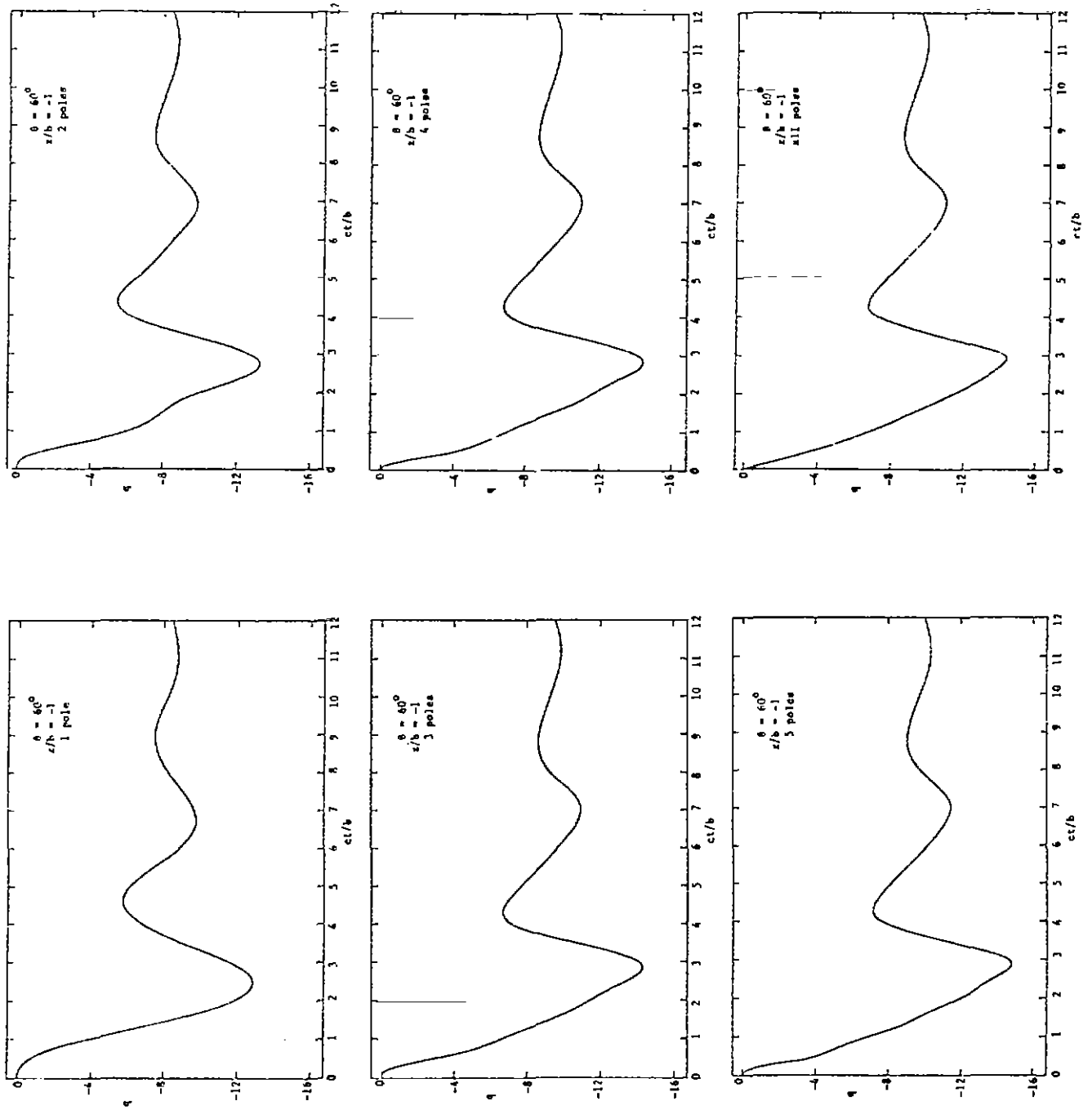

Figure 15a. The time response of the charge density at two points on a prolate spheroid as a function of the number of poles when the angle of incidence $\theta=60^{\circ}$.

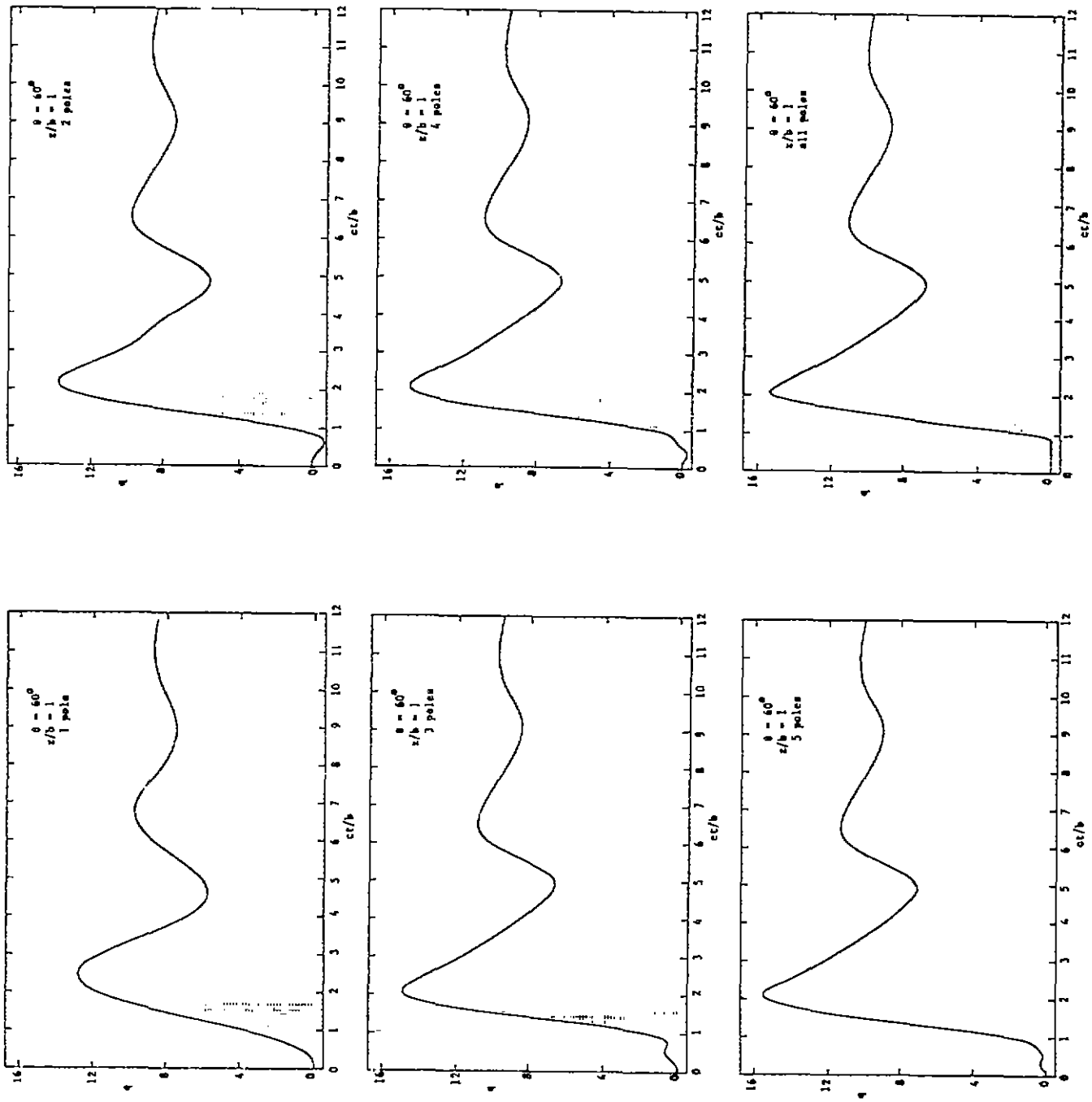

Figure 15b. The time response of the charge density at two points on a prolate spheroid as a function of the number of poles when the angle of incidence $\theta=60^{\circ}$.

Appendix A

Natural Modes of a Perfectly Conducting Sphere

Although the sphere has been the subject of extensive investigations for many years by using the method of eigen-function expansions[1,10,19] we will here determine the natural modes of a sphere by using an integral equation approach. There are several reasons for treating the sphere here: (1) we wish to give a simple example to expound the method discussed in Appendix D of [11]; (2) the analytical results derived for the natural modes of a sphere were very valuable in the numerical calculation of the natural modes of a spheroid; (3) in the sphere problem we will see some of the connections between the characteristic modes[13-16] and the natural modes[1,11].

We will start with an investigation of the eigenvalues and eigenfunctions of the integral operator $\underline{\underline{L}}$, defined by

$$\underline{\underline{L}}\cdot\underline{j} = \int_S \underline{n}\times(\nabla G\times\underline{j})\,dS, \tag{A.1}$$

when S is the surface of a sphere. The approach we will use in the following is indirect. First, we will show that the eigenfunctions of the "ordinary" expansion of the wave equation by separation of variables in spherical coordinates also are eigenfunctions of the operator $\underline{\underline{L}}$.

Introduce the functions

$$\underline{j}'_{mn}(\theta,\phi) = \frac{\partial Y_{mn}}{\partial\theta}(\theta,\phi)\hat{\theta} + \frac{1}{\sin\theta}\frac{\partial Y_{mn}}{\partial\phi}(\theta,\phi)\hat{\phi} \tag{A.2}$$

where (θ,ϕ) are the polar angles and

$$Y_{mn}(\theta,\phi) = P_n^m(\cos\theta)\exp(-im\phi), \quad n \geq 0, \quad 0 \leq m \leq n$$

are the spherical harmonics. We then have

$$(\underline{\underline{L}}\cdot\underline{j}'_{mn})(\theta,\phi) = \int_S a^3\, f(R)\underline{\underline{K}}(\theta,\theta',\phi-\phi')\cdot\underline{j}'_{mn}(\theta',\phi')\sin\theta'\,d\theta'\,d\phi' \tag{A.3}$$

where a is the radius of the sphere,

$$f(R) = -(1 + \gamma R)(4\pi R^3)^{-1} \exp(-\gamma R),$$

$$R = a(2 - 2\cos\alpha)^{\frac{1}{2}},$$

$$\cos\alpha = \cos\theta\cos\theta' + \sin\theta\sin\theta'\cos(\phi - \phi'),$$

$\underline{\underline{K}}(\theta,\theta',\psi)$ is a matrix with elements:

$$k_{\theta\theta}(\theta,\theta',\psi) = \cos\psi - \cos\theta\cos\theta'\cos\psi - \sin\theta\sin\theta',$$

$$k_{\theta\phi}(\theta,\theta',\psi) = (\cos\theta' - \cos\theta)\sin\psi,$$

$$k_{\phi\theta}(\theta,\theta',\psi) = k_{\theta\phi}(\theta,\theta',\psi),$$

and $$k_{\phi\phi}(\theta,\theta',\psi) = -k_{\theta\theta}(\theta,\theta',\psi).$$

After some lengthy algebraic manipulations equation (A.3) can be transformed into

$$(\underline{\underline{L}}\cdot\underline{j}'_{mn})(\theta,\phi) = \frac{1}{2}\left(1 + \gamma\frac{\partial}{\partial\gamma}\right)\int_S ag(R)\underline{\underline{N}}(\theta,\theta',\phi - \phi')\cdot\underline{j}'_{mn}(\theta',\phi')\sin\theta'\,d\theta'\,d\phi' \quad (A.4)$$

where

$$g(R) = (4\pi R)^{-1}\exp(-\gamma R),$$

$\underline{\underline{N}}(\theta,\theta',\psi)$ is a matrix with elements:

$$n_{\theta\theta}(\theta,\theta',\psi) = -\cos\psi,$$

$$n_{\theta\phi}(\theta,\theta',\psi) = \cos\theta'\sin\psi,$$

$$n_{\phi\theta}(\theta,\theta',\psi) = 0,$$

$$n_{\phi\phi}(\theta,\theta',\psi) = -1/\sin\theta.$$

Making use of the expansion[21]

$$g(R) = (-\gamma/4\pi) \sum_{n=0}^{\infty} (2n + 1) j_n(i\gamma a) h_n^{(1)}(i\gamma a) P_n(\cos \alpha)$$

where

$$P_n(\cos \alpha) = \sum_{m=0}^{n} \varepsilon_m (n - m)![(n + m)!]^{-1} P_n^m(\cos \theta) P_n^m(\cos \theta') \cos m(\phi - \phi')$$

equation (A.4) can be simplified to

$$(\underline{\underline{L}} \cdot \underline{j}'_{mn})(\theta,\phi) = -\frac{1}{2} [\gamma^2 a^2 j_n(i\gamma a) h_n^{(1)}(i\gamma a)]' \underline{j}'_{mn}(\theta,\phi). \tag{A.5}$$

Here the prime at the bracket denotes differentiation with respect to γa.

Introducing the modified spherical Bessel functions $i_n(z)$ and $k_n(z)$, defined by[1]

$$i_n(\zeta) = i^{-n} j_n(i\zeta),$$

$$k_n(\zeta) = i^{n+2} h_n^{(1)}(i\zeta)$$

we have

$$(\underline{\underline{L}} \cdot \underline{j}'_{mn})(\theta,\phi) = -\frac{1}{2} [\gamma^2 a^2 i_n(\gamma a) k_n(\gamma a)]' \underline{j}'_{mn}(\theta,\phi). \tag{A.6}$$

Now with the Wronskian[1]

$$W[\zeta i_n(\zeta), \zeta k_n(\zeta)] = \zeta i_n(\zeta)[\zeta k_n(\zeta)]' - [\zeta i_n(\zeta)]' \zeta k_n(\zeta) = -1$$

we have

$$(\underline{\underline{L}} \cdot \underline{j}'_{mn})(\theta,\phi) = \{\frac{1}{2} - [\gamma a i_n(\gamma a)]' \gamma a k_n(\gamma a)\} \underline{j}'_{mn}(\theta,\phi)$$

$$= -\{\frac{1}{2} + \gamma a i_n(\gamma a)[\gamma a k_n(\gamma a)]'\} \underline{j}'_{mn}(\theta,\phi). \tag{A.7}$$

To sum up we have shown that

$$\underline{\underline{L}} \cdot \underline{j}'_{mn} = \lambda'_{mn}\, \underline{j}'_{mn} \tag{A.8}$$

where

$$\lambda'_{mn} = -\frac{1}{2} + [\gamma a i_n(\gamma a)]' \gamma a k_n(\gamma a) = -\frac{1}{2} + \frac{1}{2} \gamma a i_n(\gamma a)[\gamma a k_n(\gamma a)]' \tag{A.9}$$

and $\underline{j}'_{mn}$ is given by equation (A.2).

We will now study $\underline{j}''_{mn}$, the counterpart of $\underline{j}'_{mn}$, given by

$$\underline{j}''_{mn}(\theta,\varphi) = \frac{1}{\sin\theta} \frac{\partial Y_{mn}}{\partial \varphi}(\theta,\varphi)\hat{\theta} - \frac{\partial Y_{mn}}{\partial \theta}(\theta,\varphi)\hat{\varphi}. \tag{A.10}$$

In the same way one can show that

$$\underline{\underline{L}} \cdot \underline{j}''_{mn} = \lambda''_{mn}\, \underline{j}''_{mn} \tag{A.11}$$

where

$$\lambda''_{mn} = -\frac{1}{2} + \gamma a i_n(\gamma a)[\gamma a k_n(\gamma a)]' = -\frac{1}{2} + [\gamma a i_n(\gamma a)]' \gamma a k_n(\gamma a). \tag{A.12}$$

With

$$\underline{h}'^{*}_{mn} = \underline{j}''_{mn} \tag{A.13}$$

it is now easy to show that

$$\underline{\underline{L}}_1 \cdot \underline{h}'^{*}_{mn} = \lambda_{mn}\, \underline{h}'^{*}_{mn} \tag{A.14}$$

where the operator $\underline{\underline{L}}_1$ is defined by

$$\underline{\underline{L}}_1 \cdot \underline{F} = \int_S \overline{\mathcal{G}} G^{*}(\underline{n} \cdot \underline{F})\, dS.$$

From equation (A.14) and the analysis in Appendix C of [11] it follows that

$$\underline{\underline{L}}^T \cdot \underline{h}'^*_{mn} = -\lambda'_{mn}\, \underline{h}'^*_{mn} \tag{A.15}$$

where

$$\underline{\underline{L}}^T = \underline{\underline{L}}^{\dagger *}$$

and $\underline{\underline{L}}^{\dagger}$ is the adjoint operator of $\underline{\underline{L}}$.

With

$$\underline{h}''^*_{mn} = \underline{j}'_{mn} \tag{A.16}$$

we also have

$$\underline{\underline{L}}^T \cdot \underline{h}''^*_{mn} = -\lambda''_{mn}\, \underline{h}''^*_{mn}. \tag{A.17}$$

Notice that $\underline{j}'_{mn}$ and $\underline{h}'^*_{mn}$ are proportional to the surface current density and tangential magnetic field, respectively, for transverse magnetic (TM) fields and that $\underline{j}''_{mn}$ and $\underline{h}''^*_{mn}$ are proportional to the current density and tangential magnetic field, respectively, for transverse electric (TE) fields on the sphere.

From equations (A.8), (A.11), (A.15) and (A.17) we can form the following set of equations:

$$(\tfrac{1}{2}\,\underline{\underline{I}} - \underline{\underline{L}}) \cdot \underline{j}'_{mn} = (\tfrac{1}{2} - \lambda'_{mn})\underline{j}'_{mn} = [\gamma a i_n(\gamma a)]'\, \gamma a k_n(\gamma a)\underline{j}'_{mn}, \tag{A.18}$$

$$(\tfrac{1}{2}\,\underline{\underline{I}} - \underline{\underline{L}}) \cdot \underline{j}''_{mn} = (\tfrac{1}{2} - \lambda''_{mn})\underline{j}''_{mn} = -\gamma a i_n(\gamma a)[\gamma a k_n(\gamma a)]'\, \underline{j}''_{mn}, \tag{A.19}$$

$$(\tfrac{1}{2}\,\underline{\underline{I}} - \underline{\underline{L}}^T) \cdot \underline{h}'^*_{mn} = (\tfrac{1}{2} + \lambda'_{mn})\underline{h}'^*_{mn} = -\gamma a i_n(\gamma a)[\gamma a k_n(\gamma a)]'\, \underline{h}'^*_{mn}, \tag{A.20}$$

$$(\tfrac{1}{2}\,\underline{\underline{I}} - \underline{\underline{L}}^T) \cdot \underline{h}''^*_{mn} = (\tfrac{1}{2} + \lambda''_{mn})\underline{h}''^*_{mn} = [\gamma a i_n(\gamma a)]'\, \gamma a k_n(\gamma a)\underline{h}''^*_{mn}, \tag{A.21}$$

$$(\tfrac{1}{2}\,\underline{\underline{I}} + \underline{\underline{L}}) \cdot \underline{j}'_{mn} = (\tfrac{1}{2} + \lambda'_{mn})\underline{j}'_{mn} = -\gamma a i_n(\gamma a)[\gamma a k_n(\gamma a)]'\, \underline{j}'_{mn}, \tag{A.22}$$

$$(\tfrac{1}{2}\,\underline{\underline{I}} \mp \underline{\underline{L}})\cdot\underline{j}''_{mn} = (\tfrac{1}{2} \mp \lambda''_{mn})\underline{j}''_{mn} = [\gamma a i_n(\gamma a)]' \; \gamma a k_n(\gamma a)\underline{j}''_{mn}, \tag{A.23}$$

$$(\tfrac{1}{2}\,\underline{\underline{I}} \mp \underline{\underline{L}}^T)\cdot\underline{h}'^*_{mn} = (\tfrac{1}{2} \mp \lambda'_{mn})\underline{h}'^*_{mn} = [\gamma a i_n(\gamma a)]' \; \gamma a k_n(\gamma a)\underline{h}'^*_{mn}, \tag{A.24}$$

$$(\tfrac{1}{2}\,\underline{\underline{I}} \mp \underline{\underline{L}}^T)\cdot\underline{h}''^*_{mn} = (\tfrac{1}{2} \mp \lambda''_{mn})\underline{h}''^*_{mn} = -\,\gamma a i_n(\gamma a)[\gamma a k_n(\gamma a)]' \; \underline{h}''^*_{mn}. \tag{A.25}$$

From equations (A.18) through (A.25) we observe that $\underline{j}'_{mn}$ and $\underline{j}''_{mn}$ diagonalize the operators $\frac{1}{2}\,\underline{\underline{I}} \pm \underline{\underline{L}}$, and that $\underline{h}'^*_{mn}$ and $\underline{h}''^*_{mn}$ diagonalize the operators $\frac{1}{2}\,\underline{\underline{I}} \pm \underline{\underline{L}}^T$. This diagonalization is, of course, valid for any complex frequency $s = c\gamma$.

We will now go on to compare the diagonalization procedure for the integral operator derived from the magnetic field equation with the diagonalization procedure derived from the electric field equation[13]. The integral equation derived from the electric field formulation of the electromagnetic scattering problem can be cast into the following operator form

$$\underline{\underline{Z}}\cdot\underline{j} = Z_o^{-1}\,\underline{e}^{inc} \tag{A.26}$$

where $\underline{\underline{Z}}$ is an integral operator defined by

$$\underline{\underline{Z}}\cdot\underline{j} = (\underline{\underline{I}} - \underline{n}\,\underline{n})(\nabla\phi + \gamma\underline{A}),$$

$$\underline{A} = \int_S G\underline{j}\,dS',$$

$$\phi = -\,\gamma^{-1}\int_S G\nabla\cdot\underline{j}\,dS',$$

$\underline{e}^{inc}$ is the tangential component of the incident electric field, and Z_o is the wave impedance of free space, $Z_o \approx 377\Omega$. After some algebraic manipulations we get

$$\underline{\underline{Z}}\cdot\underline{j}'_{mn} = \zeta'_{mn}\,\underline{j}'_{mn} \tag{A.27}$$

and

$$\underline{\underline{Z}}\cdot\underline{j}''_{mn} = \zeta''_{mn}\,\underline{j}''_{mn} \tag{A.28}$$

where

$$\zeta'_{mn} = - [a\gamma i_n(a\gamma)]' [a\gamma k_n(a\gamma)]'$$

and

$$\zeta''_{mn} = - (a\gamma)^2 i_n(a\gamma) k_n(a\gamma).$$

Moreover, with

$$\underline{\underline{R}} = (\underline{\underline{Z}} + \underline{\underline{Z}}^*)/2 \tag{A.29}$$

and

$$\underline{\underline{X}} = (\underline{\underline{Z}} - \underline{\underline{Z}}^*)/(2i) \tag{A.30}$$

the operators $\underline{\underline{R}}$ and $\underline{\underline{X}}$ are real and symmetric. It has been shown that for $\gamma = - ik$, (k real), we have[13]

$$\underline{\underline{X}} \cdot \underline{j}'_{mn} = \chi'_{mn} \underline{\underline{R}} \cdot \underline{j}'_{mn} \tag{A.31}$$

and

$$\underline{\underline{X}} \cdot \underline{j}''_{mn} = \chi''_{mn} \underline{\underline{R}} \cdot \underline{j}''_{mn} \tag{A.32}$$

where

$$\chi'_{mn} = - j'_n(ka)/y'_n(ka),$$

and

$$\chi''_{mn} = - j_n(ka)/y_n(ka).$$

We notice that in the case of a sphere the same functions diagonalize both the electric field integral operator and the magnetic field integral operator.

It has been shown[13] that for real frequencies ($\gamma = - ik$), the electromagnetic fields generated by surface current densities on an arbitrarily shaped body satisfying

$$\underline{\underline{X}}\cdot\underline{j} = \chi\underline{\underline{R}}\cdot\underline{j} \tag{A.33}$$

diagonalize the scattering operator. Without proof, we conjecture here that solutions of equation (A.33) also satisfies

$$\underline{\underline{L}}\cdot\underline{j} = \lambda\underline{j} \tag{A.34}$$

for real frequencies.

We now proceed to consider the natural frequencies and modes for a sphere. First we notice that $\underline{j}'_{mn}$ and $\underline{j}''_{mn}$ correspond to the eigenfunctions $\underline{\psi}_i$ as introduced in Appendix D of [11] and that $\underline{h}'_{mn}$ and $\underline{h}''_{mn}$ correspond to $\underline{\psi}_j$. The natural frequencies are given by the solutions of the equations

$$1 + 2\lambda'_{mn} = 0, \tag{A.35}$$

$$1 + 2\lambda''_{mn} = 0 \tag{A.36}$$

(c.f. equation (D.21) in [11]). In the case of a sphere equations (A.35) and (A.36) can be reduced to

$$[\gamma a i_n(\gamma a)]' \gamma a k_n(\gamma a) = 0, \tag{A.37}$$

$$\gamma a i_n(\gamma a)[\gamma a k_n(\gamma a)]' = 0, \tag{A.38}$$

and equations (A.37) and (A.38) can be split into the following set of equations

$$k_n(\gamma a) = 0, \tag{A.39}$$

$$[\gamma a k_n(\gamma a)]' = 0, \tag{A.40}$$

$$i_n(\gamma a) = 0, \tag{A.41}$$

$$[\gamma a i_n(\gamma a)]' = 0. \tag{A.42}$$

The solutions of equations (A.41) and (A.42) are pure imaginary and correspond to interior (cavity) natural frequencies. The solutions of (A.39) and (A.40) give the exterior natural frequencies of the sphere.

Assume that γ'_{mn} satisfies equation (A.39). It then follows from equations (A.18) and (A.21) that

$$(\tfrac{1}{2}\,\underline{\underline{I}} - \underline{\underline{L}})\cdot\underline{j}'_{mn} = 0, \tag{A.43}$$

and

$$(\tfrac{1}{2}\,\underline{\underline{I}} - \underline{\underline{L}}^{T})\cdot\underline{h}''^{*}_{mn} = 0. \tag{A.44}$$

Next, let γ''_{mn} satisfy equation (A.40). From equations (A.19) and (A.20) it then follows that

$$(\tfrac{1}{2}\,\underline{\underline{I}} - \underline{\underline{L}})\cdot\underline{j}''_{mn} = 0, \tag{A.45}$$

and

$$(\tfrac{1}{2}\,\underline{\underline{I}} - \underline{\underline{L}}^{T})\cdot\underline{h}'^{*}_{mn} = 0. \tag{A.46}$$

However, we have seen that $\underline{j}'_{mn} = \underline{h}''^{*}_{mn}$ and $\underline{j}''_{mn} = \underline{h}'^{*}_{mn}$ (see equations (A.13) and (A.16)). Thus, in the case of a sphere the operators $\frac{1}{2}\,\underline{\underline{I}} - \underline{\underline{L}}$ and $\frac{1}{2}\,\underline{\underline{I}} - \underline{\underline{L}}^{T}$ have the same nontrivial solutions at the natural frequencies. This fact was of great help in the numerical calculation of the natural modes of a spheroid.

Notice that equations (A.18), (A.19), (A.24) and (A.25) describe the exterior scattering problem whereas equations (A.20) through (A.23) describe the interior scattering problem (c.f. Appendix C in [11]).

Appendix B

Some Remarks Concerning the Convergence of the Numerical Solution

In this appendix we will consider some of the convergence properties of the numerical solution of the integral equation

$$\frac{1}{2} j(\xi) - \int_0^{\xi_o} L(\xi,\xi')j(\xi')d\xi' = j^{inc}(\xi) \tag{B.1}$$

where the kernel $L(\xi,\xi') = A(\xi,\xi')\rho(\xi')$ and $A(\xi,\xi')$ is defined by equation (2.13) in section II. We will pay special attention to the convergence in the numerical determination of the natural frequencies.

It is easy to show that $A(\xi,\xi')$ has a logarithmic singularity at $\xi = \xi'$ and that

$$\int_0^{\xi_o}\int_0^{\xi_o} |L(\xi,\xi')|^2 \, d\xi d\xi' < \infty. \tag{B.2}$$

Thus, the kernel $L(\xi,\xi')$ is of Hilbert Schmidt type.

Let $\mathcal{H}$ be the Hilbert space consisting of all functions $f(\xi)$, defined on the interval $(0, \xi_o)$, such that

$$\|f\|^2 = \int_0^{\xi_o} f(\xi)f^*(\xi)d\xi < \infty. \tag{B.3}$$

Moreover, let $\{f_i\}_{i=1}^{\infty}$ be a complete orthonormal set in $\mathcal{H}$. The Hilbert-Schmidt norm of the operator L,

$$(Lf)(\xi) = \int_0^{\xi_o} L(\xi,\xi')f(\xi')d\xi', \tag{B.4}$$

is then given by

$$\|L\|^2 = \sum_{i=1}^{\infty} \|Lf_i\|^2 \tag{B.5}$$

and from (B.2) it follows that $\|L\| < \infty$. The Hilbert Schmidt norm does not depend upon the particular basis used but only upon the Hilbert space[120]. Thus, the orthonormal set, $\{f_i\}_{i=1}$, used as basis for $\mathcal{H}$ can be chosen to be

independent of γ. It also follows from (B.4) that for any $\varepsilon > 0$ there exists a finite number N such that

$$\sum_{i=N+1}^{\infty} \|Lf_i\|^2 < \varepsilon^2. \tag{B.6}$$

Next we introduce some new quantities. The reason for introducing these quantities will become clear as we proceed. Let $\mathcal{H}_N$ denote the finite dimensional Hilbert space spanned by $\{f_i\}_{i=1}^{N}$. The orthogonal complement of $\mathcal{H}_N$ with respect to $\mathcal{H}$ is denoted by $\mathcal{H}_N^{\perp}$. Thus, we have

$$\mathcal{H} = \mathcal{H}_N + \mathcal{H}_N^{\perp}. \tag{B.7}$$

Let us also define a projection operator P_N so that

$$P_N\mathcal{H} = \mathcal{H}_N \tag{B.8}$$

and

$$(I - P_N)\mathcal{H} = \mathcal{H}_N^{\perp} \tag{B.9}$$

where I is the identity operator on $\mathcal{H}$.

The integral operator $L = L(\gamma)$ can then be split up into two parts

$$L = L_N + R_N \tag{B.10}$$

where

$$L_N = P_N L P_N \tag{B.11}$$

and

$$R_N = L - L_N. \tag{B.12}$$

With

$$A = \frac{1}{2} I - L \tag{B.13}$$

and

$$A_N = \frac{1}{2} I - L_N \tag{B.14}$$

we have

$$A_N = A + R_N. \tag{B.15}$$

Assume that γ is such that $A^{-1} = A^{-1}(\gamma)$ exists. From equation (B.6) it then follows that we can choose N such that $\|R_N\| < \|A^{-1}\|^{-1}$. We then have

$$A_N^{-1} = A^{-1}(I + A^{-1} R_N)^{-1}. \tag{B.16}$$

Moreover, since $\|A^{-1} R_N\| \leq \|A^{-1}\| \|R_N\| < 1$ it follows that $(I + A^{-1} R_N)^{-1}$ exists so that the inverse operator A_N^{-1} also exists. Thus, for any γ such that $A^{-1}(\gamma)$ exists then there exists an N such that $A_N^{-1}(\gamma)$ also exists. But the existence of the inverse operator A_N^{-1} ensures the existence of the inverse operator M_N^{-1},

$$M_N = P_N A P_N. \tag{B.17}$$

In reference [11] we have shown that the only singularities of A^{-1} are poles. From the analysis presented in section III it follows that the only singularities of M_N^{-1} also are poles. Let $\gamma_n^{(N)}$ be a pole of M_N^{-1} and γ_n a pole of A^{-1}. From the above it then follows that for any given $\delta > 0$ we can find a integer N such that

$$|\gamma_n^{(N)} - \gamma_n| < \delta. \tag{B.18}$$

Equation (B.18) ensures the convergence of the numerical calculation of the poles.

Appendix C

Two Numerical Methods for Determining the Natural Modes

In this appendix we will consider the matrix equation

$$M(\gamma)\cdot\bar{j} = \bar{f}. \tag{C.1}$$

There are different ways of arriving at this equation. Two examples are the matrix approximations of the magnetic-field integral equation and electric-field integral equation. For all the cases under consideration we will assume that each element of the matrix $M(\gamma)$, $m_{i\ell}(\gamma)$, is an analytic function of γ. The column vector $\bar{f}$ is determined by the incident field.

Method 1

Since $M(\gamma)$ is an analytic matrix valued function of γ it follows immediately that $M^{-1}(\gamma)$, the inverse of $M(\gamma)$, is also an analytic matrix valued function of γ except for those values of γ, (γ_n), where $\det\{M(\gamma)\} = 0$. For $\gamma \neq \gamma_n$, the solution of equation (C.1) can be written as

$$\bar{j} = M^{-1}(\gamma)\cdot\bar{f} = R(\gamma)\cdot\bar{f}/d(\gamma) \tag{C.2}$$

where

$$d(\gamma) = \det\{M(\gamma)\}$$

and $R(\gamma)$ is a matrix whose elements are the cofactors of the elements of the transposed matrix $M^T(\gamma)$. Suppose now that $\gamma = \gamma_n$ and $M(\gamma_n)$ is a $N \times N$ matrix of rank $N - 1$, so that $d(\gamma_n) = 0$ but $d'(\gamma_n) \neq 0$ (where prime denotes differentiation with respect to γ). Following the procedure in reference [11] we then have

$$\bar{j} = \sum_{\text{ext}}^{n} [(\gamma - \gamma_n)d'(\gamma_n)]^{-1} R(\gamma_n)\cdot\bar{f} \tag{C.3}$$

when $\bar{f}$ is an analytic column vector valued function of γ.

Since $M(\gamma_n)$ is a $N \times N$ matrix of rank $N - 1$ there exists one and only one nontrivial solution, $\bar{j}_n$, of the equation

$$M(\gamma_n)\cdot\bar{j}_n = 0 \tag{C.4}$$

and one and only one nontrivial solution, $\bar{q}_n$, of the equation

$$M^T(\gamma_n)\cdot\bar{q}_n = 0. \tag{C.5}$$

Each component of equations (C.4) and (C.5) takes the following form

$$\sum_{\ell=1}^{N} m_{i\ell}j_\ell = 0, \qquad 1 \le i \le N \tag{C.6}$$

$$\sum_{\ell=1}^{N} m_{\ell i}q_\ell = 0, \qquad 1 \le i \le N \tag{C.7}$$

Here

$$m_{i\ell} = m_{i\ell}(\gamma_n),$$

$$j_\ell = j_{\ell n},$$

$$q_\ell = q_{\ell n},$$

and $j_{\ell n}$ is the ℓ^{th} component of $\bar{j}_n$ and $q_{\ell n}$ is the ℓ^{th} component of $\bar{q}_n$.

Let $R(\gamma_n)$ have elements $r_{i\ell}$. From the expansion of the determinant of M it then follows that

$$\sum_{\ell=1}^{N} m_{i\ell}r_{\ell k} = 0 \tag{C.8}$$

and by comparing equations (C.6) and (C.8) we get

$$r_{\ell k} = a_\ell j_k, \qquad 1 \le \ell \le N \tag{C.9}$$

where the a_ℓ's are constants.

From the expansion of the determinant of $M^T(\gamma_n)$ we have

$$\sum_{\ell=1}^{N} m_{\ell i} r_{k\ell} = 0 \tag{C.10}$$

so that by comparing equations (C.7) and (C.10) we have

$$r_{k\ell} = b_k q_\ell, \qquad r_{\ell k} = b_\ell q_k \tag{C.11}$$

where the b_ℓ's are constants. Comparing equations (C.10) and (C.11) it follows that

$$r_{\ell k} = C j_\ell q_k \tag{C.12}$$

where C is a constant.

Thus, we have the following solution of equation (C.1)

$$\bar{j} = \sum_n \left[(\gamma - \gamma_n) d'(\gamma_n)\right]^{-1} C_n (\bar{q}_n^T \cdot \bar{f}_n) \bar{j}_n \tag{C.13}$$

where the constants C_n have to be determined by numerical methods by considering the solution of equation (C.1) in the vicinity of each pole. The derivative of the determinant can be evaluated numerically by finite difference methods.

Method 2

The second method is based on the Householder method for triangularizing matrices. To each N × N matrix M there exists a unitary transformation U such that

$$UM = T \tag{C.14}$$

where T is an upper triangle matrix with elements t_{ii} and det{U} = 1, so that

$$\det\{M\} = \det\{T\} = \prod_{i=1}^{N} t_{ii}. \tag{C.15}$$

Moreover, if $M(\gamma_n)$ is of rank N - 1 we have

$$t_{NN}(\gamma_n) = 0 \quad \text{and} \quad t_{ii}(\gamma_n) \neq 0, \qquad 1 \leq i \leq N - 1.$$

From this it follows that

$$d'(\gamma_n) = t'_{NN}(\gamma_n) \prod_{i=1}^{N-1} t_{ii}(\gamma_n). \tag{C.16}$$

For $\gamma \neq \gamma_n$ we have

$$U = TM^{-1} = TR/\det\{M\} = TR/\prod_{i=1}^{N} t_{ii}. \tag{C.17}$$

Since T is an upper triangle matrix we have

$$u_{NN} = t_{NN}r_{NN}/\prod_{i=1}^{N} t_{ii} = r_{NN}/\prod_{i=1}^{N-1} t_{ii} \tag{C.18}$$

and the last expression in equation (C.18) is well defined even for $\gamma = \gamma_n$.
For $\gamma = \gamma_n$ we have (c.f. equation (C.12))

$$R(\gamma_n) = C_n \bar{j}_n \bar{q}_n^T \tag{C.19}$$

and we normalize $\bar{j}_n$ and $\bar{q}_n$ so that

$$j_{Nn} = 1 \quad \text{and} \quad q_{Nn} = u_{NN}(\gamma_n).$$

It then follows from equation (C.19) that

$$r_{NN}(\gamma_n) = C_n u_{NN}(\gamma_n). \tag{C.20}$$

Comparing equations (C.18) and (C.20) we get

$$C_n = 1/\prod_{i=1}^{N-1} t_{ii}(\gamma_n). \tag{C.21}$$

From equations (C.13), (C.15) and (C.21) we have

$$\bar{j} = \sum_{ext} [(\gamma - \gamma_n)t'_{NN}(\gamma_n)]^{-1} (\bar{q}_n^T \cdot \bar{f}_n)\bar{j}_n \tag{C.22}$$

where $t'_{NN}(\gamma_n)$ has to be determined numerically from finite differences.

Appendix D

A Subroutine for Triangularizing a Matrix A and Solving the Equations $A\cdot\bar{p} = A^T\cdot\bar{q} = 0$ When A is a Singular Matrix

In this Appendix we will describe a computer subroutine MLRDET that triangularizes an arbitrary complex valued N × N matrix A. When the matrix A is singular, i.e. det{A} = 0, the subroutine also determines nontrivial solutions of the homogeneous equations

$$A\cdot\bar{p} = 0$$

and

$$A^T\cdot\bar{q} = 0.$$

The method used here is based on the Householder method for reducing an arbitrary matrix to an upper triangular matrix by a series of unitary transformations. The subroutine is written in Fortran IV for the CDC 6600 computer. This subroutine follows closely the subroutine CMLR for solving M linear complex equations in N unknowns[18].

The algorithm we use is based on a method developed by Householder[17]. Introduce the notations

$$\bar{e}_k = \text{the } k^{th} \text{ column of the N × N identity matrix I,} \tag{D.1}$$

$$\bar{a}_k = \text{the } k^{th} \text{ column of the N × N matrix A,} \tag{D.2}$$

$$\alpha_k = (\bar{a}_k^{\dagger}\cdot\bar{a}_k)^{\frac{1}{2}} = \text{the Euclidean norm of } \bar{a}_k, \tag{D.3}$$

$$\bar{a}^{\dagger} = (\bar{a}^T)^*, \tag{D.4}$$

$$\bar{v}_k = -(\bar{e}_k^{\dagger}\cdot\bar{a}_k)\bar{e}_k/|\bar{e}_k^{\dagger}\cdot\bar{a}_k|, \tag{D.5}$$

$$\bar{u}_k = (\bar{a}_k + \alpha_k\bar{v}_k)/[2\alpha_k(\alpha_k + \bar{v}_k^{\dagger}\cdot\bar{a}_k)]^{\frac{1}{2}}. \tag{D.6}$$

We then have

$$\bar{a}_1 - [(\bar{a}_1 + \alpha_1\bar{v}_1)^\dagger \cdot \bar{a}_1][\alpha_1(\alpha_1 + \bar{v}_1^\dagger \cdot \bar{a}_1)]^{-1} (\bar{a}_1 + \alpha_1\bar{v}_1) = -\alpha_1\bar{v}_1. \qquad (D.7)$$

Thus, the transformation U_1, defined by

$$U_1 = I - 2\bar{u}_1\bar{u}_1^\dagger, \qquad (D.8)$$

transforms the matrix A into a matrix U_1A where in the first column all elements are zero except for the first element. Next we suppress the first row and first column in U_1A and repeat the process described by equations (D.1) through (D.8) on the $(N-1)\times(N-1)$ matrix. After N steps the matrix A is trangularized so that

$$UA = T \qquad (D.9)$$

where T is an upper triangle matrix with elements $t_{i\ell}$ and U is a transformation

$$U = \prod_{\ell=0}^{N-1} U_{N-\ell} = U_N U_{N-1} \cdots U_2 U_1 \qquad (D.10)$$

where

$$U_m = I - 2\bar{u}_m\bar{u}_m^\dagger \qquad (D.11)$$

and $\bar{u}_m$ is a column vector with N - m elements determined from the m^{th} iteration of the algorithm (D.1) through (D.8). The transformation U_N actually only introduces a change in the sign of the element t_{NN}. From a lemma proved by Householder[17] it follows that U_m is a unitary transformation and that $\det\{U_m\} = 1$. Since U_m is a unitary tranformation and hence U is also a unitary transformation, the condition of A is preserved throughout the transformation, i.e.,

$$\gamma(T) = \gamma(A)$$

where

$$\gamma(A) = \|A\| \ \|A^{-1}\|$$

and $\|A\|$ is the Euclidean norm of A. We also notice that

$$\det\{A\} = \det\{T\} = \prod_{i=1}^{N} t_{ii}. \tag{D.12}$$

Let the column vector $\bar{u}_m$ have elements $u_{\ell m}$, $1 \le \ell \le N - m + 1$. The information about the transformation U can then be expressed by a lower triangular matrix W with elements $w_{i\ell}$ where

$$\begin{aligned} w_{i\ell} &= 0, && i < \ell \\ w_{i\ell} &= u_{\ell+i-1,i}, && i \ge \ell. \end{aligned} \tag{D.13}$$

When the $N \times N$ matrix A is of rank $N - 1$ so that $\det\{A\} = 0$ we have $t_{NN} = 0$, but $t_{ii} \neq 0$, $1 \le i \le N - 1$. A nontrivial solution of

$$A \cdot \bar{p} = 0 \tag{D.14}$$

can then be determined in the following way. By multiplying equation (D.14) from the left by U we get

$$UA \cdot \bar{p} = T \cdot \bar{p} = 0. \tag{D.15}$$

Since all elements in the last row of T are zero we can, without changing the value of $T \cdot \bar{p}$, put

$$p_N = 1 \tag{D.16}$$

where p_N is the last element of $\bar{p}$. Since $t_{ii} \neq 0$ for $1 \le i \le N - 1$ we can obtain the other elements of $\bar{p}$ by backsolving equation (D.15),

$$p_i = - t_{ii}^{-1} \sum_{\ell=i+1}^{N} t_{i\ell} p_\ell, \qquad 1 \le i \le N - 1. \tag{D.17}$$

A nontrivial solution of

$$A^T \cdot \bar{q} = 0 \tag{D.18}$$

can be obtained by making the following observation:

$$T^T = (UA)^T = A^T U^T, \tag{D.19}$$

so that with

$$\bar{q} = U^T \cdot \bar{s} \tag{D.20}$$

we have

$$A^T \cdot \bar{q} = A^T U^T \cdot \bar{s} = T^T \cdot \bar{s} = 0. \tag{D.21}$$

A nontrivial solution of equation (D.21) is given by

$$s_\ell = \delta_{N\ell}, \qquad 1 \le \ell \le N \tag{D.22}$$

where $\delta_{i\ell}$ is the Kronecker symbol. A nontrivial solution of equation (D.20) is then given by

$$\bar{q} = \bar{s}^{(0)} \tag{D.23}$$

where $\bar{s}^{(0)}$ is determined iteratively from the expression

$$\bar{s}^{(n-1)} = U_n^T \cdot \bar{s}^{(n)} = \bar{s}^{(n)} - 2\bar{u}_n^* \left[\bar{u}_n^T \cdot \bar{s}_n^{(n)}\right], \qquad 1 \le n \le N \tag{D.24}$$

and $\bar{s}^{(N)} = \bar{s}$. Making use of the elements of the matrix W we get

$$s_i^{(n-1)} = s_i^{(n)} - 2w_{in}^* \sum_{\ell=n}^{N} w_{\ell n} s_\ell^{(n)}. \tag{D.25}$$

Equation (D.17) was used in calculating the current distribution of each mode and equation (D.25) was used in calculating the coupling vector of each natural mode.

Appendix E

A Method for the Numerical Evaluation of the Order of Each Pole

A knowledge of the order of each pole is necessary when solving transient electromagnetic interaction problems by the singularity expansion method. For special shapes of the scattering body the order of each pole can be determined by analytical methods. For example, in the case of a perfectly conducting sphere, it has been found[1] that all poles are simple poles by considering the differential equation for spherical Bessel functions. However, for an arbitrarily shaped, finite, perfectly conducting body there seems, as of now, to exist no general analytical method that enables one to determine the order of each pole. Therefore, we will in this Appendix discuss a general numerical method to determine the order of each pole.

Let γ_n be a natural frequency, i.e., there exists $\underline{j}_n \neq 0$ such that

$$\underline{\underline{A}}(\gamma_n)\cdot\underline{j}_n = 0. \tag{E.1}$$

We also introduce the operators $\underline{\underline{B}}_{nq}$, defined by[11]

$$(\underline{\underline{B}}_{nq}\cdot\underline{f})(\underline{r}) = (-1)^q(4\pi q!)^{-1}\int_S \underline{n}(\underline{r})\times\{\nabla[|\underline{r}-\underline{r}'|^{q-1}\exp(-\gamma_n|\underline{r}-\underline{r}'|)]\times\underline{f}(\underline{r}')\}dS'. \tag{E.2}$$

The order of each pole, p, is then given by the smallest value of p such that

$$\underline{\underline{B}}_{nq}\cdot\underline{j}_n = 0, \qquad 0 \leq q \leq p-1$$

and (E.3)

$$\underline{\underline{B}}_{np}\cdot\underline{j}_n \neq 0$$

where

$$\underline{\underline{B}}_{no} = \underline{\underline{A}}(\gamma_n).$$

Translated into the numerical language this means the following. Let γ_n be a root of the equation

$$\det\{M(\gamma)\} = 0 \tag{E.4}$$

where $M(\gamma)$ is the matrix approximation of $\underline{\underline{A}}(\gamma)$. The matrix approximation of $\underline{\underline{B}}_{nq}$ is denoted by M_{nq}. The order of the pole at γ_n is then given by the smallest value of p such that

$$\det\{M_{nq}\} = 0, \qquad 0 \leq q \leq p - 1$$

and (E.5)

$$\det\{M_{np}\} \neq 0$$

where

$$M_{no} = M(\gamma_n).$$

From equation (E.5) one can determine the order of each pole.

A knowledge of the natural modes enables one to calculate the current induced on the surface of the scattering body.[11] The contribution from modes corresponding to simple poles of $\underline{\underline{A}}^{-1}(\gamma)$ are easy to obtain as we have seen in section III of this note. The contribution from higher order poles is not so easy to obtain. For example, the contribution from a double pole has been determined in Appendix E of reference [11]. Since we have not yet encountered the problem of calculating the contribution from higher order poles we find, as of now, no need to investigate this problem any further.

Acknowledgment

We thank Mr. R. W. Sassman for his invaluable assistance in the numerical computations and for his expert programming. Thanks also go to Drs. C. E. Baum, R. W. Latham, K. S. H. Lee and F. M. Tesche for many interesting discussions during the course of this work. The typing of the note and the preparation of the figures by Mrs. G. Peralta is gratefully acknowledged.

References

1. C. E. Baum, "On the Singularity Expansion Method for the Solution of Electromagnetic Interaction Problems," Interaction Note 88, December 1971.
2. M. Abraham, "Die electrischen Schwingungen um einen stabförmigen Leiter, behandelt nach der Maxwell'schen Theorie," Ann. der Physik, Vol. 66, pp. 435-472, 1898.
3. L. Page and N. Adams, "The Electrical Oscillations of a Prolate Spheroid. Paper I," Phys. Rev., Vol. 53, pp. 819-831, 1938.
4. L. Page, "The Electrical Oscillations of a Prolate Spheroid. Paper II," Phys. Rev., Vol. 65, pp. 98-110, 1944.
5. L. Page, "The Electrical Oscillations of a Prolate Spheroid. Paper III," Phys. Rev., Vol. 65, pp. 111-117, 1944.
6. C. W. Oseen, "Über die elektromagnetische Schwingungen an dünnen Stäben," Ark. Mat. Astron. Fysik, Vol. 9, No. 30, pp. 1-27, 1914.
7. E. Hallén, "Über die elekrischen Schwingungen in drahtförmigen Leitern," Uppsala Univ. Årsskr., No. 1, pp. 1-102, 1930.
8. S. W. Lee and B. Leung, "The Natural Resonance Frequency of a Thin Cylinder and its Application to EMP Studies," Interaction Note 96, February 1972.
9. F. M. Tesche, "On the Singularity Expansion Method as Applied to Electromagnetic Scattering From Thin Wires," Interaction Note 102, April 1972.
10. J. P. Martinez, Z. L. Pine, F. M. Tesche, "Numerical Results of the Singularity Expansion Method as Applied to a Plane Wave Incident on a Perfectly Conducting Sphere," Interaction Note 112, May 1972.
11. L. Marin and R. W. Latham, "Analytical Properties of the Field Scattered by a Perfectly Conducting, Finite Body," Interaction Note 92, January 1972.
12. M. G. Andreasen, "Scattering From Bodies of Revolution," IEEE Trans. Antennas Propagat., Vol. AP-13, pp. 303-310, March 1965.
13. R. F. Harrington and J. R. Mautz, "Theory of Characteristic Modes for Conducting Bodies," IEEE Trans. Antennas Propagat., Vol. AP-19, pp. 622-628, September 1971.
14. R. F. Harrington and J. R. Mautz, "Computation of Characteristic Modes for Conducting Bodies," IEEE Trans. Antennas and Propagat., Vol. AP-19, pp. 629-639, September 1971.

15. R. J. Garbacz and R. H. Turpin, "A Generalized Expansion for Radiated and Scattered Fields," IEEE Trans. Antennas Propagat., Vol. AP-19, pp. 348-358, May 1971.

16. R. J. Garbacz, "Modal Expansions for Resonance Scattering Phenomena," Proc. IEEE, Vol. 53, pp. 856-864, August 1965.

17. A. S. Householder, "Unitary Triangularization of a Nonsymmetric Matrix," J. Assoc. Comp. Mach., Vol. 5, pp. 339-342, October 1958.

18. R. W. Sassman, "CMLR, A Subroutine to Solve M Linear Complex Equations in N Unknowns," Mathematics Note 11, February 1970.

19. J. A. Stratton, Electromagnetic Theory, Chapter IX, McGraw-Hill, New York, 1941.

20. N. Dunford and J. T. Schwartz, Linear Operators, Part II Spectral Theory, Interscience Publishers, New York, 1963.

21. W. Magnus, F. Oberhettinger and R. P. Soni, Formulas and Theorems for the Special Functions of Mathematical Physics, Springer-Verlag, New York, 1966.